

# Annual Report

## *Authors*

Ronald Adamson  
Fremont, CA, USA

Kit Coleman  
Deep River, ON, Canada

Friedrich Garzarolli  
Fürth, Germany

Malcolm Griffiths  
Deep River, Canada

Clément Lemaignan  
Voreppe, France

Albert Machiels  
Brentwood, CA, USA

Tahir Mahmood  
Pleasanton, CA, USA

Charles Patterson  
Clovis, CA, USA

Peter Rudling  
ANT International, Tollerød, Sweden



A.N.T. INTERNATIONAL®

© December 2018

Advanced Nuclear Technology International  
Spinnerivägen 1, Mellersta Fabriken plan 4,  
448 50 Tollerød, Sweden

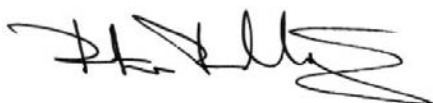
[info@antinternational.com](mailto:info@antinternational.com)

[www.antinternational.com](http://www.antinternational.com)

## Disclaimer

The information presented in this report has been compiled and analysed by Advanced Nuclear Technology International Europe AB (ANT International®) and its subcontractors. ANT International has exercised due diligence in this work, but does not warrant the accuracy or completeness of the information. ANT International does not assume any responsibility for any consequences as a result of the use of the information for any party, except a warranty for reasonable technical skill, which is limited to the amount paid for this assignment by each ZIRAT/IZNA programme member.

**Quality-checked and authorized by:**

A handwritten signature in black ink, appearing to read 'Peter Rudling', with a stylized, flowing script.

Mr Peter Rudling, President of ANT International

## Contents

<b>1</b>	<b>Introduction (P. Rudling)</b>	<b>1-1</b>
<b>2</b>	<b>Burnup and Fuel Technology Achievements (C. Patterson)</b>	<b>2-1</b>
2.1	Introduction	2-1
2.2	Trends in Fuel and Reactor Operating Conditions	2-1
2.2.1	General Trends	2-1
2.2.2	Fuel Cycles	2-7
2.2.3	Power Upgrades	2-10
2.2.4	Burnup Extensions	2-12
2.3	Fuel Performance and Reliability	2-15
2.4	PCI and Anticipated Operating Occurrences	2-25
2.4.1	Assessment of Core-Wide PCI Risk due to AOOs	2-25
2.4.2	Regulatory Perspective	2-28
2.4.3	PCMI/PCI Models and Cladding Failure Criteria	2-30
2.4.4	Cladding Failure Criteria	2-63
2.5	Summary	2-78
<b>3</b>	<b>Fabrication and Microstructure (K. Coleman)</b>	<b>3-1</b>
3.1	Common Path to Fuel Cladding	3-1
3.2	Surface Coating Methods	3-9
3.2.1	Physical Vapour Deposition (PVD)	3-9
3.2.2	Chemical Vapour Deposition (CVD)	3-11
3.2.3	Cold Spraying (CS)	3-14
3.3	Summary	3-16
<b>4</b>	<b>Mechanical Properties (K. Coleman)</b>	<b>4-1</b>
4.1	Introduction	4-1
4.2	Response to Accidents	4-1
4.2.1	LOCA: Loss Of Coolant Accident	4-1
4.2.2	RIA: Reactivity Initiated Accident	4-7
4.3	Effects of Hydrogen	4-11
4.3.1	Non-destructive Evaluation	4-11
4.3.2	Phases, Solubility Limit and Delayed Hydride Cracking	4-17
4.3.3	A New Failure Mechanism	4-24
4.4	Summary	4-28
<b>5</b>	<b>Dimensional Stability (M. Griffiths and R. Adamson)</b>	<b>5-1</b>
5.1	Part I – Experimental and Operational Data	5-1
5.1.1	Introduction	5-1
5.1.2	Measure of Radiation Damage to Zirconium Alloy Microstructure	5-3
5.1.3	Previous Creep and Growth Reviews	5-5
5.1.4	Comparisons between Creep and Growth in a Reactor Environment as a Function of Variables	5-8
5.1.5	Recent Literature	5-19
5.1.6	Summary	5-27
5.2	Part II – Mechanisms & Modelling of Irradiation Creep and Growth of Zr Alloys	5-28
5.2.1	Irradiation Growth	5-28
5.2.2	Irradiation Creep	5-49
5.2.3	Summary	5-80
<b>6</b>	<b>Corrosion and Hydriding (F. Garzarolli and C. Lemaignan)</b>	<b>6-1</b>
6.1	Out-of-pile Corrosion and HPU (Friedrich Garzarolli)	6-1
6.2	Corrosion in PWR and VVER (Friedrich Garzarolli)	6-5
6.3	Corrosion in BWR and RBMK (Friedrich Garzarolli)	6-12
6.4	Coated Zr Alloy Cladding for Enhanced Accident Tolerant Fuel (Friedrich Garzarolli)	6-26
6.5	Progresses in Scientific Understanding (Clément Lemaignan)	6-37

6.5.1	Transition in Corrosion Kinetics	6-38
6.5.2	Irradiation Effects on Corrosion Mechanisms	6-47
6.5.3	Hydrogen Pick-Up and Localisation	6-50
6.6	Summary (Friedrich Garzarolli and Clément Lemaignan)	6-54
7	Fuel Performance and Design (P. Rudling)	7-1
7.1	Introduction	7-1
7.1.1	Primary Failures	7-1
7.1.2	Secondary Degradation	7-5
7.2	Results Presented in Year 2017-2018	7-5
7.3	Summary of Recent Key Results 2017–2018	7-17
8	LOCA, RIA, Seismic Event (P. Rudling and C. Patterson)	8-1
8.1	Introduction	8-1
8.1.1	Seismic Event (P. Rudling)	8-1
8.1.2	Loss of Coolant Accident (P. Rudling)	8-2
8.1.3	Reactivity Initiated Accident	8-12
8.1.4	Fuel Cladding Failure Threshold	8-17
8.1.5	Coolable Core Geometry Criteria	8-22
8.1.6	Radiological Fission Product Inventory Guidance	8-24
8.2	New Results 2016-2018	8-26
8.2.1	Seismic Event	8-26
8.2.2	RIA	8-26
8.2.3	LOCA	8-33
8.3	Summary of Recent Key Results 2016–2018	8-100
8.3.1	RIA	8-100
8.3.2	LOCA	8-101
9	Accident Tolerant Fuels (ATFs) (Tahir Mahmood)	9-1
9.1	Introduction	9-1
9.2	Accident Tolerant Fuel Materials	9-2
9.3	DOE Funded ATF Development Programs	9-4
9.3.1	National Laboratory, Industry, and University Directed Efforts	9-7
9.3.2	ATF Irradiation Testing	9-9
9.4	ATF Claddings	9-11
9.4.1	Coated and Improved Zirconium Alloy Claddings	9-13
9.4.2	Cr Coated Claddings	9-18
9.4.3	Ceramic Coated Claddings	9-20
9.4.4	Westinghouse-lead ATF R&D	9-23
9.4.5	Framatome-lead ATF R&D	9-30
9.4.6	Coated Cladding R&D in Korea	9-35
9.4.7	Advanced Steels (FeCrAl) Claddings	9-40
9.4.8	GE-lead ATF R&D	9-45
9.4.9	FeCrAl-ODS R&D in Japan	9-51
9.4.10	ATF R&D in China	9-61
9.4.11	SiC/SiC Composite Claddings	9-68
9.4.12	Lined Mo Alloy Claddings	9-72
9.5	Accident Tolerant Fuel Designs	9-73
9.5.1	Improved UO <sub>2</sub>	9-73
9.5.2	High Density Fuel	9-74
9.5.3	TRISO-SiC Composite Pellets	9-75
9.6	Non-Fuel Components	9-78
9.6.1	SiC Composite BWR Channels	9-78
9.6.2	Accident Tolerant Control Rods	9-80
9.7	Evaluation of Accident Tolerant Fuel Systems	9-82
9.7.1	Standard Screening Analyses for ATF Concepts	9-82
9.7.2	Analysis of Severe Accident Behavior	9-83
9.8	Irradiation Facilities for In-core Testing of ATF Materials	9-90
9.9	Summary	9-90



<b>10</b>	<b>Storage and Transportation of Commercial Spent Nuclear Fuel Under Dry Inert Conditions (Albert Machiels)</b>	<b>10-1</b>
10.1	Introduction	10-1
10.2	Thermal Creep of Zr-based Alloys	10-3
10.2.1	Introduction	10-3
10.2.2	Creep Testing Set-up	10-4
10.2.3	Experimental Creep Curve Shapes	10-6
10.2.4	Thermal Creep Deformation Mechanisms	10-7
10.2.5	Thermal Creep Equations for Zr-based Alloys	10-10
10.2.6	Effect of Material Condition and Composition	10-12
10.2.7	Creep of Closed Systems such as Fuel Rods	10-19
10.2.8	Allowable Diametral Strain and Creep Rupture	10-20
10.2.9	Conclusions	10-22
<b>11</b>	<b>Trends and Needs</b>	<b>11-1</b>
<b>References</b>		
<b>Appendix A - Determination of the Creep Anisotropy Factors, F, G and H</b>		
A.1	Determination of F, G and H by Measurement	
A.2	Determination of F, G and H using a Polycrystalline Model	
<b>Appendix B - References</b>		
<b>Nomenclature</b>		
<b>Unit conversion</b>		

# 1 Introduction (P. Rudling)

The objective of the Annual Review of ZIRconium Alloy Technology (ZIRAT) and Information on Zirconium Alloys (IZNA) is to review and evaluate the latest developments in ZIRAT as they apply to nuclear fuel design and performance.

The objective is met through a review and evaluation of the most recent data on zirconium alloys and to identify the most important new information and discuss its significance in relation to fuel performance now and in the future. Included in the review are topics on materials research and development, fabrication, component design, and in-reactor performance presented in conferences, journals and reports.

The primary issues addressed in the review and this report is zirconium alloy research and development, fabrication, component design, ex- and in-reactor performance including:

- Regulatory bodies and utility perspectives related to fuel performance issues, fuel vendor developments of new fuel design to meet the fuel performance issues.
- Fabrication and Quality Control (QC) of zirconium manufacturing, zirconium alloy systems.
- Mechanical properties and their test methods (that are not covered in any other section in the report).
- Dimensional stability (growth and creep).
- Primary coolant chemistry and its effect on zirconium alloy component performance.
- Corrosion and hydriding mechanisms and performance of commercial alloys.
- Cladding primary failures.
- Post-failure degradation of failed fuel.
- Cladding performance in postulated accidents (Loss of Coolant Accident (LOCA), Reactivity Initiated Accident (RIA)).
- Performance of accident tolerant fuel (ATF)
- Dry storage.
- Potential Burn-up (BU) limitations.
- Current uncertainties and issues needing solution are identified throughout the report.

Background data from prior periods have been included wherever needed. The data published in this Report is only from non-proprietary sources; however, their compilation, evaluations, and conclusions in the report are proprietary to ANT International and ZIRAT/IZNA members as noted on the title page.

The authors of the report are Mr. Friedrich Garzarolli, Dr. Malcolm Griffiths, Dr. Charles Patterson, Clément Lemaignan, Dr. Ronald Adamson, Dr. Christopher Coleman, Dr. Tahir Mahmood, Dr. Albert Machiels (EPRI) and Mr. Peter Rudling, President of ANT International.

The work reported herein will be presented in four Seminars:

- February 5-7, 2019, Clearwater Beach, FL., USA,
- March 11-13, 2019, Palma de Mallorca, Spain
- November, 2019 in China
- November, 2019 in Japan

The Term of ZIRAT23/IZNA18 started on February 1, 2018 and ends on March 31, 2019.

All literature that we refer to in this Report is available in the ANT International Literature Database (LDB). Key information from previous A.N.T. International reports are easily accessible in the A.N.T. International Wikipedia (AWIKI). Please contact Ms. Mikaela Strand at [mikaela.strand@antinternational.com](mailto:mikaela.strand@antinternational.com) for more information.

## 2 Burnup and Fuel Technology Achievements (C. Patterson)

### 2.1 Introduction

The objective of this Section is to summarize recent achievements within the nuclear industry and to review key performance issues that could affect fuel design, fabrication or operation of nuclear fuel in the near or longer terms. The information sources reviewed, screened and evaluated include nearly all the related publications and technical meeting presentations of the past, approximately 18 months. This Section is intended to be a guide to current issues related to these topics and to provide an alert to items that could affect fuel related operations. The extensive volume of information involved limits the presentations to the most significant features and conclusions, and the reader is urged to refer to the referenced publications for more detail.

### 2.2 Trends in Fuel and Reactor Operating Conditions

#### 2.2.1 General Trends

The driving forces in the evolution of fuel technology and operating conditions are improved fuel reliability and economics while maintaining acceptable margins to operating and regulatory safety limits. Driving forces also include improvements in margins to fuel damage thresholds and mitigation of the consequences of severe accidents. These forces provide incentives for significant advances in materials technology, software for designing and predicting fuel performance, sophisticated instrumentation, modifications in water chemistry and methods for post-irradiation examinations. These forces are also causing shifts in the utilization of nuclear power in established and developing nuclear countries. Activities related to accident tolerant fuel are reviewed in a separate section of the Annual Report.

Advances in technology have increased the demands on fuel performance levels and put pressure on regulatory agencies to license operations to increased burnup levels. The types of changes in LWR design and operating methods intended to achieve improved safety and economics have not changed in the past years and still include:

- Plant power uprates that range from 2 to ~20%,
- More aggressive fuel designs with a larger amount of fuel at or near the near-universal limit for civilian power reactors of 5%  $^{235}\text{U}$ ,
- Increased concentrations and more widespread use of burnable neutron absorbers,
- More aggressive fuel management practices, with increased power peaking factors and increased amounts of fuel operating closer to design limits,
- Annual fuel cycles extended to 18 and 24 months at many NPPs,
- Increased discharge burnups as high as 64 GWd/MT batch average exposures by means of higher enrichments, increased amounts of burnable absorbers in the assemblies (absorber concentrations, increased length of burnable absorber pellets in rods with axially-zoned enrichments (BWR fuel) and increased number of rods with neutron absorbers) and, in PWRs, higher lithium and boron levels or enriched boron in the coolant,
- Development of cladding and fuel assembly materials with increased resistance to corrosion, hydrogen pickup irradiation growth and creep,
- Reduced activity transport by Zn injection into the coolant,
- Improved water chemistry controls and increased monitoring,
- Component life extension with hydrogen water chemistry (HWC), noble metal chemistry (NMC) and more extensively with on-line noble metal chemistry (OLNC) in BWRs.

A combination of environmental, economic, social and political issues are contributing to changes in the worldwide application of nuclear power. As of late 2018, the International Atomic Energy Agency reported 454 operating nuclear power reactors with a total installed electrical generating capability of 399.3 GWe<sup>1</sup>, [IAEA, 2018c]. The number of reactors with operational status and the associated generating capacities are shown by country in Figure 2-1. The number is changing due to the closure of plants in some countries and the startup of new plants in others. The net change between 2017 and 2018 was an increase in the number of reactors by six and an increase in the total generating capacity by 7.6 GWe. The amount of electricity supplied by nuclear power plants increased 2 506 TWeh in 2017 as shown in Figure 2-2. The installed capacity of the U.S., France, China, Japan, Russia and the Republic of Korea accounts for approximately 70% of the total, worldwide nuclear generating capability.

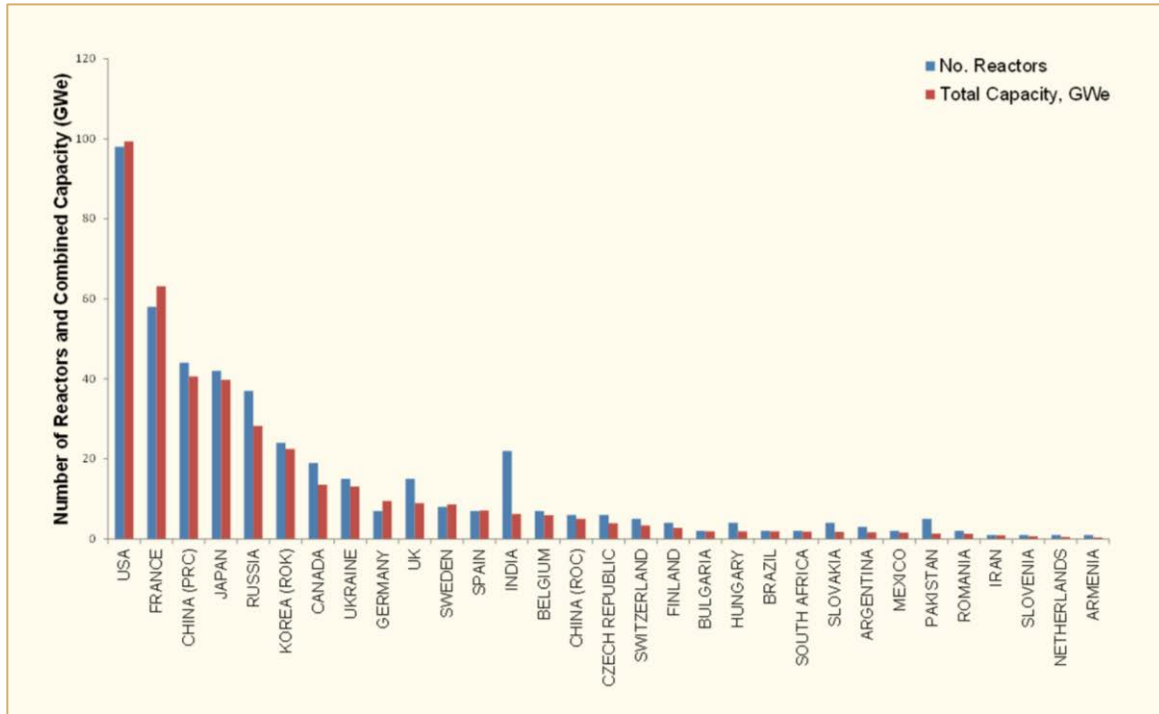


Figure 2-1: Electrical generating capabilities of nuclear reactors by country, after [IAEA, 2018c].

<sup>1</sup> The Power Reactor Information System (PRIS) database of the IAEA includes experience of all nuclear countries. Information compiled in PRIS through the end of 2017, with updates through September 2018, is used as a primary source for information in this section. Although the database is updated at frequent intervals, information in PRIS can differ from regional databases and other periodic tabulations due to the timing of the updates.

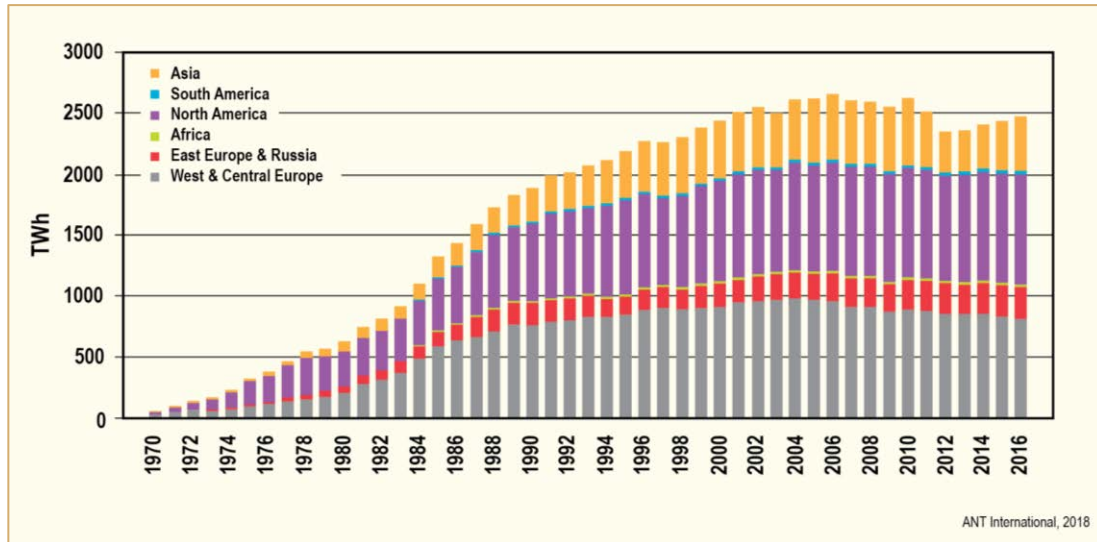


Figure 2-2: Nuclear generating capacity by year and region, [WNA, 2018].

The energy produced by the existing fleet of nuclear reactors constitutes about 13% of the electrical energy produced in countries with nuclear power plants, [IAEA, 2018c]. However, as shown in Figure 2-3, the relative role of nuclear power varies markedly among countries; e.g., 72% of electrical power is produced by nuclear reactors in France and less than 4% in Japan. The large generating capacity (Figure 2-1) and large nuclear fraction in France represents the historic policy of this country. The large capacity and the small production fraction in Japan represents the lingering effects of the 2011 Tohoku earthquake and tsunami; i.e., continued plant shutdowns with ongoing assessments of nuclear and plant safety by the utilities, regulators and politicians. The large generating capacity and small nuclear share in the U.S., China and Russia reflects the reliance of these countries on alternate sources of energy – primarily fossil fuels, but with increasing amounts of energy from solar and wind sources.

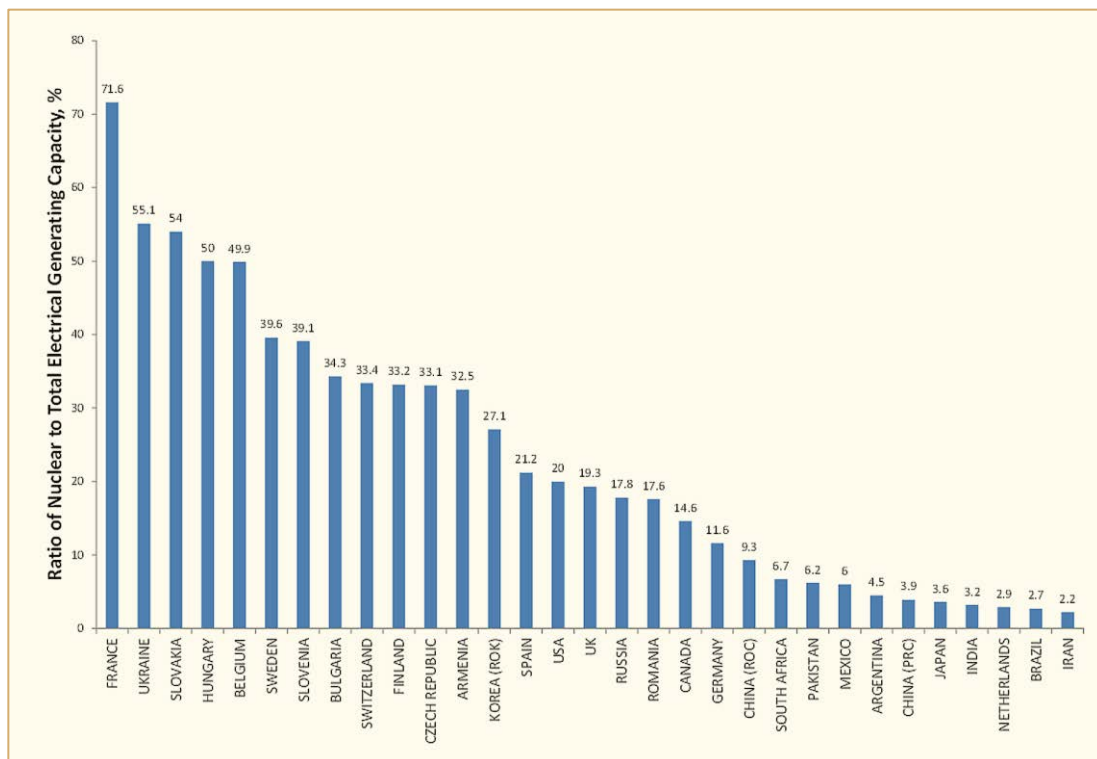


Figure 2-3: Electrical production by nuclear power plants relative to the total electrical production by country in 2018, [IAEA, 2018c].

Light water reactors continue to be the most commonly used source of nuclear energy. As shown in Figure 2-4, PWRs and VVERs constitute the greatest number of reactors and the largest generating capacity; viz., 292 out of 448 reactors and ~70% of the operable nuclear generating capacity. This condition is expected to continue since 45 of the 55 reactors currently under construction are PWRs or VVERs, [IAEA, 2018c].

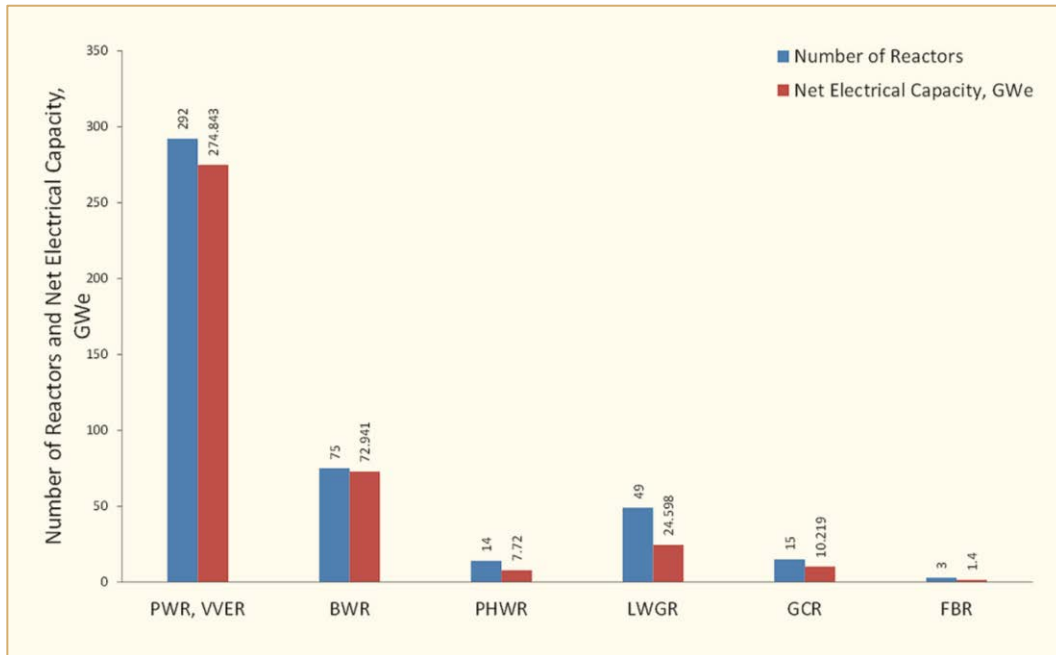


Figure 2-4: Number of operating nuclear reactors and the net electrical generating capacity by reactor type, after [IAEA, 2018b].

As shown in Figure 2-5 and Figure 2-6, a large number of new reactors are being constructed. The majority (82%) of the reactors currently under construction are PWRs or VVERs. Twenty eight reactors (51% of the total number) are being built in China (PRC and ROC), Russia and India. The remainder are being built in the rest of Asia, Europe and North and South America.

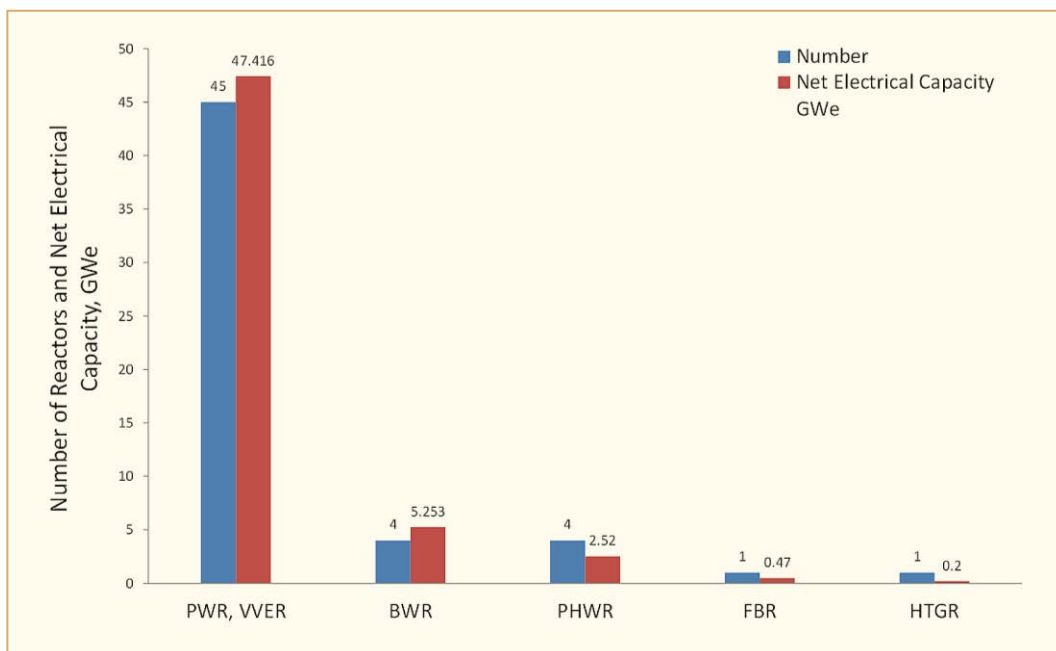


Figure 2-5: Nuclear power plants under construction in 2017 by reactor type, after [IAEA, 2018c].



Figure 2-6: Nuclear power plants under construction in 2016 by country, after [IAEA, 2018c].

The age of the existing fleet of reactors is approaching the point at which life extension or plant shutdown will be needed (e.g., 40 years in the U.S.), Figure 2-7. The generating capacity in GWe corresponds closely to the number of plants as indicated in Figure 2-1. So, decisions regarding life extension or shutdown will affect both the number of plants and the contribution of nuclear to the total energy production of the affected countries.

Based on the capacity factor of NPPs relative to age, shown Figure 2-8, there is no degradation in performance as plants reach the end of their initial license.<sup>2</sup> The original 40-year license interval was based on the amortization of capital expenditures combined with design and operational conservatism rather than an intrinsic limitation on reactor lifespan; [WNA, 2017a]. Experience has identified life-limiting factors, which have been or are being addressed, generally in the 30-40 year range of NPP age. Extensions in increments of 20 years are now common in countries where sociopolitical and economic climates are supportive or at least not hostile to nuclear power. Most NPPs in the U.S. (89 out of 99 plants) have already extended their licenses to 60 years. Three of these plants have subsequently ceased operation, while 47 are operating under extended licenses. In addition, the NRC is preparing to consider license extensions beyond 60 years, with applications submitted in January 2018 for the Turkey Point Unit 3 and Unit 4 PWRs, [NRC, 2018b]. The license renewal process in the U.S. typically costs \$16-25 million and requires 4-6 years for review by the NRC.

<sup>2</sup> The lower capacity factor at 49 years is due to the prolonged safety review of the Beznau-1 reactor in Switzerland (since late 2015) and the planned inspection and maintenance activity at Tarapur-1 in India. The capacity factors of the other four plants range from 94 to 99%.

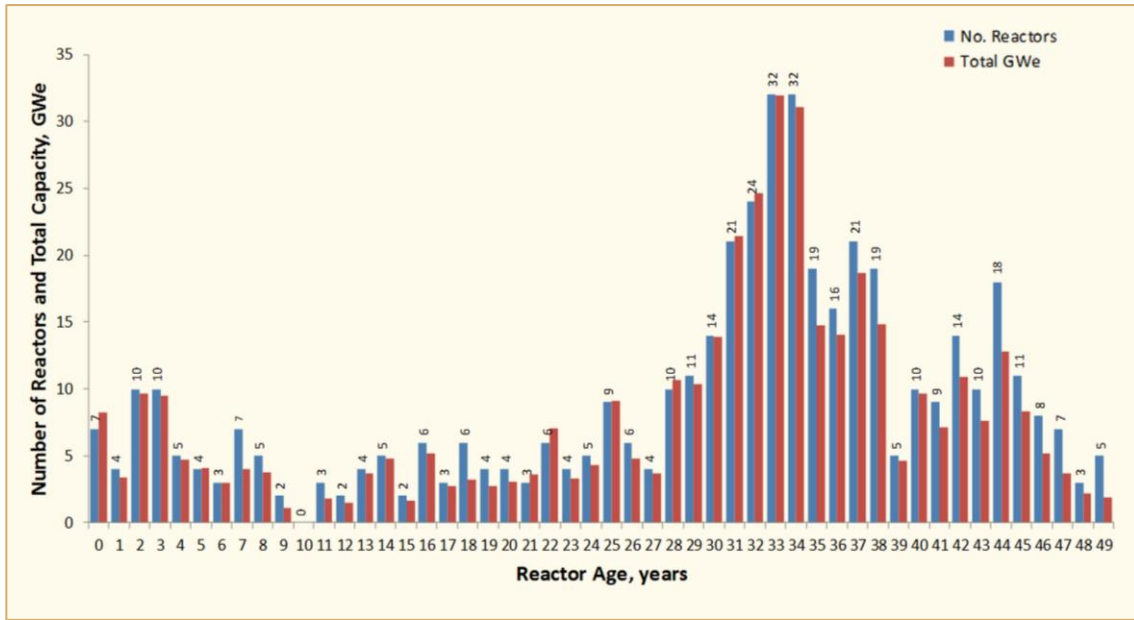


Figure 2-7: Age of operating reactors, after [IAEA, 2018c].

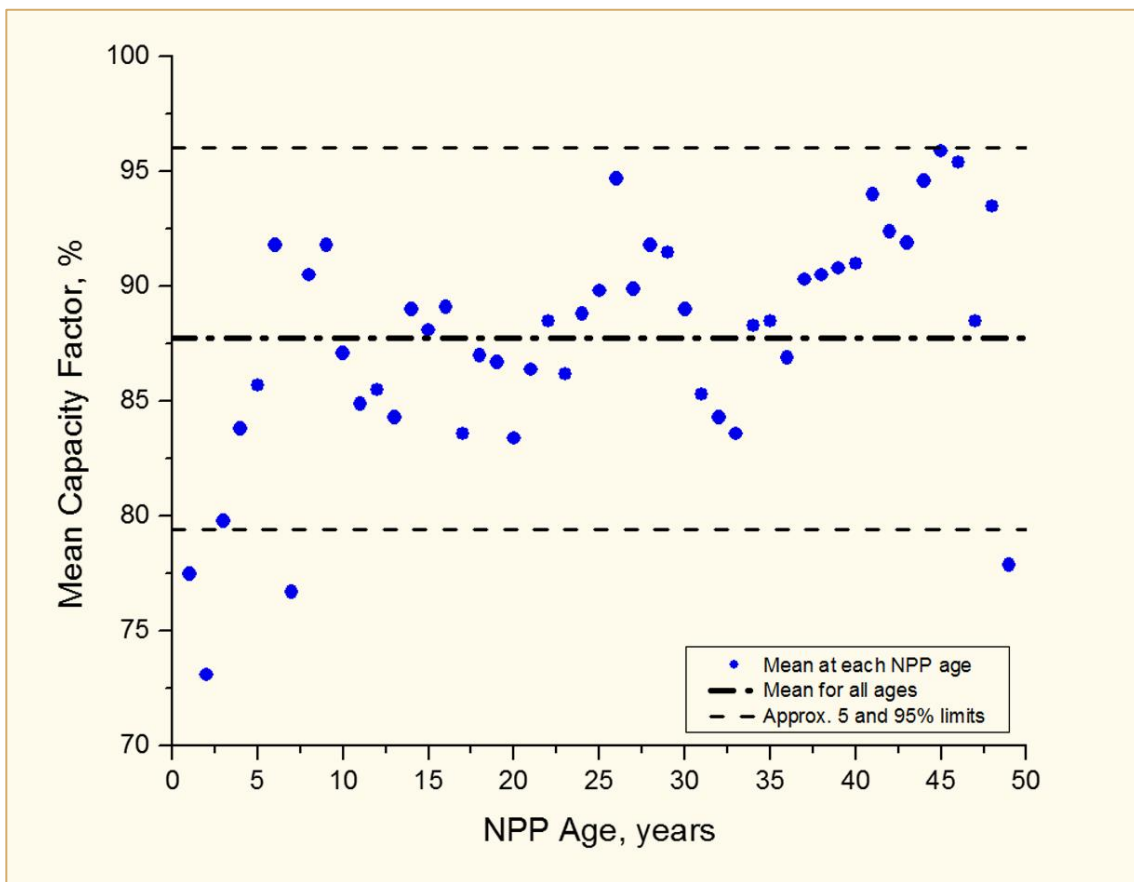


Figure 2-8: Median capacity factor relative to NPP age during 2012-2017, after [WNA, 2018].



Despite the ability to extend operating licenses, the perception of nuclear power relative to alternate, carbon-free sources (primarily wind and solar) along with the low cost of natural gas and subsidies for renewable energy sources in some countries is adversely affecting the economic viability of a number of NPPs. This condition is leading to early plant closure, particularly of those NPPs in merchant-based (deregulated) markets; see WNA [2017a] for background. This trend has been recognized as detrimental to long-term stability of power supplies given the intermittent nature of solar and wind sources. Financial pressures on NPPs is being addressed by credits for the capability of continuous power production and for the carbon-free capabilities of nuclear power. Although national and international public relation programs to improve the social and political acceptability of nuclear power as a necessary means to reduce the emissions of greenhouse gases (see IAEA [2018a] for example), both the number of plants and the nuclear generation capabilities are expected to decrease in established nuclear (OECD) countries and to increase in other countries (primarily Asian) over the next few decades.

## 2.2.2 Fuel Cycles

### 2.2.2.1 Cycle Length

The trend for increased fuel cycle lengths has come to a near “equilibrium” in the U.S. with PWRs operating at an average of 500 effective full power days (EFPD) per cycle and BWRs an average of 620 EFPD per cycle, up to a maximum of about 680 days for PWRs and 720 days for BWRs.

Nearly all of the U.S. BWRs are trending toward 24 month cycles except for an unusual move by Exelon, which changed the Clinton BWR NPP to a 12 month cycle. This change is reported to be in preparation for plant closure due to the economic effects of abundant, low-cost natural gas and subsidized, renewable sources. Some older, lower power density PWRs have implemented the 24 month cycles. But, fuel management limitations such as the reload batch sizes required for long cycles have impeded implementation of 24 month cycles in the high power density plants. The economics of 24 month cycles tend to be plant specific since they depend on the balance of a variety of parameters unique to each plant. The potential economic gains for cycle extension have decreased in the U.S. as the downtimes for reloading and maintenance procedures have been significantly reduced, thereby increasing the capacity factors.

Most countries have one winter power peak annually compared to the two, winter and summer peaks in the US. This condition has tended to keep plants outside of the U.S. on annual cycles. Changes in load management, economics, maintenance practices and licensing procedures are influencing this condition; some countries, such as France, Belgium, Switzerland and Germany are applying both annual and 18 month cycles. The fuel supplier TVEL has increased the fuel cycle length from 12 to 15 months in the 440 VVERs by increasing the enrichment from 4.2% to 4.7% in Russian, Finnish, Czech, Slovak and, more recently, in Hungarian plants.

### 2.2.2.2 Capacity Factors

The capacity factors of NPPs increased on both a global and local basis through the 1990s and have remained relatively constant since that time, as shown in Figure 2-9 and Figure 2-10. Globally, capacity factors have remained in the range of 78% to 83% since 2000. Capacity factors in the U.S. have followed a similar trend with yearly averages of 88% to 92% since 2000. The distributions of capacity factors on a global basis are shown relative to time in Figure 2-11. These data show that 64% of reactors achieved a capacity factor higher than 80% in 2017, compared to 25% in 1977. Conversely, only 6% of reactors had a capacity factor below 50% in 2017, compared to 23% in 1977.

### 3 Fabrication and Microstructure (K. Coleman)

#### 3.1 Common Path to Fuel Cladding

The usual starting material for zirconium alloy components is  $\text{ZrSiO}_4$  usually in the form of sand from Australia, South Africa or Ukraine. It is often associated with Hf. Several other undesirable impurities are controlled at this stage by judicious analysis and physical separation. Thus the two starting processes involve reducing the oxide, removing the Si and minimising Hf to maintain low capture cross-section for thermal neutrons. Ore-unlocking processes that have been used, or are currently being used in production, include carbothermic reduction, alkali fusion, fluorosilicate fusion, and carbochlorination. The product is a Zr halogen salt. Hf may be removed by fractional crystallization, methyl isobutyl ketone-thiocyanate (MIBK) and tributyl phosphate (TBP) solvent extraction, and extractive distillation. Reduction to the metal is by one of two methods: reduction of the metal tetrachloride with Mg to produce sponge Zr (Kroll Process) or electrolytic reduction to yield Zr powder. The metal production processes used around the world are summarised in Table 3-1.

Table 3-1: Main processing steps for conversion of zircon sand to metallic zirconium.

	NFC (India)	ChMP (Russia)	ATI Metals/WZr	CEZUS (France)
Ore decomposition	Caustic fusion	Fluorosilicate fusion	Carbochlorination	Carbochlorination
Separation	TBP-nitric	Fractional crystallization	MIBK	Extractive distillation
Reduction	Kroll	Electrolytic	Kroll	Kroll
© ANT International 2018				

The next step is to mix the sponge or powder with alloying elements in the required proportion then compact the materials into cylindrical briquettes. The briquettes are welded together and an ingot is formed by vacuum arc melting (VAR) the stack of briquettes, Figure 3-1 [Schemel, 1989]. Double melting is the minimum practice for all zirconium based alloys, but for better homogeneity, and to reduce surface and subsurface defects, and to remove critical gaseous impurities, triple or quadruple melting is also carried out. Multiple melting can reduce the hydrogen and halogen concentrations, both of which are harmful for fracture properties.

The ingots are cooled under vacuum, or inert gas such as argon or helium. After completion of the melting the ingot is stripped from the copper crucible. The rough surface of the ingot is machined and samples from several places of the ingot are taken in the form of turnings or solids for chemical and spectroscopic analysis and gas analysis. Hardness may be measured at various places on the surface of the ingot to further check for compositional heterogeneities. The ingot is also tested ultrasonically to ascertain integrity of the material and to locate any shrinkage cavity or piping-type defects. The microstructure of the ingot is very inhomogeneous at this stage consisting of transformed large  $\beta$ -grains and variations in size and shape from top to bottom and in the cross-section.

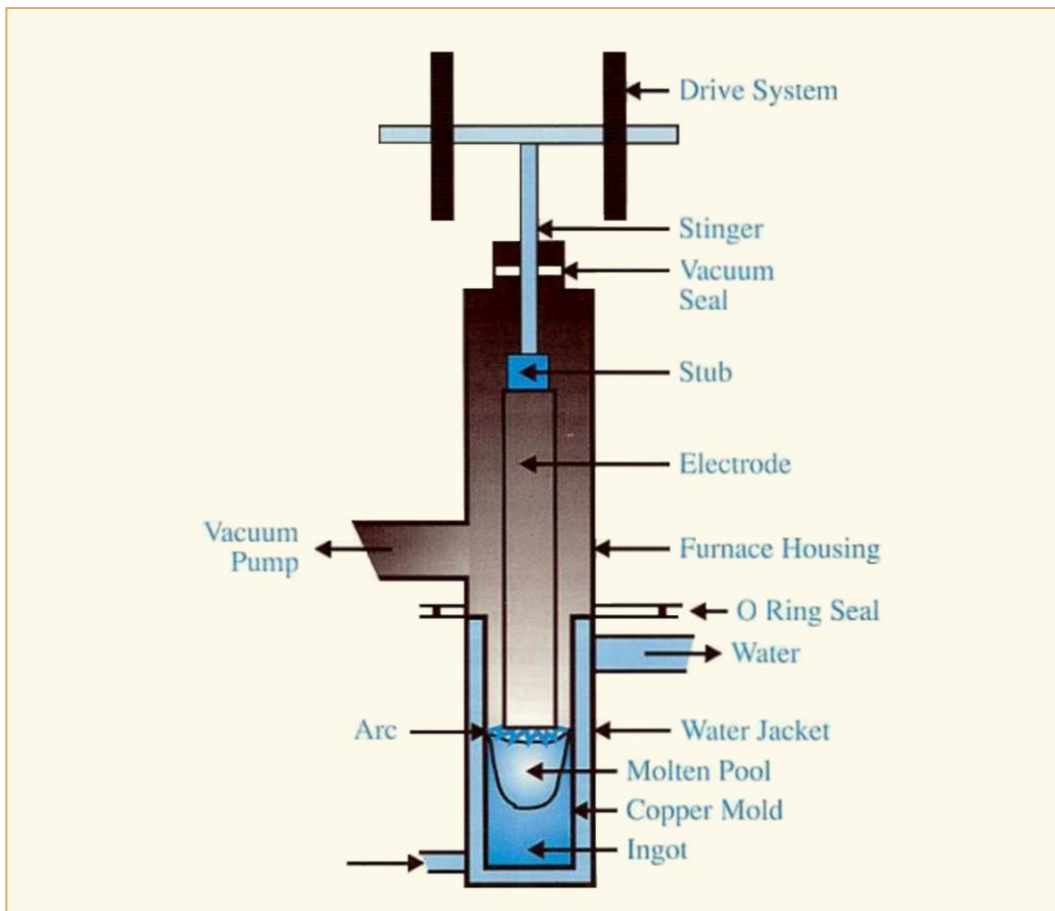


Figure 3-1: Melting zirconium alloys by consumable electrode process in a vacuum [Schemel, 1989].

The ingot is cut into smaller lengths to ease handling. Then hot deformation, for example forging, is used to refine the as-cast microstructure of zirconium alloy ingots and to achieve shape control. This dual function requires balancing processing conditions to achieve an intermediate shape and size while reducing grain size and improving microstructural homogeneity. The refinement of microstructure exploits dynamic recrystallization (DRX) in which grain nucleation and growth are simultaneous. DRX is a beneficial process in hot deformation since it not only gives stable flow and good workability to zirconium by simultaneously softening it, but also refines the as-cast microstructure. DRX breaks down the as-cast microstructure to produce a wrought (equiaxed  $\alpha$  or  $\alpha+\beta$ ) microstructure. Figure 3-2 illustrates a typical recrystallized microstructure for Zircaloy-2.

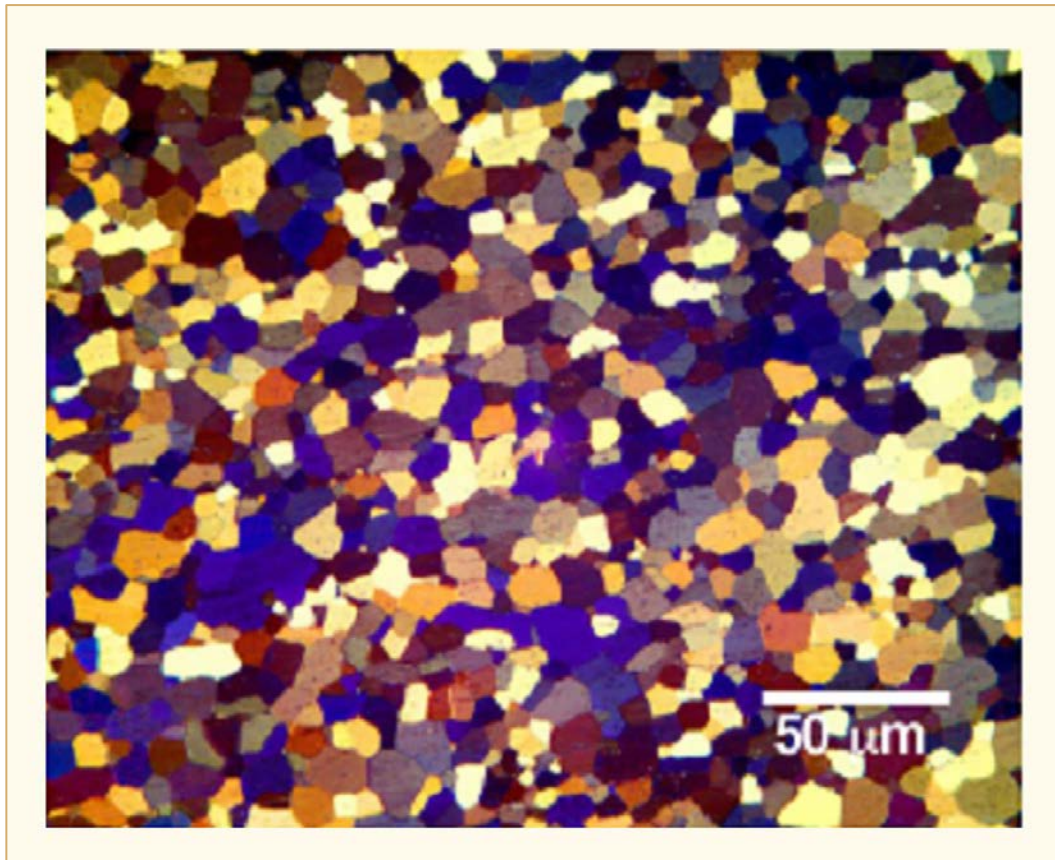


Figure 3-2: Recrystallized grains in Zircaloy-2.

The dynamic recrystallization domain is in the temperature range of 730–870 °C and at intermediate strain rates  $0.1\text{--}1\text{ s}^{-1}$  for zirconium alloys. Conventional open-die press forging is typically carried out in the strain rate-temperature domain of dynamic recrystallization.

Depending on the fabricator, at some intermediate stage the pre-component is heated into the  $\beta$ -phase, above 1000 °C, then cooled rapidly by quenching into water. The purpose of this  $\beta$ -quenching is to refine the size of intermetallic particles during aging at modest temperatures; the slow cooling from high temperature in the early stages of fabrication produces large particles, mostly along grain boundaries. This microstructure provides material with poor corrosion resistance and mechanical properties. Subsequent reductions towards the final dimensions of a component are attained by several processes including hot extrusion, hot and cold rolling, pilgering and drawing. Intermediate heat-treatments allow much further deformation and control microstructure and strength. Sheets or plates are made by rolling while tubes start off by piercing or machining a central hole in a cylindrical billet.

With mainly  $\alpha$ -alloys, after final forging to a log about 180 mm in diameter, for a typical cladding the billet is carefully machined to control straightness, wall thickness and concentricity then extruded at  $700 \pm 50\text{ °C}$  to form an extrusion hollow. The process is shown schematically in Figure 3-3.

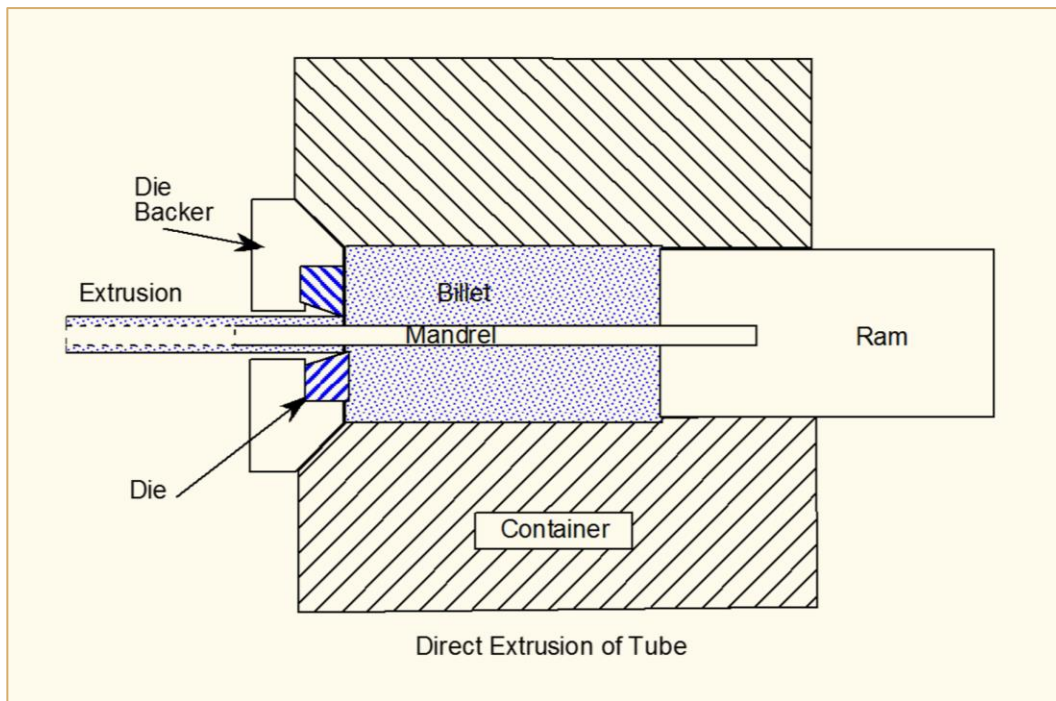


Figure 3-3: Schematic diagram of direct extrusion to form a hollow for cold-working [Dieter, 1988].

The microstructure, importantly including crystallographic texture, is controlled by the extrusion ratio, the starting cross-sectional area/cross-sectional area of the final extrusion. Texture is often characterised by the distribution of the basal plane of the zirconium hexagonal crystals and expressed as a pole figure or by Kearns' factors,  $f$  [Kearns, 1965] using the component's principal directions for reference, for example, radial  $f_R$ , transverse  $f_T$  and axial  $f_A$ . After extrusion the basal poles tend to be half way between the radial and transverse directions of the hollow,  $f_R$  and  $f_T$  about 0.45 with very few in the axial direction,  $f_A$  of 0.06. Subsequent cold-working is by pilgering.

Pilgering, Figure 3-4, is a cold working operation where the outside diameter, inside diameter and wall thickness of tubes are simultaneously reduced over a short working length under a pair of dies with almost semi-circular tapered grooves cut on them. The groove shape provides the reduction of the outside diameter from the incoming tube-shell to the finished tube. A tapered mandrel, matching the contour of the dies, is placed centrally between the grooves, which in turn determines the wall thickness of the reduced tube along the working length. Large amounts of cold work can be imparted in the process of cold pilgering by this application of large biaxial compressive stresses. During pilgering the ring dies rotate back and forward and reduce the tube, analogous to a rolling pin preparing pastry. At the end of each stroke the work-piece advances and rotates. The forming process often requires more than ten small steps of feeding and rotation to attain the full reduction in area, and it is the large number of small steps that ensures a constant wall thickness and homogeneous microstructure. A typical final texture is  $f_R = 0.64$ ,  $f_T = 0.31$  and  $f_A = 0.05$ . For zirconium alloys, pilgering is the main cold-working process used for fuel cladding, and some pressure and calandria tubes, indicating its flexibility and range of application.



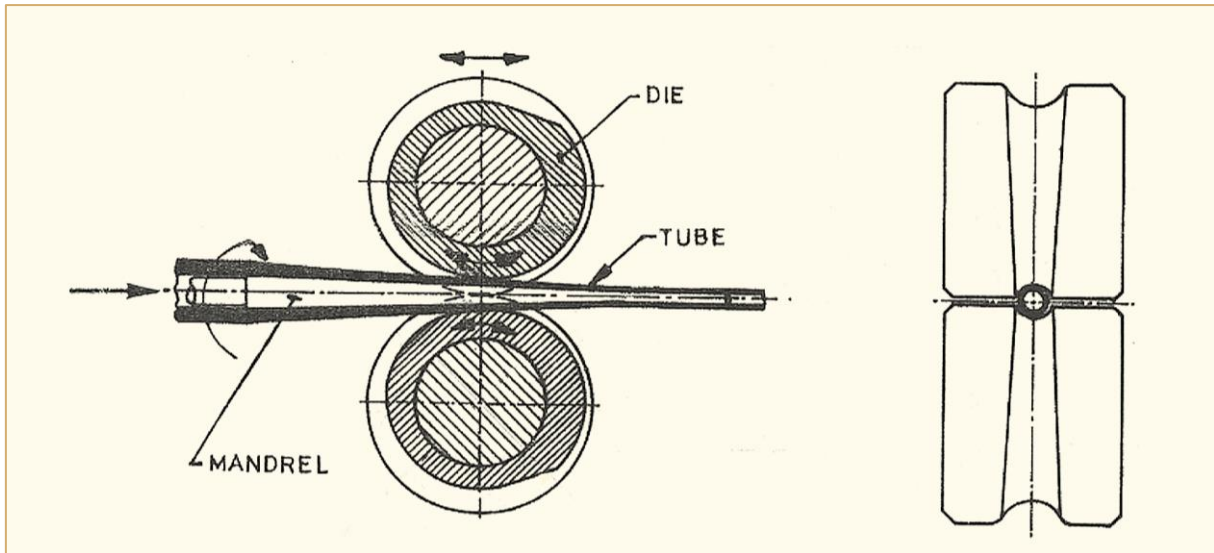


Figure 3-4: Schematic diagram illustrating the pilgering process.

The  $Q$ -factor is defined as the ratio of percentage wall thickness reduction to percentage diameter reduction and influences the final crystallographic texture of the finished product, Figure 3-5. It is generally necessary to maintain a high ' $Q$ ' (not less than 1.05), particularly during the final cold pilger pass in the fabrication of anisotropic materials like zirconium alloys. In all cases,  $Q > 1$  is beneficial to reduce the propensity for inside surface cracking.

At the end of each deformation step the tube is annealed to reduce its strength and increase its ductility as well as providing a precipitate distribution that ensures good corrosion resistance. Parameter,  $A$ , based on the dependence of the annealing temperature,  $T$ , on the amount of recrystallization in a given time,  $t$ , is given by [Steinberg et al., 1984]:

Equation 3-1: 
$$A = t \cdot \exp[-Q/(R \cdot T)]$$

where  $Q$  equals the activation energy for the process  
 $R$  equals the Gas Constant.

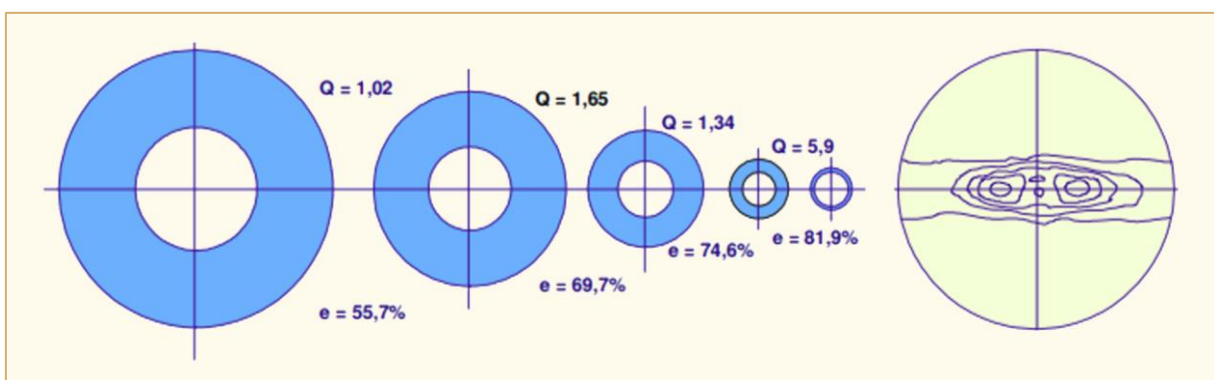


Figure 3-5: Typical sequence of % reductions,  $e$ , and  $Q$  values at various stages of pilgering resulting in tight distributions of  $\langle 0002 \rangle$  [Perez and Reschke, 1993].

The measure of recrystallization for any starting metallurgical condition can then be plotted against  $A$  for several combinations of annealing time and temperature on a single curve. As an example, Figure 3-6 depicts as a function of  $A$  the change in the yield strength at 400 °C of Zircaloy-4 cold-worked 63.4%.

## 5 Dimensional Stability (M. Griffiths and R. Adamson)

### 5.1 Part I – Experimental and Operational Data

#### 5.1.1 Introduction

Dimensional stability of the core components of a nuclear reactor is critical to safe and efficient operation. Primary structural materials are Zr-based alloys, originally chosen because of a low capture cross-section for thermal neutrons and adequate strength and corrosion resistance in about  $300\text{ }^{\circ}\text{C} \pm 50\text{ }^{\circ}\text{C}$  ( $573 \pm 50\text{ K}$ ) water; consequentially this review will be mostly limited to this temperature range. Although it was known that materials in general deformed under the influence of stress, at the time of first use (about 1955), almost nothing was known about the dimensional stability of zirconium, in-or-out of a radiation field. Another unknown was the influence on all the properties of the anisotropy induced by the hexagonal close packed (HCP) structure of Zr. Even at the time of the successful demonstrations of the Naval Reactor prototype core (Mark, I, 1953) using un-alloyed Zr, and the Nautilus submarine core (1955) [Lustman, 1979; Rickover, 2010] using Zircaloy-2, almost nothing was known about the topics of this review – irradiation growth (henceforth called “growth”) and irradiation creep (henceforth called “creep”) of zirconium alloys.

Irradiation growth is a change in the dimensions of a zirconium alloy reactor component even though the applied stress is nominally zero. It is considered to be a constant volume process, so if there is, for example, an increase in the length of a component, the width, or thickness, or both, must decrease to maintain constant volume. Understanding of the detailed mechanism is still evolving, see Section 5.2; however, a clear correlation of growth to microstructure evolution exists, and many empirical observations have revealed key mechanistic aspects. The inherent anisotropy of the Zr crystallographic structure and the texture induced during fabrication play strong roles in the mechanism, as materials with isotropic crystallographic structure (like stainless steel, copper, Inconel) do not undergo irradiation growth. Growth is not to be confused with irradiation swelling (primarily induced by microscopic voids or gas bubbles in the matrix,) which does not conserve volume and does not occur in zirconium alloys under normal reactor operating conditions.

Creep is defined as a time dependent change in dimension of a reactor component (or any material) under a stress. Creep is deformation occurring as a constant volume process, normally at low stresses below the usual yield strength, which is usually measured at strain rates  $10^6$  to  $10^7$  times greater than creep rates [ASTM Standard E6]. During normal reactor operation, failure of components by creep rupture is unlikely because large safety margins are included by design. For pressure bearing structures, specifications usually require that the material has a certain strength that is several times that of the design stress. For example, pressure-retaining components may follow the principles of Section III of the American Society of Mechanical Engineers (ASME) Boiler and Pressure Vessel Code; at the maximum operating temperature the imposed stress must not exceed the lowest of:

- 1/3 of the ultimate tensile strength (UTS),
- 2/3 of the yield strength,
- 3/5 of the stress to produce rupture within 100 000 hours, or
- the stress to provide a creep rate of  $10^{-7}$  per hour. The creep strain is sometimes restricted to 1%.

As with the early applications of Zircaloy-2, this code was applied to components before information on in-reactor effects were known.

For materials in an irradiation field, the most important for purposes of ZIRAT 23 being the neutron environment of a nuclear reactor. The deformation occurs by the motion of dislocations and irradiation-produced defects under the influence of stress. Neutron irradiation produces large quantities of point defects – vacancies (V) and self-interstitial atoms (SIA) – that migrate to and collect at various sinks. Due to the anisotropy of the zirconium crystal lattice, motion of both dislocations and

irradiation-produced defects is anisotropic, with SIAs preferring to diffuse parallel to the basal plane in the  $\langle a \rangle$  directions of the lattice and V more randomly. Dislocations are sinks for both vacancies and SIAs, but an edge dislocation attracts SIAs more than vacancies. In addition, an important factor is the concept that anisotropic diffusion is enhanced by stress. Many mechanisms of irradiation creep have been proposed, as discussed in detail later in this AR section.

Irradiation creep is distinguishable from creep without irradiation in the shape of the creep curve: at moderate temperatures e.g. 300 °C, after a small amount of strain with no irradiation the strain rate declines rapidly while during irradiation the strain rate does not decline and, after the same time, can appear to be much larger than that with no irradiation.

Growth occurs simultaneously with creep if there is an applied stress, as is almost always the case with any reactor component. The two processes are often assumed to be independent and additive, even though mechanistically they compete for the same radiation-produced defects. The subject of “independency” is examined in detail in Part 2 of this AR report.

Design and operational issues can arise when allowances for dimensional change are insufficient or not possible because of the component’s configuration; for example, BWR channels or PWR guide tubes that are subjected to large gradients in neutron fluence, may result in gradients in creep and growth. BWR flow channels are susceptible to bowing that may restrict control blade motion, an issue described in detail by [Garzarolli et al., 2011], [Mahmood et al., 2011] and [Franklin and Adamson, 1988]. Issues can also arise when growth or creep allowances depend on the behaviour of different materials, or components that operate at different temperatures, or neutron flux or both. For example, pressure tubes in CANDU reactors operate for decades rather than years and have gradients of temperature, flux and microstructure along their lengths of 6 m. In CANDU reactors, axial and differential axial elongation may cause interference between fuel channel components, as described by [Field, 1988].

Schematic diagrams of two types of fuel assemblies are given in Figure 5-1. One of the distinguishing features is the bundle length: about 4 m for PWR/BWR and about 0.5 m for CANDU.



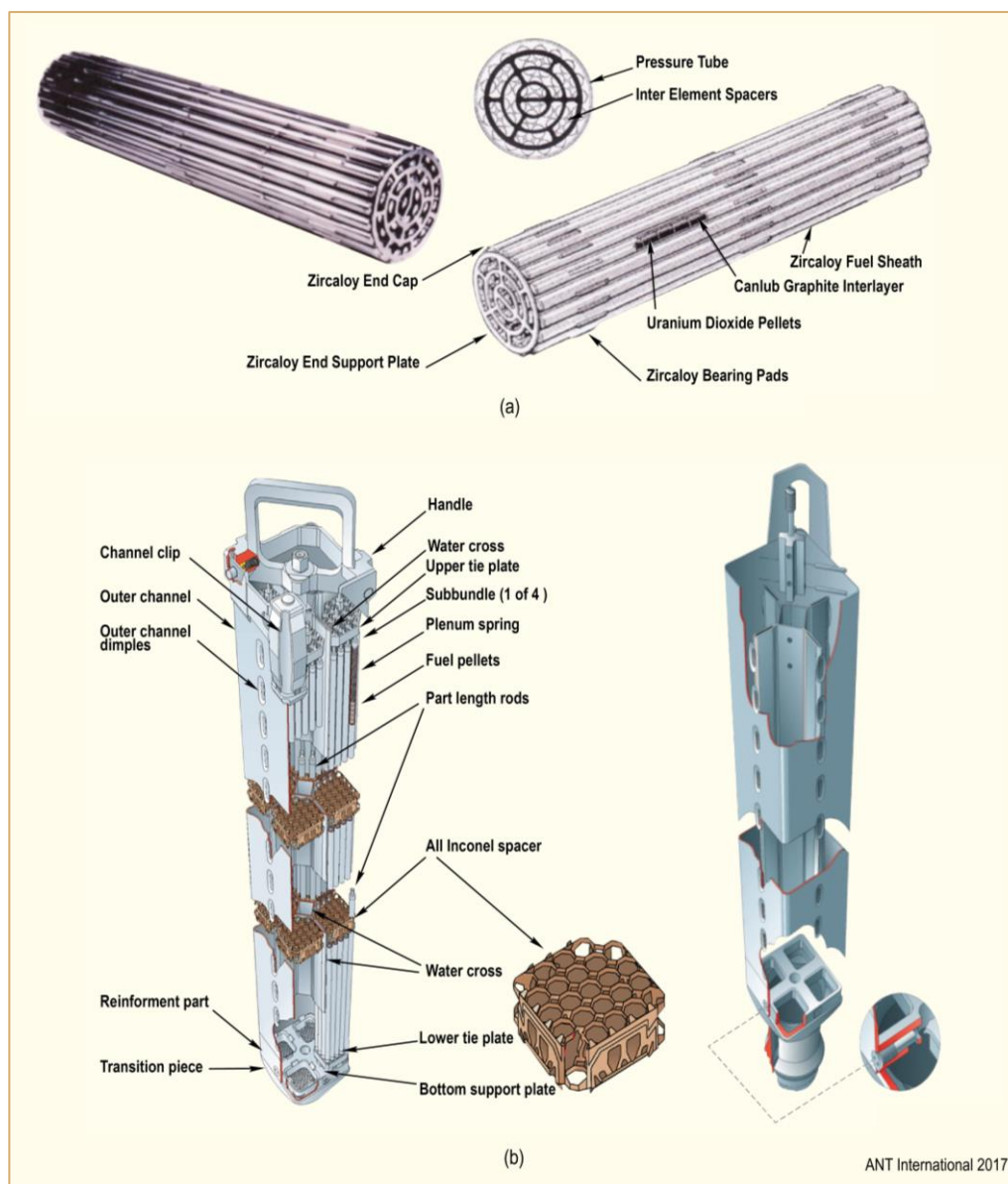


Figure 5-1: Typical fuel assemblies (a) CANDU; (b) BWR.

### 5.1.2 Measure of Radiation Damage to Zirconium Alloy Microstructure

Most of the “irradiation damage” in-reactor components is caused by neutrons. The energy of neutrons produced by fission ranges up to about 10 MeV. Common terms for energy ranges are: thermal (up to 0.03 eV), epithermal (up to 100 eV) and fast (> about 0.1 MeV, although often classed as >1.0 MeV). The amount of energy required to displace an atom of Zr from its normal lattice position is about 40 eV, and from straight forward energy transfer theory (see, for example [Norgett et al., 1975]) it is seen that any “fast” neutron can easily transfer enough energy to displace a Zr atom (the “primary knock-on”), which in turn can displace additional atoms. For purposes of this review, the immediate results are small clusters of vacancies (depleted zones), individual vacancies, individual interstitials<sup>20</sup> (although interstitials are often thought to cluster in pairs) and, after some short time (<

<sup>20</sup> “Interstitials” are often be called SIAs (self-interstitial atoms) to distinguish them from impurities or alloying elements that occupy interstitial lattice sites, for example, hydrogen, oxygen, nitrogen and carbon.

$10^{-10}$  seconds), vacancy and interstitial dislocation loops form. Collectively this rearrangement of the crystal lattice is termed “irradiation damage”. Only 1-10% of the individual defects survive their original creation.

The absolute amount of irradiation damage produced in a reactor component depends on the neutron energy spectra within a specific reactor. The energy spectra vary with reactor type, and for the location within the reactor. Typical pressurized (PWR/VVER) and boiling (BWR) water reactors have similar energy spectra, but in a BWR they vary along the core length depending on local void fraction. CANDU reactors differ from both PWR and BWRs, and test reactors (particularly fast or sodium cooled reactors) can have quite different neutron energy spectra across their volume. Therefore, it is useful to use a parameter more closely related to “irradiation damage” than the conventional fluence,  $n/m^2$ ,  $>1$  MeV or  $>0.1$  MeV. If the complete energy spectrum is considered and a consistent estimate of the energy needed to “knock” an atom from its normal lattice position is used (40 eV is standard, but 25 eV is sometimes used), it is helpful to use displacement per atom, dpa, as a measure of irradiation damage. Dpa refers to the average number of times an individual atom is displaced from its normal lattice position during a given reactor exposure.

Reactor engineers frequently use a measure of radiation damage or component exposure called fuel burnup, usually expressed as:

$$\text{Burnup} \equiv \text{GWd/MT or MWd/kgU}$$

Burnup is a measure of the amount of energy produced by fission in a given amount of fuel. The conversion of burnup to neutron fluence is complex, depending on neutron energy spectrum, fuel enrichment, void fraction, and other factors. But for a rule of thumb for a PWR it is close to:

$$50 \text{ GWd/MT} \approx 1 \times 10^{26} \text{ n/m}^2 \text{ (E>1 MeV)} \approx 15 \text{ dpa}$$

Conversion factors have been calculated by [Walters et al., 2018]. An abbreviated conversion chart, (in this case for neutron energies  $>1$  MeV, but also available for  $E>0.1$  MeV in Walters et al.) is given in Table 5-1.

Table 5-1: Comparison of Radiation Damage for Zirconium in Different Reactors for  $E > 1$  MeV [Walters et al., 2018].

Neutron Fluence, $10^{24}/m^2$ , $E > 1$ MeV	
Reactor	per 1 dpa
CANDU (pressure tube)	5.8
BWR core	6.2
PWR core	6.5
ATR	7.0
DIDO	5.9
BOR-60 (6th row)	4.9
OSIR15	6.5
EBR2	3.2
Halden 13 w/o booster fuel	5.6
NRU (fast neutron rod)	6.1
HFIR (peripheral target)	6.6
HFIR (removable Beryllium)	6.0
SM2 (C4W)	5.8
RBMK (site 33, H = 1.9m)	5.1
© ANT International 2017	

Typical damage rates for different types of reactors are given in Table 5-2. Irradiation damage accumulates, therefore, over different times in different reactors.

Table 5-2: Approximate typical damage rates for different types of reactors.

Reactor	Peak neutron flux, $n/m^2/s$ $E > 1\text{MeV}$	Damage rates dpa/s
BOR-60	$4.3 \times 10^{17}$	$8.9 \times 10^{-7}$
BWR	$6.0 \times 10^{17}$	$1.0 \times 10^{-7}$
PWR	$8.1 \times 10^{17}$	$1.3 \times 10^{-7}$
CANDU	$4.0 \times 10^{17}$	$6.4 \times 10^{-8}$
© ANT International 2018		

### 5.1.3 Previous Creep and Growth Reviews

Very little information on irradiation creep of zirconium alloys was known before the start-up of the Nautilus in 1955, the first power reactor, Shippingport, in 1957 and the first commercial power reactors in the early 1960s. The first comprehensive review of creep data was by [Fidleris, 1968] and more followed regularly, as listed in Table 5-3. In addition to the reviews listed in Table 5-3, three major conferences were held to discuss only irradiation growth and creep:

- M.R. Cundy, P. von der Hardt and R.H. Loelgen, Proceedings of International Conference on Measurement of Irradiation-Enhanced Creep in Nuclear Materials, Petten 1976 May (also Journal of Nuclear Materials, 65 [1977]).
- G.J.C. Carpenter, C.E. Coleman, S.R. MacEwen, "Proceedings of the International Conference on Fundamental Mechanisms of Radiation Induced Creep and Growth, Chalk River, May 8-10, 1979 (also Journal of Nuclear Materials 90 [1980]).
- C.H. Woo and R.J. McElroy, Proceedings of the International Conference on Fundamental Mechanisms of Radiation-Induced Creep and Growth, Hecla Island, Manitoba, Canada, June 22-25, 1987. (Also, Journal of Nuclear Materials 159 [1988]).

Other reviews of irradiation creep and growth are given in Table 5-3.

Table 5-3: Significant reviews of creep and growth.

Year	Author
1968	Fidleris
1975	Rickover
1975	Fidleris
1975	Lustman
1980	Carpenter, Coleman and MacEwen
1983	Franklin, Lucas and Bement
1987	Nichols
1988	Woo and Carpenter
1988	Fidleris
1996a	Garzarolli, Stehle and Steinberg
2000	Adamson
2008	Holt
2009	Griffiths
2009a	Adamson, Garzarolli and Patterson
2010	Adamson
2010	Shishov
2010	Cheadle
2017	Adamson, Griffiths and Patterson
2019	Adamson, Griffiths and Coleman
© ANT International 2018	

Both creep and growth are influenced by the many variables listed in Table 5-4. The large number of parameters is a reminder about why it is difficult to predict strain magnitudes during in-reactor service.

## 6 Corrosion and Hydriding (F. Garzarolli and C. Lemaignan)

### 6.1 Out-of-pile Corrosion and HPU (Friedrich Garzarolli)

Zirconium and its alloys are highly reactive metals and in oxygen containing atmospheres always have at least a thin oxide film on their surfaces. At intermediate temperatures, at  $>200\text{ }^{\circ}\text{C}$ , the oxide grows by oxygen diffusion through the oxide layer to the metal oxide/metal (M/O) interface by migration of oxide ions into the metal, increasing the oxygen content of the Zr metal at the M/O interface and if the O content exceeds the solubility limit by formation of  $\text{ZrO}_2$ . For the selection of alloy elements in early days and partially also today out reactor corrosion tests were applied. As corrosion environment oxygen,  $\text{CO}_2$ , pressurized water, steam, or supercritical water have been used. For tests in water and steam the oxygen content, hydrogen content and potential additions of boric acid,  $\text{LiOH}$ ,  $\text{H}_2\text{S}$ , etc. are important issue.

The corrosion behaviour of the Zr alloy depends on (1<sup>st</sup>) the alloying (Sn, Nb, Fe, Cr, V, etc.), (2<sup>nd</sup>) the impurity (N, C, Si, Al, etc.) content, and (3<sup>rd</sup>) the material condition (annealing temperatures (SPP size), final condition (final cold work, final anneal, and grain size), but (4<sup>th</sup>) also on the corrosion environment.

The present conclusions on the effect of alloying elements on Zr-alloy corrosion are:

- Sn, being dissolved in the metal, decreases the sensitivity against impurities in the alloy (e.g. N), and the coolant (e.g. Li) but increases the corrosion in oxygen-free water and steam.
- Nb, being dissolved up to 0.5% and forming second phase particles (SPP) at higher concentration, reduces the corrosion significantly in oxygen-free water and steam, depending on the final annealing temperature, but increases corrosion in oxygen containing water and steam. Addition of Sn increases the corrosion rate in oxygen free water but decreases the sensitivity against oxygen in the water significantly.
- Fe, Cr, and V, having a very low solubility in Zr and exist as SPP with a size and distribution depending on fabrication temperatures, improve the corrosion depending on the SPP size. In oxygen free  $\leq 370\text{ }^{\circ}\text{C}$  water and  $400\text{ }^{\circ}\text{C}$  steam an increased corrosion occurs if the average SPP size is  $<80\text{ nm}$ , and in oxygen free  $480\text{--}540\text{ }^{\circ}\text{C}$  high pressure steam nodular corrosion occurs if the average SPP size is  $>100\text{ nm}$ .
- In water with a high  $\text{LiOH}$  content Zr alloys showed a significant reduction of the corrosion at a high Sn, a medium Sn + high Fe+Cr+V, or a medium Sn + Nb content.

The hydrogen pickup (HPU) examinations during corrosion showed a low hydrogen pick up fraction (HPUF) at high Sn, in case of Nb containing alloys, and in high Zircaloy type alloys with a high Cr content.

*In the Journal of Nuclear Material, Corrosion Science and other journals some papers were reported in 2016-2018 dealing with out reactor the corrosion of Zr alloys.*

[Zhang et al., 2016] reported on Chinese studies on the effect of Ge additions (soluble in Zr up to  $<0.01\%$ ) to  $\text{Zr1Nb}$  on out of pile corrosion (deionized water at  $360\text{ }^{\circ}\text{C}/18.6\text{ MPa}$ ). The results are shown in Figure 6-1.  $\text{Zr-1Nb}$  shows the worst corrosion.  $0.05\text{--}0.2\%$  Ge addition can improve the corrosion resistance. The  $\text{Zr-1Nb-0.05Ge}$  alloy shows the highest corrosion resistance. A similar benefit of Ge was previously observed for  $\text{Zr0.7Sn0.35Nb0.3Fe}$  with 0, 0.05, 0.1, and 0.2% Ge on corrosion in  $360\text{ }^{\circ}\text{C}$  water with 0.01 mol  $\text{LiOH}$ .

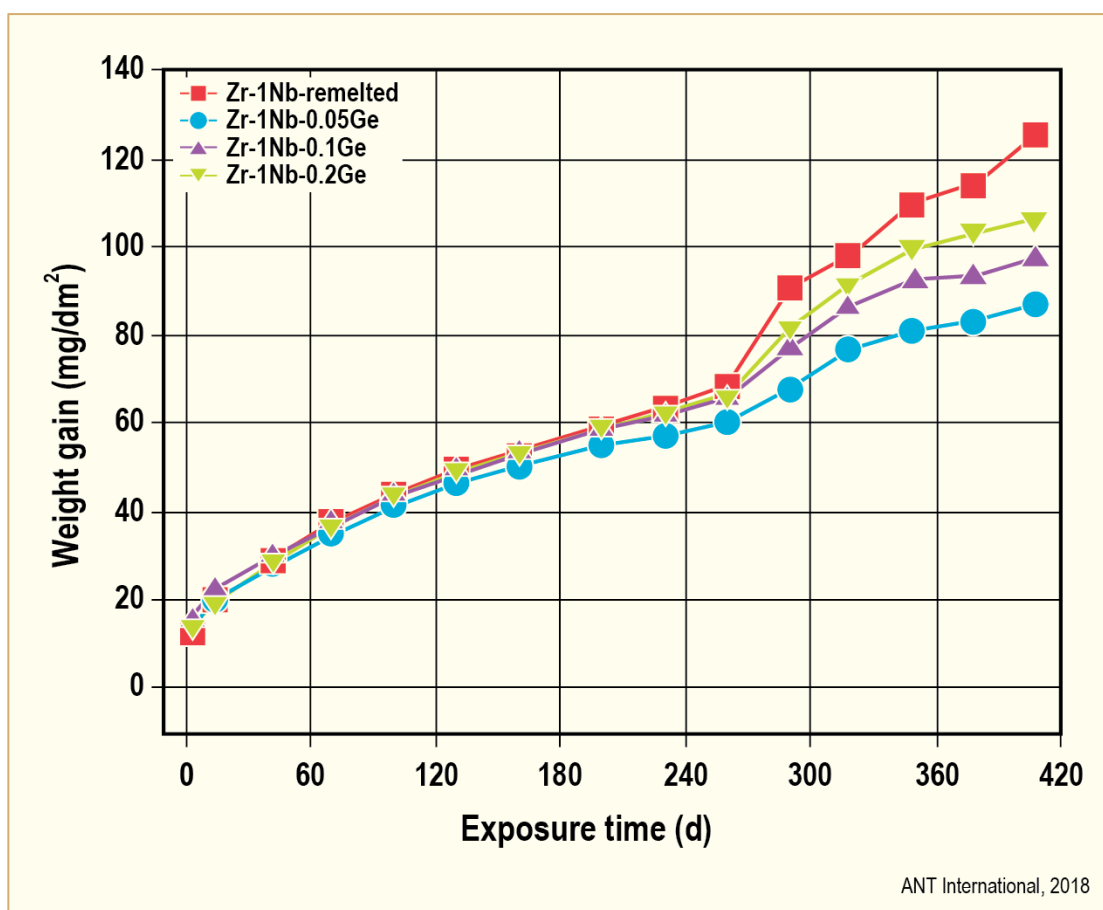


Figure 6-1: Weight gain vs. exposure time for Zr-1Nb-xGe alloys corroded in deionized water at 360 °C [Zhang et al., 2016].

[Bell et al., 2016] investigated the influence of Sb, Sn, Sb, and Nb on the corrosion and hydrogen pick-up (HPU) in deionized water at 360 °C. Sc is fully dissolved, Sb and Sn have a solubility of >1-2% and Nb of ~0.5%. The corrosion results of the tested alloys are shown in Table 6-1. Alloys with 0.5Nb and 0.2-0.3Sc have an extremely high corrosion, alloy 4, a Zr-alloy with 0.25% Sb shows a very high corrosion, but alloy 3 (Zr0.5Nb0.1Sb) shows a significantly lower corrosion and HPU as alloy 5 (Zr0.5Nb).

Table 6-1: Weight gain and HPU after max. exposure in deionized water at 360 °C.

Alloy	Weight gain at 360°C	Transition at	HPU
(3) Zr0.5Nb0.1Sb	38 mg/dm <sup>2</sup> after 210 d	>210 d	6 ppm after 195 d
(5) Zr0.5Nb	48 mg/dm <sup>2</sup> after 210 d	>210 d	22 ppm after 195 d
ZIRLO	77 mg/dm <sup>2</sup> after 210 d	100 d	96 ppm after 195 d
(4) Zr0.2Sb	515 m/dm <sup>2</sup> after 105 d	30 d	
(1) Zr0.5Nb0.2Sc	Extremely fast corrosion		
(2) Zr0.5Nb0.3Sc	Extremely fast corrosion		

© ANT International 2018

From the published reports it can be concluded, that ZrNb alloys are sensitive against oxygen and LiOH in the coolant. Fe additions do not reduce the corrosion significantly, only Cu was found to have a positive effect, but obviously additions of  $\leq 0.1\%$  Ge or  $\sim 0.2\%$  Sb have also a significant positive effect.

[Garner et al., 2015] reported on a detailed study of the texture and microstructure of oxides formed on two Zr alloys which exhibit different corrosion behaviour (high corrosion and HPUF of Zr1Sn1Nb0.1Fe and low of Zr1Nb0.1Fe) to investigate the effect of the removal of Sn on oxide texture formation during aqueous corrosion. The following conclusions are made:

- The removal of Sn leads to a delayed transition in the corrosion kinetics ( $\sim 200$  days) and a reduction in hydrogen pickup.
- The average columnar grain width and length is larger in the oxide layer on Zr1Nb0.1Fe and is also more ordered.
- A higher tetragonal phase fraction is observed in oxide formed on Zr1Sn1Nb0.1Fe, probably because Sn stabilizes the tetragonal oxide (Figure 6-2).
- There is more lateral cracking in the oxide formed on Zr1Sn1Nb0.1Fe (Figure 6-3), what the authors attributed to the effect of Sn on the mechanical properties of the substrate and its influence on the formation of undulations in the metal-oxide interface.
- It is concluded that the improved corrosion performance of Zr1Nb0.1Fe is due to the reduced stabilization of tetragonal grains in the absence of Sn, resulting in the formation of larger, well-oriented columnar grains and less transformation and consequently a delayed transition.

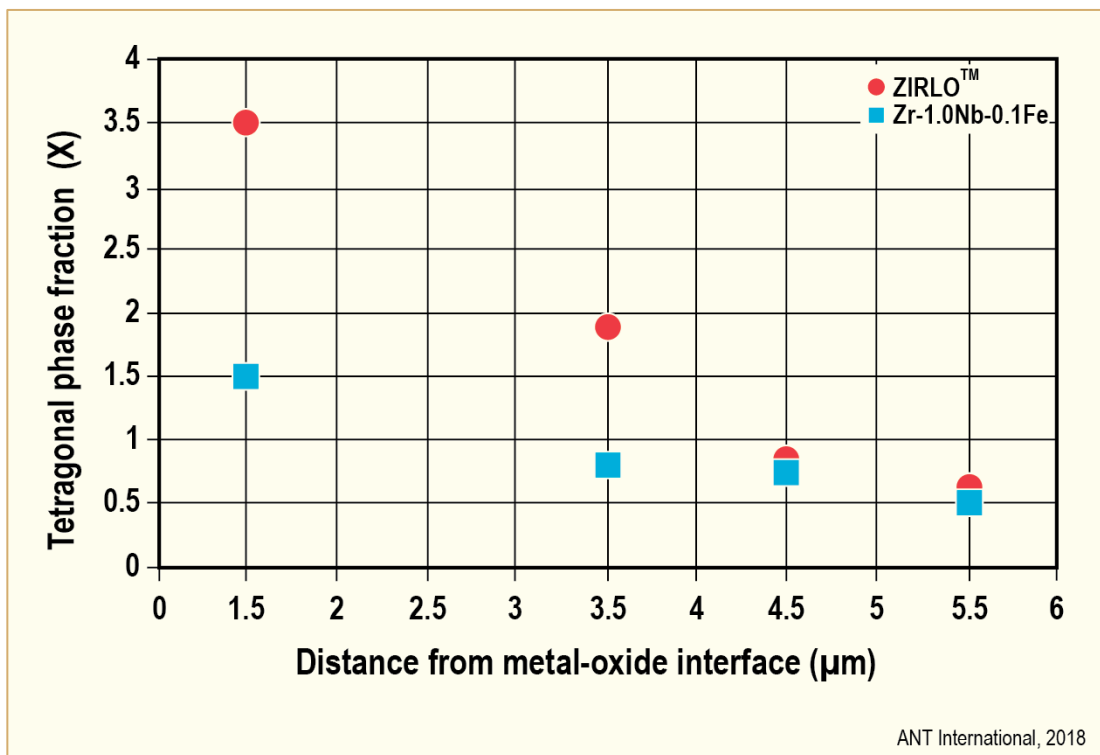


Figure 6-2: Tetragonal phase fraction of Zr1Sn1Nb0.1Fe and Zr1Nb0.1Fe as function of distance from the metal-oxide interface [Garner et al., 2015].



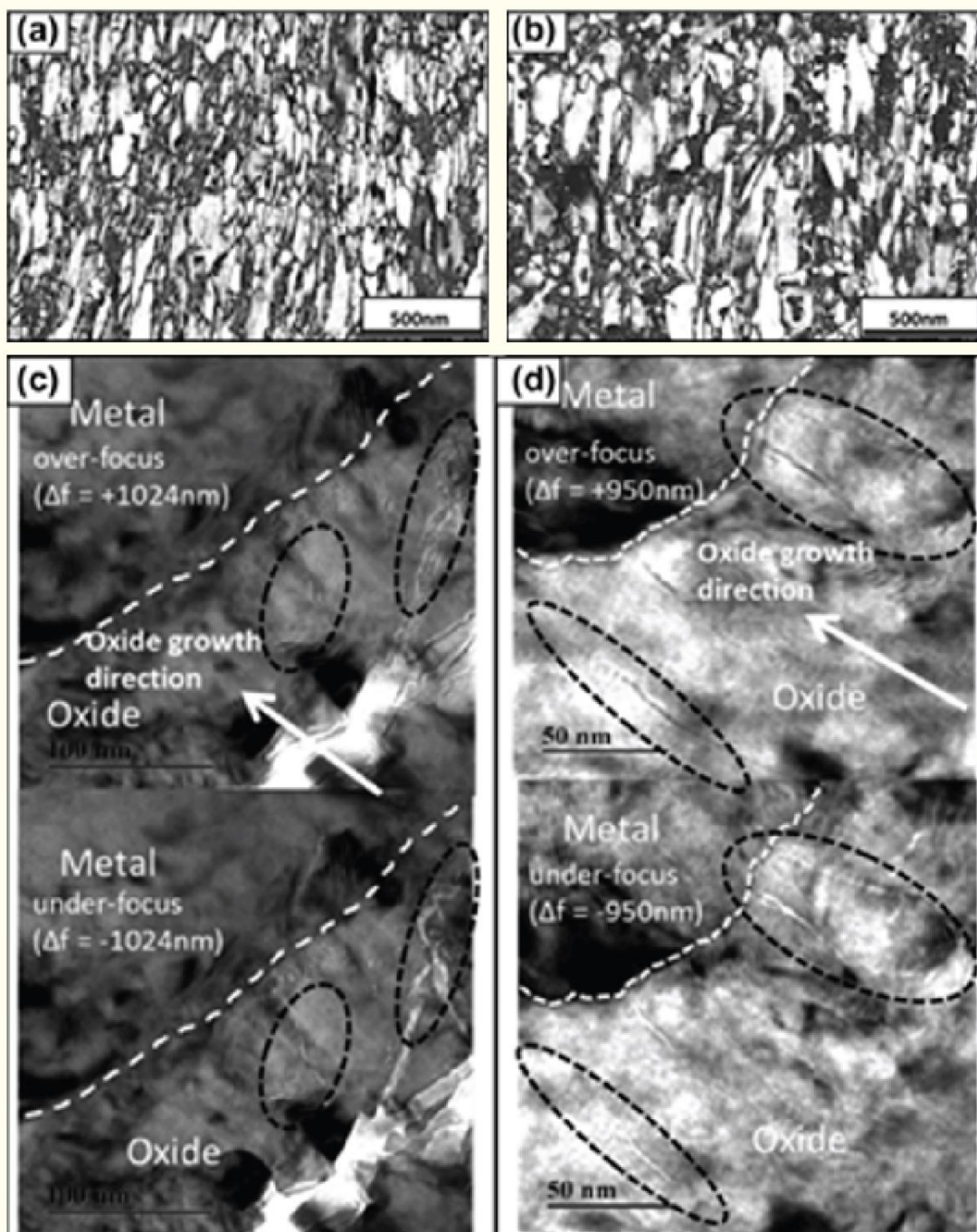


Figure 6-3: Monoclinic orientation reliability maps from columnar grain region of oxide formed on (a) Zr1Sn1Nb0.1Fe and (b) Zr1Nb0.1Fe. Image of fine pores (circled) at the metal-oxide interface from the oxide on (c) Zr1Sn1Nb0.1Fe and (d) Zr1.0Nb0.1Fe. [Garner et al., 2015].



## 6.2 Corrosion in PWR and VVER (Friedrich Garzarolli)

There are two *different types of reactors operating under hydrogenated coolant* conditions:

1. The Pressurized-Water Power Reactors (Closed Cycle) operates at a system pressure of 155-158 bar, with a reactor core contained in a pressure vessel through which H<sub>2</sub>O supplied by a feed pump is entering the core with a temperature of 284-294 °C. The water is heated up over the FA height to an outlet temperature of 300 °C to saturation temperature (~345 °C) and circulates to an external steam generator. The cladding surface temperature is higher than the coolant temperature and may lead to a surface boiling and in certain PWRs even to steam void formation up to 25%. The average FA discharge burnup has increased from 1980 to 2010 from ~ 30 to ~55 MWd/kgU (Figure 6-4) due to an increase of the enrichment from ~2.5 to 5%. The allowed radial peaking factor, that is limited by departure of nucleate boiling, depends on the power control which is done in case of Westinghouse type PWRs by measurements out of the pressure vessel and in case of the Siemens PWRs by measurements by measurements within the core at positions close to the peak power position, resulting in a lower uncertainty. Thus, the allowed peak power is higher in Siemens PWRs, where a void fraction up to 25% may occur, than in Westinghouse PWRs. The water chemistry is governed by addition of 2-4 ppm H<sub>2</sub> avoiding the formation of oxidative radicals and reducing the irradiation induced increase of the corrosion potential significant. However, in case of high void formation more oxidative conditions may rise in the upper FR end, which have led to an accelerated corrosion in Siemens PWRs in case of M5 claddings, which are sensitive to oxidative conditions. Such an increased corrosion at the upper end of M5-FRs were reported by e.g. [Schmidt & Hoffmann, 2007].

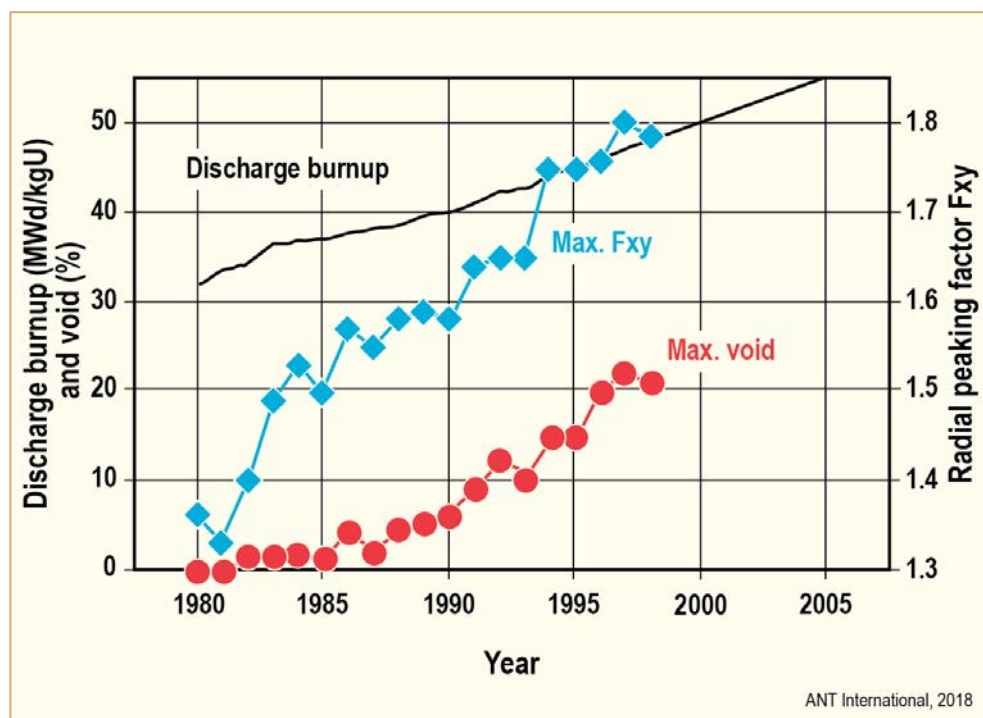


Figure 6-4: Evolution of operating conditions (discharge burnup, local power, void) for Siemens PWR fuel assemblies [Seibold et al., 2000].

2. The other reactor is the Russian VVER. Its operation conditions are similar as in PWR. However, for pH control KOH addition is used instead of LiOH addition in PWR, NH<sub>3</sub> is added to keep the H<sub>2</sub> at a similar level as in PWR, and as cladding Zr1Nb was applied from the early beginning. Today, Zr-Nb (E110) and Zr-Nb-Sn-Fe (E635) type alloys are used as fuel cladding materials.

*The state of knowledge on the more modern Zr-alloys used in PWRs is summarized in the following.*

For PWR fuel claddings Zry-4 was used in early days. In the late 1970's early 1980's corrosion induced fuel rod (FR) failures occurred in **Siemens** PWRs with experimental FRs respectively FAs with increased enrichment, e.g. [Garzarolli et al., 1985]. For estimation of the allowable burnup models were developed to predict corrosion of PWR fuel rods including the effect of irradiation which was found to become important at an oxide layer thickness of  $>5\text{ }\mu\text{m}$ , e.g. [Garzarolli et al., 1985].

In the late 1980's it became obvious, that for plants with high power density and coolant inlet temperatures even a corrosion optimized Zry-4 material has insufficient corrosion resistance, to reach the burnups envisaged shown in Figure 6-4. Therefore, several promising alternative Zr alloys were examined with test fuel rods and corrosion coupons in water rods in PWRs since 1985. The following alloying systems were tested **Siemens (today Framatome)**:

- Zr 0.2-1.2%Sn 0.1-0.7%Fe 0-0.7%Cr 0-0.3%V
- Zr 0.2-1%Nb 0.2-0.6%(Fe+Cr+V)
- Zr 0.2-1.5%Sn 0.2-3%Nb 0-1%(Fe+Cr+V)
- Zr 0.5-2.6%Nb
- Zr 0.5-1.1% (Fe+Cr+V)

Most of these tests were performed in Goesgen NPP in Switzerland under quite demanding thermal hydraulic conditions. Test fuel rods with alternative Zr alloys were irradiated for up to 9 years up to almost 100 MWd/kgU. In 1987, as consequence of the observation, that SR Zr alloys with an excellent corrosion resistance had the disadvantage of a very low creep resistance, and the prevention to modify the ASME Code yield stress licensing criteria, a DUPLEX (DX) cladding with a 100 nm thick outer layer of the corrosion resistant Zr-alloy was defined for the future commercial cladding tubes, and tested since 1988. In 1991 the first reload with **DX-ELS 0.8a** (with 0.8%Sn in the outer layer) was inserted and in 1992 the first reload with **DX-ELS0.8b** claddings (with an increased Fe and Cr content compared with Zry-4). In the late 1990s, as consequence of the further increasing enrichment, power densities, and burnup, the cladding of the reloads was changed to **DX-D4** (Zr0.5Sn0.5Fe0.2Cr), exhibiting a still higher corrosion resistance (Figure 6-5). All the applied claddings (Low-Sn-Zry-4, Opt-Zry-4, DX-ELS 0.8 and DX-D4) showed at an oxide thickness of  $\sim 30\text{ }\mu\text{m}$  a significant increase of the corrosion rate (an  $\sim 2\text{x}$  rate increase) due to the formation of a dense hydride rim. Figure 6-6 shows an example of such a dense hydride rim. Extensive examinations showed that such hydride rims forms at an av. H-content of  $>300\text{ ppm}$  in the cladding and a heat flux of  $>50\text{ W/cm}^2$ . To avoid this type of corrosion increase alloys with lower hydrogen pickup fraction (HPUF) as DX-HPA-4, DX-Zr2.5Nb and Zr1Nb, which have a significantly lower HPUF were consequently extensive tested.

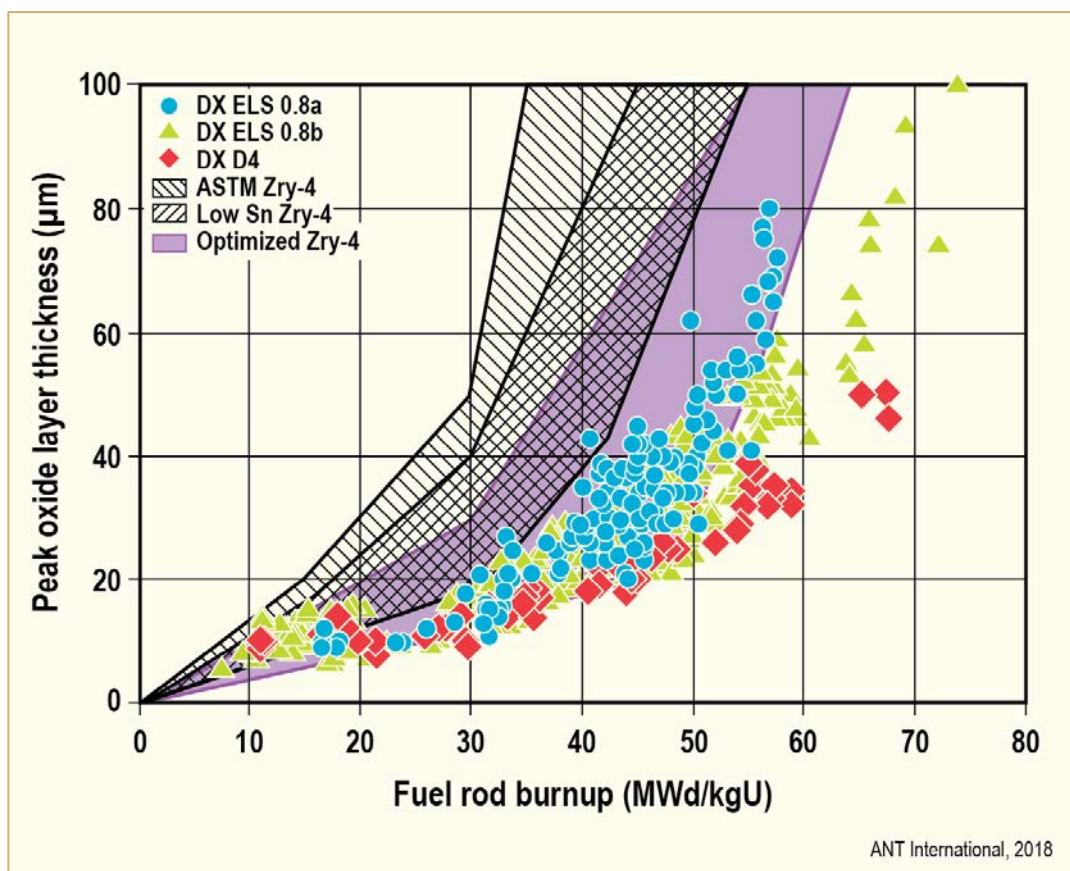


Figure 6-5: Corrosion behaviour of several DX ELS cladding materials at high heat fluxes [Garzarolli 2000].

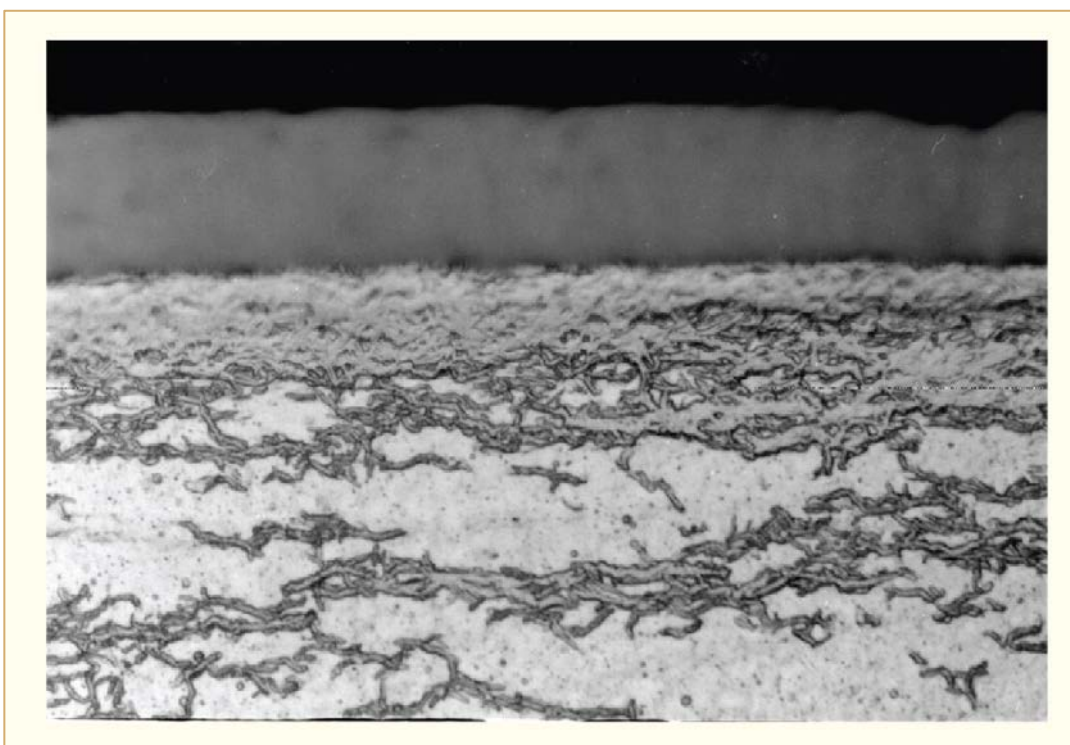


Figure 6-6: Hydride rim observed in a fuel rod cladding exposed at a high power [Garzarolli et al., 1998].

## 7 Fuel Performance and Design (P. Rudling)

The open literature data are provided in the following sections.

### 7.1 Introduction

#### 7.1.1 Primary Failures

During reactor operation, the FR may fail due to a primary cause such as fretting, PCI manufacturing defects, corrosion, etc. (Table 7-1).

Table 7-1: Primary failure causes for LWR fuel during normal operation and Anticipated Operational Occurrences (AOO).

Primary failure cause	Short description
Excessive corrosion	An accelerated corrosion process results in cladding perforation. This corrosion acceleration can be generated by e.g., CRUD deposition (CILC) <sup>a</sup> , Enhanced Spacer Shadow Corrosion, (ESSC) <sup>b</sup> , (in BWRs), dry-out due to excessive FR bowing.
Localised hydriding	Fuel may fail in hydrided regions fractured under tensile loading that arose with accumulation of exposure during the course of normal operation (BWRs) <sup>c</sup> . Li seems to be involved in the failure mechanism (It is not clear from where the Li originated since Li does not normally occur in BWR coolants). More work is needed to understand the mechanism that led to the localised hydriding.
Manufacturing defects	Non-through-wall cracks in the fuel cladding developed during the cladding manufacturing process. Defects in bottom and/or top end plug welds. Primary hydriding due to moisture in fuel pellets and or contamination of clad inner surface by moisture or organics. Too large a gap between the FR and the spacer grid supports (poor spacer grid manufacturing process) leading to excessive vibrations in PWR fuel causing fretting failures. Chipped pellets may result in PCI failures both in liner and non-liner fuel.
PCI	PCI – an iodine assisted SCC phenomenon that may result in fuel failures during rapid power increases in a FR. There are three components that must occur simultaneously to induce PCI and they are: 1) tensile stresses—induced by the power ramp, 2) access to freshly released iodine—occurs during the power ramp, provided that the fuel pellet temperature becomes large enough and 3) a sensitised material—Zircaloy is normally sensitive enough for iodine stress-corrosion cracking even in an unirradiated state.
Cladding collapse	This failure mechanism occurred due to pellet densification. This failure mode has today been eliminated by fuel design changes and improved manufacturing control.
Fretting	This failure mode has occurred due to: Debris fretting in BWR and PWR. Grid-rod fretting – Excessive vibrations in the PWR FR causing fuel failures. This situation may occur for example due to different pressure drops in adjacent FAs causing cross-flow. Baffle jetting failures in PWRs – Related to unexpectedly high coolant cross-flows close to baffle joints.
<p><sup>a</sup> CILC – an accelerated form of corrosion that has historically resulted in a large number of failures in BWRs. Three parameters are involved in this corrosion phenomenon, namely: 1) Large Cu coolant concentrations as a result of e.g., aluminium brass condenser tubes, 2) Low initial fuel rod surface heat flux – occurs in Gd rods and 3) Fuel cladding that shows large initial corrosion rates- occurs in cladding with low resistance towards nodular corrosion.</p> <p><sup>b</sup> This corrosion phenomenon resulted in a few failed rods. The mechanism is not clear but seems to be related to galvanic corrosion. This corrosion type may occur on the fuel cladding in contact or adjacent to a dissimilar material such as Inconel. Thus, this accelerated type of corrosion occurred on the fuel cladding material at spacer locations (the spacer springs in alloy BWR fuel vendors fuel are made of Inconel). Water chemistry seems also to play a role if the fuel cladding material microstructure is such that the corrosion performance is poor. Specifically coolant chemistry with low Fe/(Ni±Zn) ratio seems to be aggressive (provided that the cladding material shows poor corrosion performance. A fuel cladding material with good corrosion resistance does not result in ESSC, even in aggressive water chemistry).</p> <p><sup>c</sup> Sixty-three GE13B 9×9 fuel assemblies in Browns Ferry, Unit 2 (BF2) during Cycle 12 failed. Seven rods were examined in hot cell to determine the primary failures cause.</p>	
© ANT International, 2018	

The following table below, Table 7-2 and Table 7-3, Table 7-4 and Table 7-5 provide key data for some of the most recent fuel-failure cases.

Table 7-2: Summary of previous PWR/PHWR failure key events, see previous ZIRAT/IZNA-reports for details.

Nuclear unit	Type of primary failure	Comment
TMI-1, Cy 10, 1995	Nine high peaking FRs, Zry-4 Cladding, failed after 122 days of operation. CRUD/corrosion related failures.	All failed and degraded pins reportedly had Distinctive CRUD Pattern (DCP) <sup>21</sup> . High peaking factors, thermal-hydraulic conditions. Calculations indicated that no boiling should have occurred on the pins with DCP, although the pins with DCP were calculated to have a slightly higher temperature. Water chemistry (low pH at BOC, pH < 6.9, max LiOH 2.2 ppm). Some, AOA effect was found reaching a maximum in the middle of cycle 10. The source of the CRUD could not be determined. The CRUD sampling showed that the nickel-to iron ratio was in the range 1.25 to 16.7, which was reportedly somewhat lower than in previous investigations.
Seabrook, Cy 5, 1997	Five one-cycle ZIRLO rods failed. CRUD/corrosion related failures.	Longer cycle in transition to 24-month cycle. Possibly CRUD-induced overheating resulting in substantial nucleate boiling.
EdF data reported in 2009 [Thibault et al., 2009]	The main failure causes in the EdF plants are: GTRF wear, Clad manufacturing defects and, Excessive fuel assembly bowing (resulting in assemblies grids hanging-up during loading and unloading and IRI)	A significant number of fuel failures were related to the M5 fuel cladding in 1300 MWe and 1450 MWe units. The M5 FR failures were due to fabrication defects either related to the end plug girth or fill hole weld or defects in the fuel clad itself at grid levels (related to the pulling of the rods into the assembly structure). To resolve these manufacturing issues, AREVA has modified the welding techniques as well as the rod pulling procedure. It was observed that there were no GTRF failures in 2008 (in previous years there have always been some GTRF failures). The reasons for the great improvement is thought to be due to that both AREVA and Westinghouse have introduced reinforced FAs design (AFA3GLr – AREVA and RFA2- Westinghouse). Since the introduction of the AREVA AFA3G design in 1999, a decrease of the average core bow in EdF NPPs has been observed, especially on the 900 MW units, but not as fast as expected. The maximum values of bowing remain relatively high on the 1300 MW units, typically between 15 and 19 mm for a “S shape” bow. The Westinghouse RFA fuel design behaves in the same way with similar bowing range while HTP assembly deformations are twice less. Incomplete Rod Insertions (IRIs) due to bowing have been significantly reduced since the AFA3G FA's design has been loaded in EdF NPPs and despite the increasing of the average discharge bumup of the FAs. In 2008, no anomaly of RCCA drop time was observed in EdF NPPs during the BOC tests. Concerning the EOC tests, no anomaly was observed in the 12 feet units whereas four RCCAs dropped without recoil in the 14 feet units. Three of them was AFA3G FAs (two “2nd cycle” FAs and one “4th cycle” FA) and one was the older design (AFA2G). The number of FAs damaged during handling operations has decreased in 2008 but remains significant. The damages concern only AFA 2G or 3G design and mainly the 14 feet units. It occurs during the unloading operations. The damages generally occur during a “three-sided box” extraction and result from grids' hanging due to bowing and to a reduced gap between FAs following unexpected grid growth due to re-crystallized Zircaloy-4.

<sup>21</sup> This acronym implies that the fuel inspection revealed CRUD deposits on the fuel rod and that the deposits were uneven in the rod circumference.



Table 7-3: Summary of previous PWR/PHWR failure key events, see previous ZIRAT/IZNA-reports for details. New results added to the table from the ZIRAT 18/IZNA13 AR [Rudling P. et al., 2013] is in red text. (cont'd)

Nuclear unit	Type of primary failure	Comment
Kakrapar Atomic Power Station (KAPS) unit#2, India	Manufacturing defect	A PHWR fuel rod with an incomplete fusion end plug weld. The fuel rod operated at very low power for the first 18 months as the fuel bundle was in a peripheral location of the core during that period. For the next 5 months, the fuel pin operated at a linear power rating of 410 W/cm when the fuel bundle was shifted to a high flux location in the core. In total the rod operated in failed condition for a period of 710 days and accumulated a burnup of 4400 MWd/tU. See ZIRAT18/IZNA13 AR for more details.
Korean PWR plant, identification not known	2 debris-induced fuel failures	PWR debris-induced fuel failures on a thrice-burned fuel rod, not showing any degradation and a first-burned fuel rod, which degraded. See ZIRAT18/IZNA13 AR for more details.
© ANT International, 2018		

Table 7-4: Summary of previous BWR failure key events, see previous ZIRAT/IZNA-reports for details.

Nuclear unit	Type of primary failure	Comment
KKL	1997, 1998	Excessive Shadow Corrosion on LK II Zry-2 Cladding under the Inconel x-750 grid springs. The oxide thickness was locally above 500 µm. The most notable cladding corrosion attacks were found on fuel that had experienced a fourth, fifth, or sixth operational cycle. Zn-injection. Low level of Fe in coolant.
River Bend	Cy 8, 1999	At least 12 GE First cycle FRs were failed. Heavy CRUD – The failures appeared in bundles with a significant iron CRUD deposition. The heavy deposits almost filled the gaps between the FRs. Some 700 pounds (320 kg) iron was estimated to have been input to the River Bend-1 RPV during cycle 8 (1998-1999). CRUD deposit thickness in the range 37–55 mils (940 – 1400 µm) was reported. Analysis of the CRUD showed that the major phases were hematite and spinel, reportedly magnetite or zinc ferrite. Significant amounts of copper, up to 15% were found in some cases. No NMCA. Zn-injection.
Vermont Yankee, 2001-2002	5 FRs failed due to CRUD corrosion.	A total of 5 failed GE rods in 4 bundles were removed from the core at Vermont Yankee in a mid-cycle outage in May 2002, along with 40 other bundles deemed most at risk of failure due to being similar to the leakers in terms of duty, exposure, and tubing material.
Browns Ferry 2, Cy 12, 2001-2003	63 FAs failed due to localised massive hydriding	Affected fuel was GE13B claddings that failed in their second cycle with burnups of 29-30 MWd/kgU. Bundles that failed tended to be leading for the reload batch, indicating some impact of duty on tendency for failures. HWC started in BOC Cy 11 and NMCA at EOC 11 was implemented (3/01), Depleted Zinc Oxide (DZO) started in 1997 at 3 to 5 ppb. Maximum oxide thickness both in lower and upper part of the failed rods. Maximum CRUD deposition towards the bottom of the rods. BF2 changed out their condenser tubes to Ti-tubes 8-10 years ago. Cladding material - Corrosion behaviour was sensitive to alloying content, primarily iron and tin; - Multiple ingots were affected; - Ingots supplied by two different vendors were affected. An update of the root cause examinations of the sixty-three failed GE13B 9X9 fuel assemblies in Browns Ferry, Unit 2 (BF2) during Cycle 12 was presented. Seven rods were examined in hot cell to determine the primary failures cause. The authors, [Lutz et al., 2012] and [Lutz et al., 2013] suggest that the BF2 Reload 10 fuel failed by hydrided regions fractured under tensile loading that arose with accumulation of exposure during the course of normal operation. The results also suggest that Li contributed to the failures at least by aggravating the late stage corrosion of the BF2 Reload 10 rods, regardless of any role it may have had in initiating the corrosion. See ZIRAT18/IZNA13 AR for more details.

Table 7-5: Summary of previous BWR failure key events, see previous ZIRAT/IZNA-reports for details.

Nuclear unit	Type of primary failure	Comment
Browns Ferry 3, Cy 11, 2002-2004	3 FAs failed due to localised massive hydriding	DZO started in 1995 at 3 to 5 ppb, NMCA at EOC 9 was implemented and HWC started in BOC Cy 10, DZO went to 5 to 10 ppb after the HWC was started. Affected fuel was GE13B claddings that failed in their third cycle with burnups of 43-47 MWd/kgU. Rod oxide thickness peaked at lower and upper part of the rods but maximum oxide thickness was found in upper part of the failed rods.
River Bend, Cy 11, 2003	7 rods failed due to CRUD related corrosion.	Water chemistry apparently within specification. Cy 11 – No NMCA but HWC and Zn-injection, also high Cu coolant content was observed. First cycle fuel with burnup ranging from 14.6-19.0 MWd/kgU. Siemens ATRIUM-10 (LTP). All failed rods were on periphery in FA on bladed surfaces (high power positions). Failures and peak oxide thicknesses in span 2 (of peripheral rods) where max. CRUD deposition was noted.
Hatch 1, Cy 21, 2003	PCI related failures in five (5) liner (barrier) FRs	Five duty related FRs failed at 19 months into a 22 month cycle in one cycle GE14 barrier fuel with an estimated burnup of 26 MWd/kgU.
Fitzpatrick, 2004	PCI related failures in two (2) non-barrier fuel	Two duty related failures occurred in non-barrier GE12 assemblies late in their second cycle at a burnup of about 45 MWd/kgU.
Kuosheng 2, 2003-2004 (Cycle 16) [Chiu et al., 2009]	PCI related failures in three (3) liner (barrier) FRs suspected to be due to MPS	Duty related failures in two ATRIUM-9B fuel bundles, KAG115 and KBH069 in Cycle 16. The estimated bundle burnup of KAG115 and KBH069 was 28.87 GWd/MTU and 28.64 GWd/MTU respectively. Poolside examinations showed that both bundle had one failed rod at the F2 location. KAG115-F2 failed rod exhibited secondary degradation including a 470 mm axial crack resulting in some fuel washout. The KBH069-F2 failed rod exhibited three defects including a blister, a bulge and, a 5 mm long circumferential crack – fuel washout was noted. A similar fuel failure to those reported above occurred in Cycle 14
Several BWRs	Excessive fuel channel bowing	[Cantonwine et al., 2010] reported on the measured settle times at Monticello and Peach Bottom 3 and compared to the data collected at LaSalle 1. To quantify control rod interference, the amount of interference was calculated in two ways: A Channel Interference Metric (CIM) is defined as the total deflection of both channels toward the blade minus the available gap and the Half-Gap Channel Interference Metric (HGCIM) is defined as the total deflection of an individual channel side minus the available half gap. [Cantonwine et al., 2010] concluded that the new data fits well into the previously developed correlation (reported in ZIRAT14/IZNA9 AR [Adamson et al., 2009b]) which showed that an interference (the sum of all 4 blade wings) of <0.5 mm (20 mils) correlated to normal or near normal settling times, 0.5 to 1.0 mm (20 to 40 mils) correlated to slow or no-settle conditions and >1.0 mm would indicate a no-settle condition. The results of half gap interference (the sum of half gap interference of each channel side that faces the blade) showed that >5 mm (200 mil) half gap interference is necessary before a slow or no-settle condition occurs. Cofrentes have experience of >7 mm measured bow in one channel without friction problems in the cell [Sedano & Mata, 2011]. However friction problems can be expected for bows >5 to 6 mm based on the experience in other reactors. If the maximum fuel channel bow exceeds 4 mm there is a risk that the CR does not settle.

© ANT International, 2018

## 8 LOCA, RIA, Seismic Event (P. Rudling and C. Patterson)

### 8.1 Introduction

#### 8.1.1 Seismic Event (P. Rudling)

To assure safe operation following a seismic event, additional criteria are defined. Two levels of ground motion excitation, corresponding to two earthquake levels, are defined for safety-related structures, systems, and components in operating nuclear power plants. Compliance with specified criteria assure that plant safely is maintained following each event.

For the first-level earthquake, the Operating Basis Earthquake (OBE), the load factors and acceptable allowable stresses ensure that the stresses in plant structures remain at least 40 percent below the yield stress of the material for the event.

For the second-level earthquake, the Safe Shutdown Earthquake (SSE), whose vibratory motion is usually twice that of the OBE), the associated load factors and allowable stresses ensure that the stresses in the plant structure and assembly remain close to the yield stress of the specific materials; a small excursion in the inelastic range is allowed when the SSE load is combined with accident loads, usually those associated with a LOCA event.

The following criteria relates to a seismic event:

- OBE-Allow continued safe operation of the FA following an OBE event by establishing that the FA components do not violate their dimensional requirements. This is most simply assured by requiring that the stresses in components remain below the yield stress of the unirradiated components.
- SSE-Ensure safe shutdown of the reactor by maintaining the overall structural integrity of the fuel assemblies, control rod insertability and a coolable geometry within the deformation limits consistent with the ECCS and safety analysis. Requirements to assure safe shutdown are:
  - Fuel rod or assembly fragmentation does not occur due to seismic loads.
  - Control rod insertability is maintained by confirming no or small plastic deformation of components.
    - Adequate static and dynamic crush strength of the spacer assembly (PWR/VVER) and fuel channel (BWR), including requirements for Condition III and IV accidents must be ensured. The grid should maintain the fuel rods in a coolable configuration. The seismic criteria are particularly critical since the PWR/VVER spacers and BWR fuel channels absorb the lateral seismic shocks. This means that the hydrogen content in the Zr alloy spacer (PWR/VVER) and fuel channel (BWR) should be limited.
  - Confirmation that the FA (top and bottom nozzles) maintains engagement with the reactor internals.

To ensure that the criteria above are met, fuel vendors limit the maximum allowable amount of hydrogen in grids (for PWRs/VVERs) and fuel channels (for BWRs) to limit the hydrogen embrittlement effect (Figure 8-1). If the hydrogen content becomes too large in these components, the grids or the fuel channel may fracture due to the seismic load making it difficult to insert the control rods and shut down the reactor.



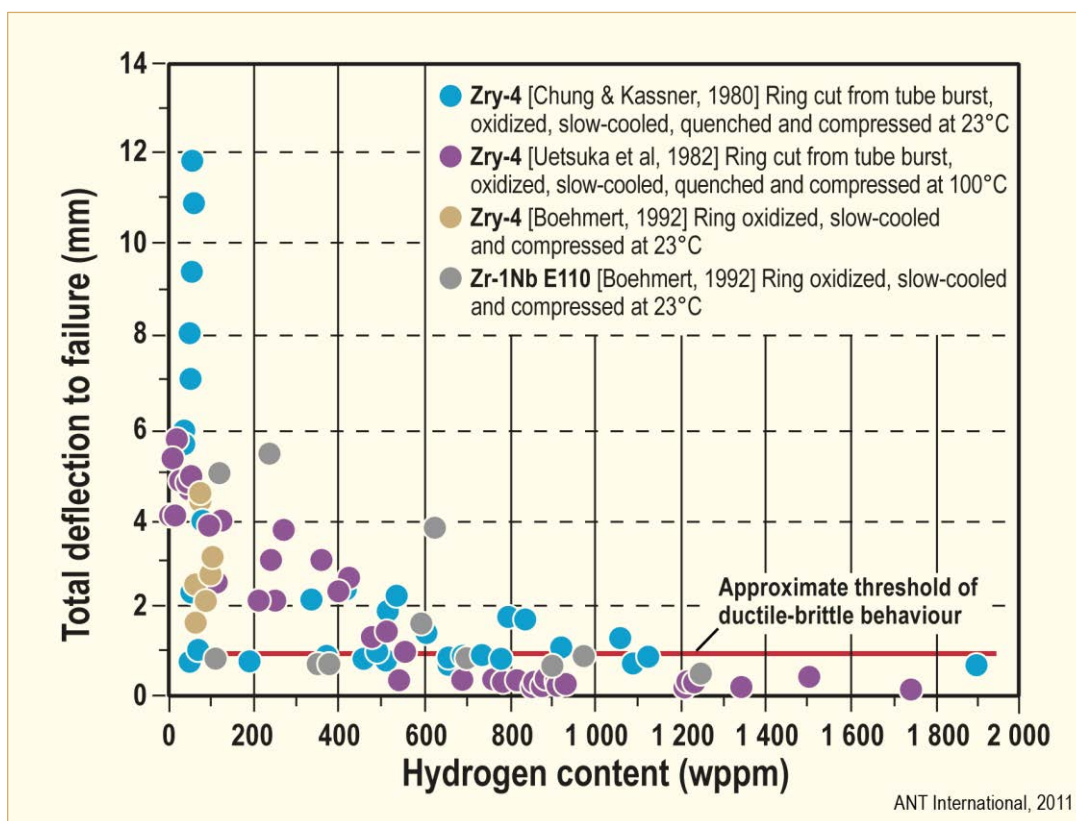


Figure 8-1: Effect of hydrogen on ring compression ductility of unirradiated samples prehydrided before RCT, after [Chung et al., 2001].

Increased burnup may lead to additional HPU through Zr-alloy corrosion of the grids (for PWRs/VVERs) and fuel channels (for BWRs) which may reduce the margins towards satisfactory performance of these components during the seismic event.

### 8.1.2 Loss of Coolant Accident (P. Rudling)

The design basis Loss of Coolant Accident (LOCA) is a break in a pipe that provides cooling water to the reactor vessel. Analyses are performed for a variety of break sizes and locations to demonstrate that the Emergency Core Cooling System (ECCS) can maintain the fuel in a coolable geometry. The limiting break is typically in one of the cold, main coolant pipes of a PWR or one of the intake pipes to the recirculation pump of a BWR.

The LOCA process starts by the decrease and ultimate loss of coolant flow at the same time that the reactor is depressurized (Figure 8-2). The loss of coolant flow decreases heat removal from the fuel, increasing the fuel temperature and causing a significant temperature rise of the cladding. The decrease in system pressure causes an outward pressure differential and a hoop stress in the cladding wall. The result is the plastic deformation, or *ballooning* of the cladding. Ballooning may also result in *fuel relocation*<sup>25</sup> that may impact the cladding temperature as well as the Equivalent Cladding Reacted (ECR)<sup>26</sup> in the later phase of LOCA.

<sup>25</sup> Fuel relocation may occur, if during LOCA a section of the fuel rod experiences ballooning, by slumping of fuel fragments from upper location in the ballooned section.

<sup>26</sup> The ECR is defined as the total thickness of cladding that would be converted to stoichiometric ZrO<sub>2</sub> from all the oxygen that are contained in the fuel cladding as ZrO<sub>2</sub>, and oxygen in solid solution in the remaining clad metal phase.

Ballooning of the fuel rods may result in *blockage* of the coolant sub-channel that in turn may impact the fuel coolability. If large fuel clad burst strains occur at the same axial elevation, *co-planar deformation*, in the FA, the coolability may be significantly degraded. Specifically, the clad azimuthal temperature gradient will strongly impact the burst strain. The extent of the ballooning is also dependent on:

- Creep strength of the cladding.
- Stress in the cladding and the corresponding strain rate (related to the rod internal gas pressure).
- Temperature and the rate of temperature increase.

Depending on the temperature, the cladding ductility and the rod internal pressure, the cladding will either stay intact or may burst which will allow steam to oxidize the fuel clad inner surface. In addition, some of the hydrogen released by the water/zirconium corrosion reaction inside the burst fuel may be picked up by the cladding resulting in very high local hydrogen concentrations (1000-3000 wtpm H). A fuel cladding with such high hydrogen concentrations will be very brittle even though the cladding is not oxidised at all, i.e. ECR is 0. The fuel clad axial temperature distribution will determine the axial elevation of the ballooned and burst fuel rods in the assembly. The axial and azimuthal fuel clad temperature distribution is a result of the heat transfer mechanisms at the surfaces of the cladding.

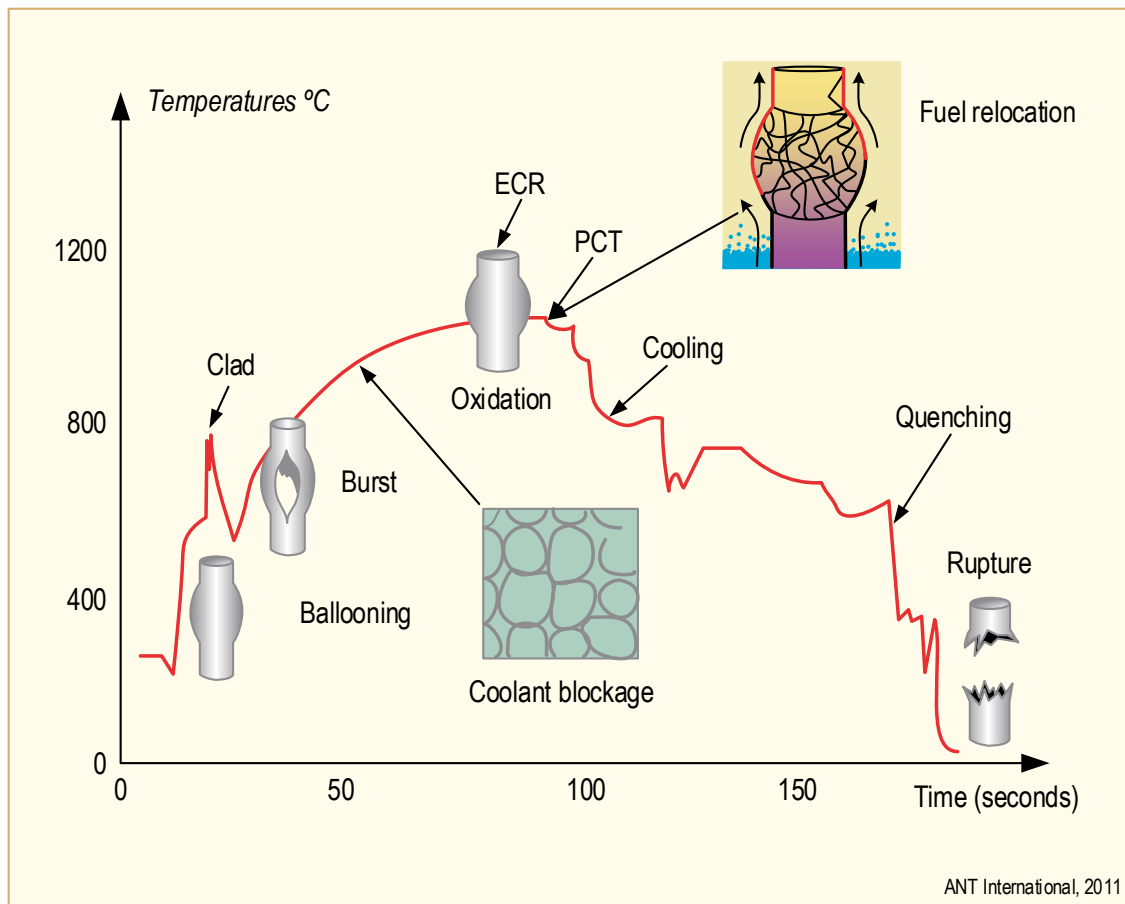


Figure 8-2: Typical LOCA in a PWR.

The increasing temperatures and presence of steam will cause the intact cladding to oxidize on the OD and the burst cladding to oxidize on both the OD and ID (two sided oxidation) until the ECCS is activated and the water quenches the cladding. The oxidation process at the high LOCA temperatures will increase the oxygen and hydrogen content in the cladding, reducing its ductility and resistance to

rupture. The process and final structure of the cladding after a LOCA cycle is shown in Figure 8-3 and described in the following:

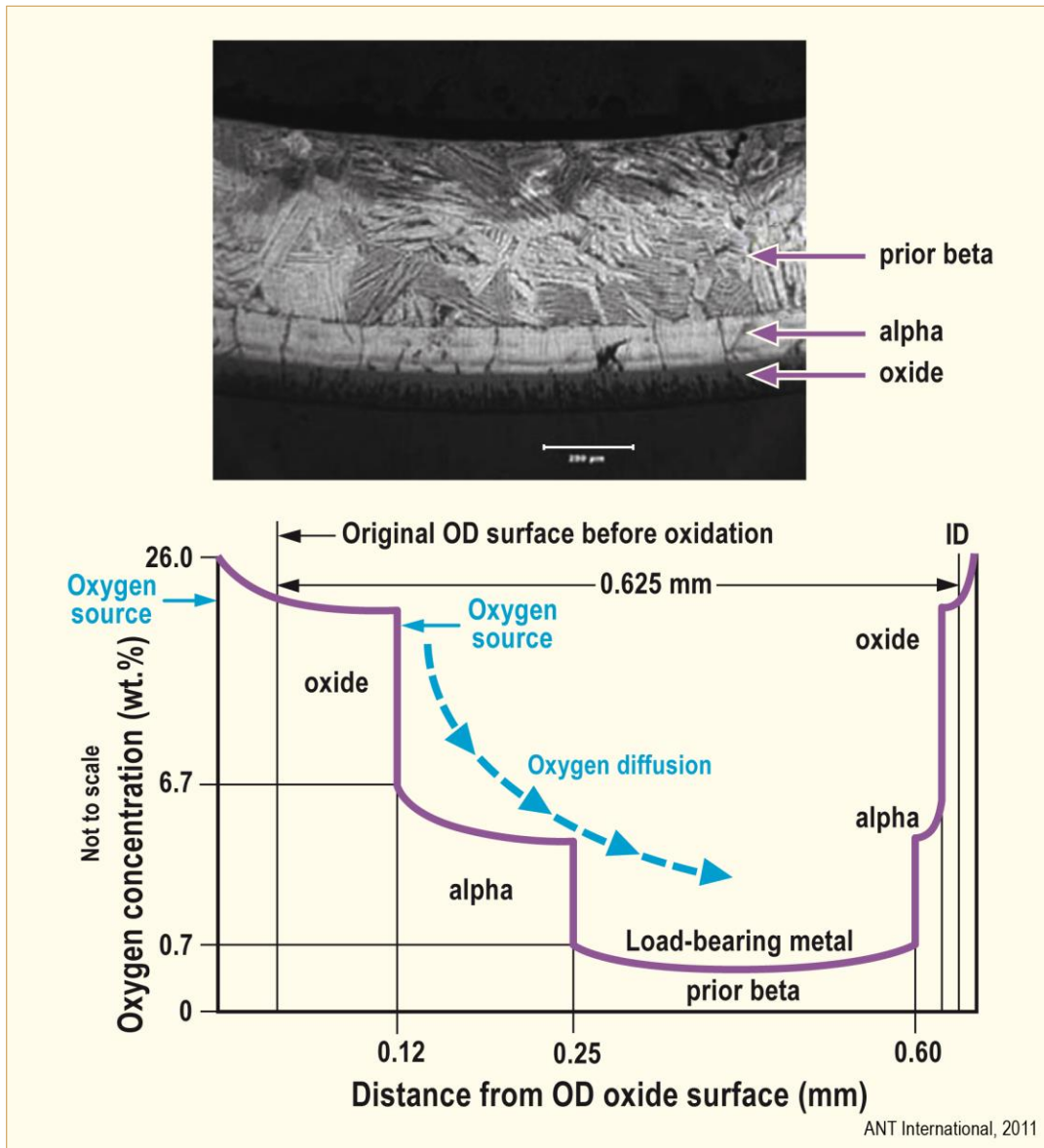


Figure 8-3: Structure of oxidized cladding, after [Meyer, 2013].

- First, the high water and steam temperatures increase their reaction rates with the cladding and increase the conversion of the cladding surface into thicker  $\text{ZrO}_2$  films.
- As the LOCA temperature passes the levels where  $\text{Zr } \alpha \rightarrow \beta$  transformations start and finish, the resulting structure consists of:
  - The growing  $\text{ZrO}_2$  layer.
  - A brittle zirconium alloy layer with a very high oxygen content which stabilizes the  $\text{Zr-}\alpha$  phase, formed by diffusion of oxygen from the oxide layer.
  - The bulk cladding, which is now in the  $\beta$ -phase, has a high solubility for hydrogen; the hydrogen picked up by the cladding from the water-metal reaction increases the solubility of oxygen in the  $\text{Zr-}\beta$  layer.

- The  $\text{ZrO}_2$  and oxygen stabilized  $\alpha$  layers grow with continued diffusion of oxygen and hydrogen from the water reaction. The increasing amount of oxygen convert some of the Zr  $\beta$ -phase to oxygen stabilized Zr  $\alpha$  phase with the concurrent shrinkage of the Zr  $\beta$ -phase. The remaining Zr  $\beta$ -phase cladding wall thickness is transformed to Zr  $\alpha$  phase, or “prior  $\beta$ -phase”, on cooling and is the only structural part of the cladding that can insure its integrity.

During the LOCA oxidation, the first oxide formed is adherent and protective. However, after an extended exposure, *breakaway oxidation* may occur manifested by the change from parabolic to quasi-linear oxidation kinetics and a dramatic increase in Hydrogen PickUp Fraction (HPUF). High temperature oxidation studies have shown that the Zr-Nb materials M5, ZIRLO have similar LOCA oxidation kinetics compared to that of Zry-4 and Zry-2, i.e., an intact black oxide layer is preferentially formed which is associated with low HPUF. However, the earlier Russian Zr-Nb alloys E110 (with similar chemical compositions to that of M5 and ZIRLO) show a much larger tendency to breakaway oxidation and high hydrogen pickup. The reason for this difference in behaviour is related to that different source material for the earlier E110 (iodide/electrolytic Zr) and M5/ZIRLO where (Zr sponge) are used. Also, another reason for the difference in behaviour between these two groups of materials is that the clad outer surface is HF pickled for E110/E635 materials while belt-polishing is used for M5/ZIRLO materials. However, today the earlier used iodide/electrolytic Zr source material has been replaced by Zr sponge for the E110 fuel cladding.

The sources and role of hydrogen in the embrittlement of the cladding includes hydrogen from the corrosion reaction during normal operation and hydrogen from the reaction with steam during the LOCA. In addition hydrogen increases the solubility of oxygen and diffusivity of oxygen in the  $\beta$ -phase at high temperatures. Oxygen, in combination with hydrogen, are the two major elements that cause cladding embrittlement by the growth of the  $\alpha$  layer and the shrinkage of the structural, prior  $\beta$  layer.

Integrity of the cladding is based partly on the properties of the former  $\beta$  zone, since the  $\text{ZrO}_2$  and oxygen stabilized  $\alpha$  zones are too brittle to sustain a load. The embrittlement criteria are based on properties of the prior  $\beta$  layer measured on post-simulated LOCA tests of unirradiated Zircaloy-4, by ring compression tests [Hobson & Rittenhouse, 1972] and related to oxidation, or ECR, calculated by the Baker-Just equation. It should be noted that the oxide thickness of the samples were never actually measured during those tests. The United States Nuclear Regulatory Commission (USNRC) accepts ECR calculations by the Cathcart-Pawel equation or others that may be submitted for approval.

The re-entrance of the coolant via the ECCS will quench and cool the cladding. The cladding may rupture due to thermal stresses, or differential expansion of FA components, in the event the cladding ductility is insufficient to accommodate the strain. The cladding temperature will be reduced at a rapid rate (1-5 °C/sec) by re-wetting the cladding surface at the Lidenfrost temperature (about 600-700 °C). The process will collapse the vapour film on the cladding OD and cooling will be by nucleate boiling. Thermal shock due to the sudden change in heat transfer conditions can fracture the cladding at this stage of the transient. The ability of the cladding to withstand the thermal stresses will depend on the extent of oxidation that occurred during the heat-up stage of the transient. Since, however, all the hydrogen is likely to be in solution at these temperatures, hydrogen is unlikely to contribute to the embrittlement except to the extent that its presence increased the oxygen solubility and increased oxygen content, in turn, increased the embrittled condition of the cladding.

Upon further cooling, the hydrogen stabilized  $\beta$ -phase will decompose below the  $\alpha$ - $\beta$  transformation temperature and the hydrogen will precipitate in the form of hydrides in the  $\alpha$  phase and embrittle and potentially crack the cladding. At temperatures of about 135 °C/275 °F (saturation temperature after the LOCA event) the forces imposed on the FA by the coolant, by handling, by transport and by hypothetical accidents such as seismic events have the potential of cracking the embrittled cladding. The embrittlement effect of hydrogen (in form of hydrides) on ductility during this phase of the LOCA is much stronger than during the quenching phase. The volume fraction of hydrides precipitated will be a function of the cooling rate.

There are several test methods to evaluate the effects of oxidation and quenching on the integrity of the cladding. Integrated tests, or thermal shock tests appear to approach LOCA conditions most closely. Mechanical tests include *ring compression tests*, three point bend tests and Charpy impact

tests. The samples used are usually unirradiated, pre-hydrated and oxidized to represent the pre-quench conditions except in the integral thermal shock test, which includes the ballooning and oxidation cycle.

The *thermal shock tests* consist of isothermal heating of the fuel to the selected oxidation temperature and then quenched with water at a selected rate. The electrically heated cladding, usually filled with alumina pellets, is placed in a tube with inlets, usually at the bottom for steam to oxidize and for water to quench the cladding. The fuel rods may be free to expand axially or be restrained. The integral thermal shock test simulates the entire LOCA.

### 8.1.2.1 Current US Regulations (C. Patterson)

The section 50.46 “Acceptance criteria for emergency core cooling systems for light-water nuclear power reactors” deals with the Emergency Core Cooling System (ECCS) design requirements in the event of a loss of coolant accident. In its present (approved) form, 10 CFR 50.46 requires that, [NRC, 2017]:

- (a)(1)(i) Each boiling or pressurized light-water nuclear power reactor fueled with uranium oxide pellets within cylindrical zircaloy or ZIRLO cladding must be provided with an emergency core cooling system (ECCS) that must be designed so that its calculated cooling performance following postulated loss-of-coolant accidents conforms to the criteria set forth in paragraph (b) of this section...
- (b)(1) *Peak cladding temperature*. The calculated maximum fuel element cladding temperature shall not exceed 2200 °F.
- (2) *Maximum cladding oxidation*. The calculated total oxidation of the cladding shall nowhere exceed 0.17 times the total cladding thickness before oxidation...
- (3) *Maximum hydrogen generation*. The calculated total amount of hydrogen generated from the chemical reaction of the cladding with water or steam shall not exceed 0.01 times the hypothetical amount that would be generated if all of the metal in the cladding cylinders surrounding the fuel, excluding the cladding surrounding the plenum volume, were to react.
- (4) *Coolable geometry*. Calculated changes in core geometry shall be such that the core remains amenable to cooling.
- (5) *Long-term cooling*. After any calculated successful initial operation of the ECCS, the calculated core temperature shall be maintained at an acceptably low value and decay heat shall be removed for the extended period of time required by the long-lived radioactivity remaining in the core.

Applicable cladding alloys are Zry-2, Zry-4 and, ZIRLO.

### 8.1.2.2 Modifications being Considered to US Regulations

Section 50.46c is being revised and is in the final stages of rulemaking by the NRC, Table 8-1 [NRC, 2011]. The change is a major revision which is likely to be adopted in-whole or in-part by regulatory agencies outside of the U.S. given the international effort to develop the technical bases for the change and ongoing efforts to harmonize regulations.

Table 8-1: Summary of Significant Changes to § 50.46c [NRC, 2011].

Item	§ 50.46	§ 50.46c	Benefit to Industry
Rule Structure	Prescriptive	Performance-Based	More flexibility
Applicability	Zircaloy or ZIRLO Cladding	All LWR Cladding	Eliminates exemption requests for modern alloys
Burnup Related Phenomena	None	Cladding Inner Surface Oxygen Ingress	Supports current, high efficiency, high burnup core loading patterns
Corrosion Related Phenomena	None	Hydrogen-Enhanced Embrittlement	Supports current, high efficiency, extended operating cycles
Fabrication Related Phenomena	None	Breakaway Oxidation	Confirms cladding performance without interfering with manufacturing flexibility
Debris Consideration	Implicit	Explicit	Regulatory certainty
Debris Treatment	Deterministic	Deterministic or Risk-Informed	Supports closure of GSI-191 and reduces need for costly fibre removal
LTC Regulatory Criteria	General	Explicit	Supports closure of GSI-191 and reduces need for costly fibre removal
Crud Treatment	None	Explicit	Regulatory certainty
© ANT International 2018			

The proposed revision of 10 CFR 50.46c is given in NRC [NRC, 2011]. A comprehensive review of the revision is contained in a report by the Advisory Committee on Reactor Safeguards (ACRS), [NRC, 2016a]. Significant changes to the existing requirements of 10 CFR 50.46c include, [NRC, 2016a]:

- “The final rule replaces prescriptive analytical requirements with performance-based requirements. To demonstrate compliance with the requirements, ECCS performance will be evaluated using fuel-specific performance objectives and associated analytical limits that take into consideration all known degradation mechanisms and unique performance features of the particular fuel system, along with an acceptable ECCS evaluation model.”
- “The final rule applies to all fuel designs and cladding materials. The final rule defines two principal ECCS performance requirements:
  - Core temperature during and following the postulated LOCA does not exceed the analytical limits for the fuel design used for ensuring acceptable performance.
  - The ECCS provides sufficient coolant so that decay heat will be removed for the extended period of time required by the long-lived radioactivity remaining in the core.”



## 9 Accident Tolerant Fuels (ATFs) (Tahir Mahmood)

### 9.1 Introduction

Uranium dioxide ( $\text{UO}_2$ ) pellets contained within a zirconium (Zr) alloy cladding has been the fuel of choice for light water reactors (LWRs) for over 40 years and the behavior of this fuel is well understood. Since the introduction of Zr alloy clad  $\text{UO}_2$  fuel in the 1970s, fuel rod failure rates have decreased by three orders of magnitude (Figure 9-1), such that they are now a rare occurrence [Terrani et al., 2014]. This has been achieved through improvements in fuel assembly design, materials, manufacturing reliability, quality assurance, and reactor operation procedures.

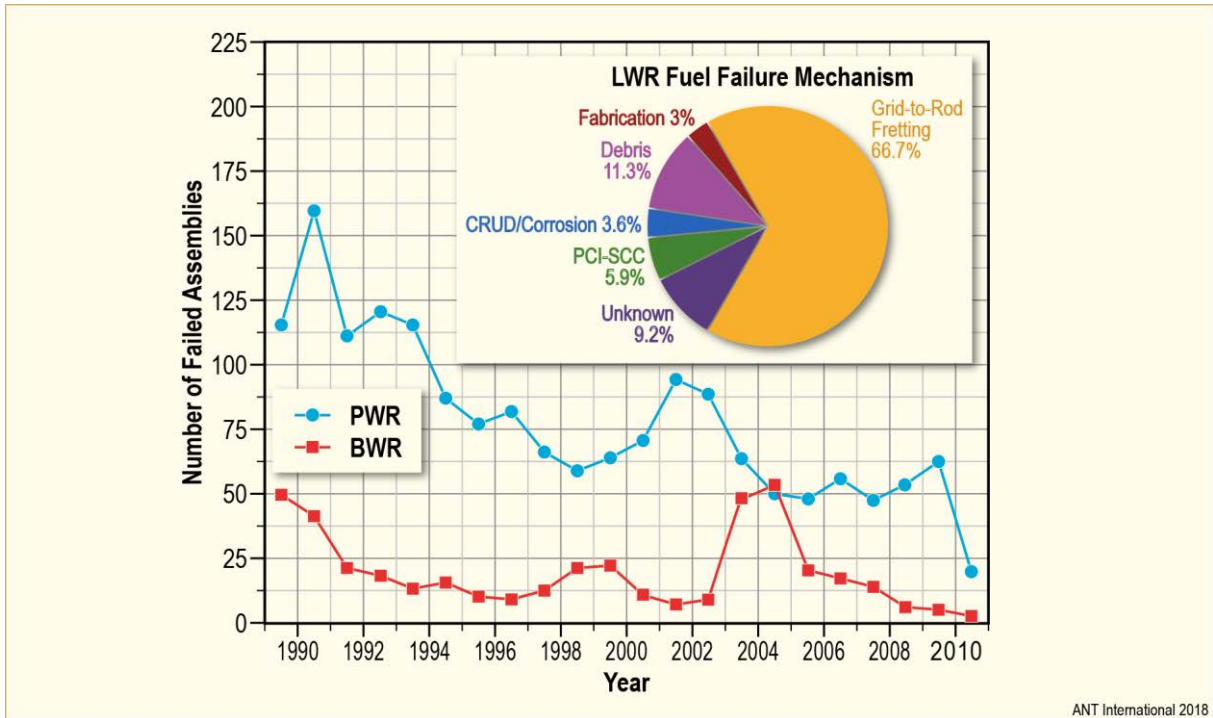


Figure 9-1: Performance over the years of the existing  $\text{UO}_2$ -Zr alloy system [Bragg-Sitton, 2012].

The events at the Fukushima-Daiichi plant in Japan in 2011 revealed  $\text{UO}_2/\text{Zr}$  alloy system's inherent vulnerability to a prolonged station blackout. Although this type of event is extremely rare, the consequences are significant: the current estimate for the removal of fuel debris, clean-up of contaminated land and compensation payments resulting from Fukushima are estimated to be \$191Bn [WNA, 2017b]. This has led researchers to focus their efforts on what can be done to improve the resilience of fuels in severe accident scenarios. Any improvements however must be economically viable to ensure that nuclear continues to be a competitive source of clean energy.

During a prolonged station blackout, the accident tolerance of a fuel is directly related to the ability of the fuel to withstand increasingly high temperatures. This can also be thought of in terms of “coping time”, a measure of the time that operators have to re-instate cooling of the reactor to prevent major consequences. If the coping time could be extended from minutes to hours to days (or even indefinitely), it could significantly reduce the consequences of possible future severe accidents [NNL, 2018].



Developing Accident Tolerant Fuels (ATF) could be considered as one of the options to address the challenges. An ATF cladding that will survive in 1200-1500 °C steam

- can extend the time without meltdown of the fuel,
- may significantly reduce the generation of hydrogen, and hence
- will provide additional coping time for operators to recover from the accident.

The introduction of a new fuel type requires extensive testing and evaluation. Typically, this entire process can take between 10-15 years, from concept to a fully commercial product. For ATF to play a role in providing added protection to existing LWR fleets acceleration of this fuel qualification process is desirable. This is because of the age of existing reactor fleets. In 10 years, when ATF might be available, 85% of the US LWR fleet and 73% of European LWRs will have been operating for more than 40 years [WNA, 2017b]. The urgency to proceed quickly is reflected in the US Department of Energy ambition to have ATF deployed in commercial reactors in the form of lead test rods or assemblies as early as 2022 [DOE, 2015].

Development efforts have focused on the screening and characterization of material candidates with the highest degree of promise to produce a technically viable cladding/fuel in the shortest amount of time. The performance of these materials under accident conditions is such that potential exists for relaxation of safety system performance requirements, which in turn can result in substantial economic incentive for adoption of ATF. Therefore, several large ATF development programs are being pursued around the world.

Independent of the outcomes of the current investigations, it is important to mention that developing ATF is a motivating driver for the entire nuclear fuel community, including young engineers and researchers. Thanks to the countless ATF related research projects, significant progress is being made towards

- physical understanding of the fuel behavior under irradiation,
- advanced techniques to better analyze data, and
- development of advanced calculations tools and methods.

The ATF development is still at the lab testing/in-reactor irradiation level. Before implementing a new type of fuel on an industrial scale, utilities and regulators will require to collect trouble free in-reactor data over a long period of time (to cover the entire burnup range) and a successful qualification PIE program on irradiated specimens.

Another important consideration which has both safety and cost implications is what to do with the spent fuel. This will depend on the policy adopted by different countries.

## 9.2 Accident Tolerant Fuel Materials

The leading candidate technologies identified in the Trade-off Study [Bragg-Sitton, 2016] and ATF status report [NEA, 2018] include

- Cladding and fuel component materials
  - Coated and Improved Zr alloys
  - Advanced steels – FeCrAl
  - SiC/SiC composite cladding
  - Refractory metals – Lined Mo alloy cladding

- Advanced fuel designs
  - Improved  $\text{UO}_2$ 
    - Doped  $\text{UO}_2$
    - High thermal conductivity  $\text{UO}_2$
  - High density fuel
    - Nitride fuel
    - Silicide fuel
    - Carbide fuel
    - Metallic fuel
  - Non-fuel components
    - Accident tolerant control rods
    - SiC composite BWR channels

Among the multiple variants of ATF concepts under development all around the world (Figure 9-2) [Waeckel, 2017], the short-term concepts (e.g. coated Zr alloy cladding, FeCrAl cladding) have better chance to be used in the current nuclear power plants. The longer-term fuel system concepts (e.g. SiC/SiC cladding, refractory Molybdenum cladding, metallic fuels, micro-cells fuel, or uranium nitride fuel), despite their potential high level of performance in accidental conditions, will need decades before they could be implemented on an industrial scale (i.e. beyond the expectation life of the current fleet).

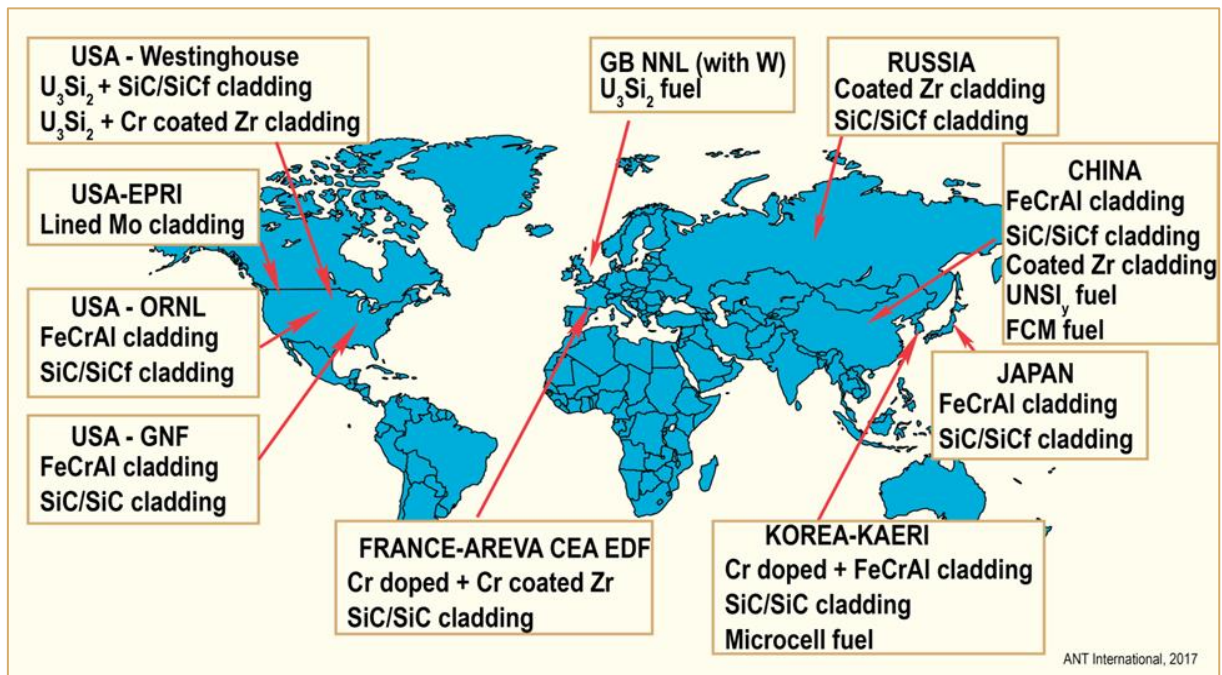


Figure 9-2: Similar ATF concepts are under development all around the world [Waeckel, 2017].

Each ATF concept has some pros and cons across the spectrum of operating and transient conditions of interest, therefore, systematic analytical and experimental evaluations are being performed during the feasibility and material property investigations.

## New Results and Status – 2017 - 2018

### 9.3 DOE Funded ATF Development Programs

After Fukushima, enhanced accident tolerance became a priority topic. The US congress approved funding to DOE to start developing nuclear fuel with enhanced accident tolerance. Aggressive ten-year schedule started in 2012 that has three phases [McCaughey, 2017].

- Phase 1: Feasibility - complete
- Phase 2: ATF development and qualification - started in October 2016
- Phase 3: DOE insertion of LTR/LTA in commercial reactor by 2022 (industry is working to further accelerate this schedule)

The ten-year schedule is shown in Figure 9-3 [McCaughey, 2017].

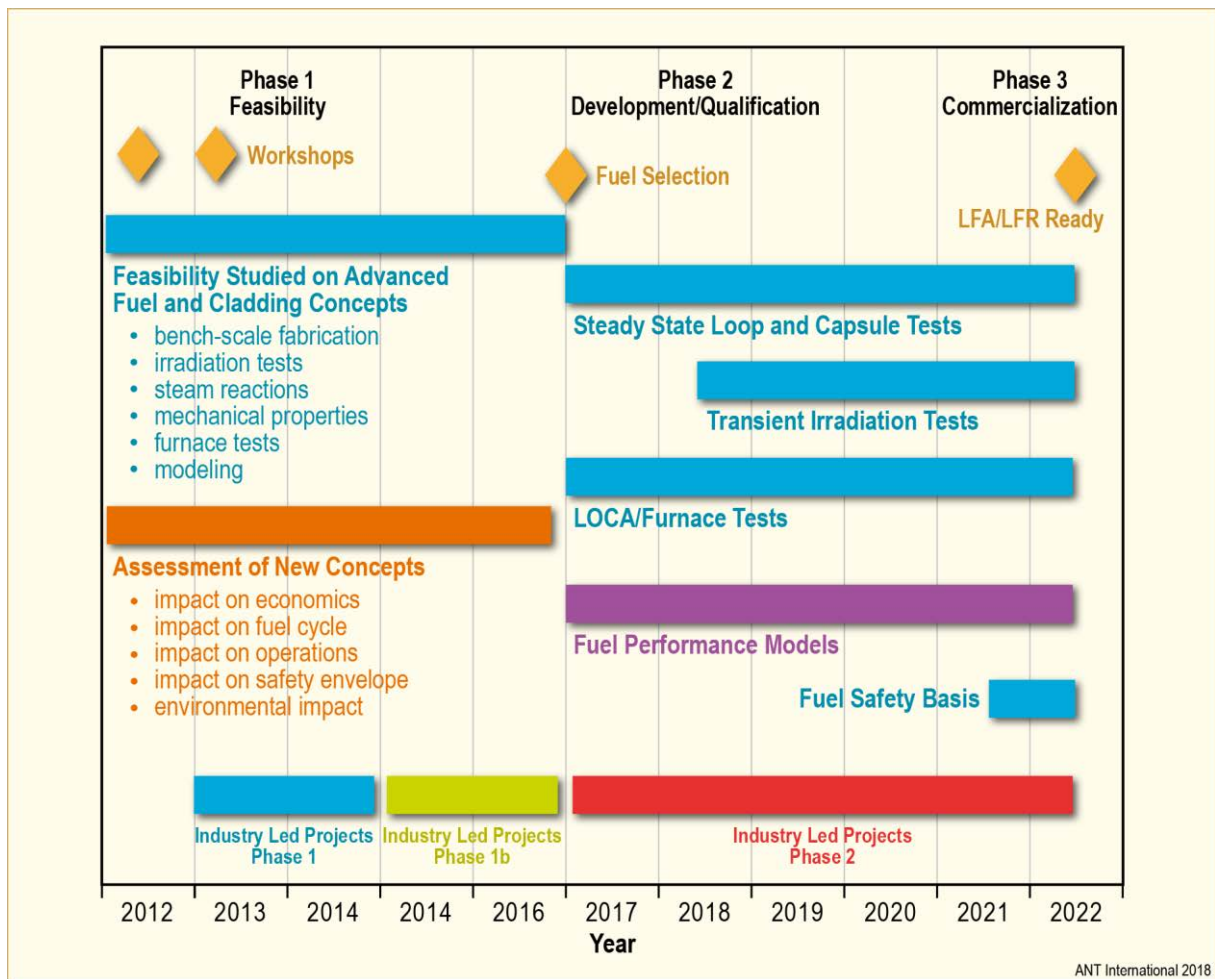


Figure 9-3: US strategy for ATF R&D- development and qualification of ATF [after McCaughey, 2017].

The ATF development effort adopts a three-phase approach to commercialization, as illustrated in Figure 9-3. Each development phase roughly corresponds to the Technology Readiness Levels (TRL) defined for nuclear fuel development, where

- TRL 1-3 corresponds to the “proof-of-concept” stage,
- TRL 4-6 to “proof-of-principle,” and
- TRL 7-9 to “proof-of-performance”.

Each step in the fuel development effort necessarily considers the requirements set out by the Nuclear Regulatory Commission (NRC) to support the fuel licensing effort in planning, executing, and documenting all phases of fuel development, including fabrication, experiments, model development, and validation, etc. Sufficient data for licensing of a new fuel system should be available at TRL 7, as shown in Table 9-1. As shown in Figure 9-4, there are two key attributes that are important in assessing the TRL for the fabrication process and performance maturity evaluation elements.

Table 9-1: Summary of TRL definitions for advanced nuclear fuels [NEA, 2018].

TRL	Function	Definition
1	Proof of concept	A new concept is proposed. Technical options for the concept are identified and relevant literature data reviewed. Criteria are developed.
2		Technical options are ranked. Performance range and fabrication process parametric ranges are defined based on analysis.
3		Concepts are verified through laboratory-scale experiments and characterisation. Fabrication process is verified using surrogates.
4	Proof of principle	Fabrication of small samples (rodlets) at bench-scale. Irradiation testing of rodlets in a relevant environment. Design parameters and features are established. Basic properties are compiled.
5		Fabrication of full-length rods using prototypic materials at laboratory scale. Rod-scale irradiation testing in a relevant environment (test reactor). Primary performance parameters with representative compositions under normal operating conditions are quantified. Fuel compositions under normal operating conditions are quantified. Fuel behaviour models are developed for use in fuel performance code(s).
6		Fabrication of rods using prototypic materials at laboratory scale and using prototypic fabrication processes. Rod-scale irradiation testing at relevant (test reactor) and prototypic (commercial LWR, referred to as lead test rods) environment (steady-state and transient testing)a. Predictive fuel performance code(s) and safety basis are established.
7	Proof of performance	Fabrication of test assemblies using prototypic materials at engineering-scale and using prototypic fabrication processes (also referred to as lead use assemblies). Assembly-scale irradiation testing in prototypic (commercial LWR) environment. Predictive fuel performance code(s) are validated. Safety basis established for full-core operations.
8		Fabrication of a few core-loads of fuel and operation of a commercial reactor with such fuel.
9		Routine commercial-scale operations. Multiple reactors operating.

© ANT International 2018

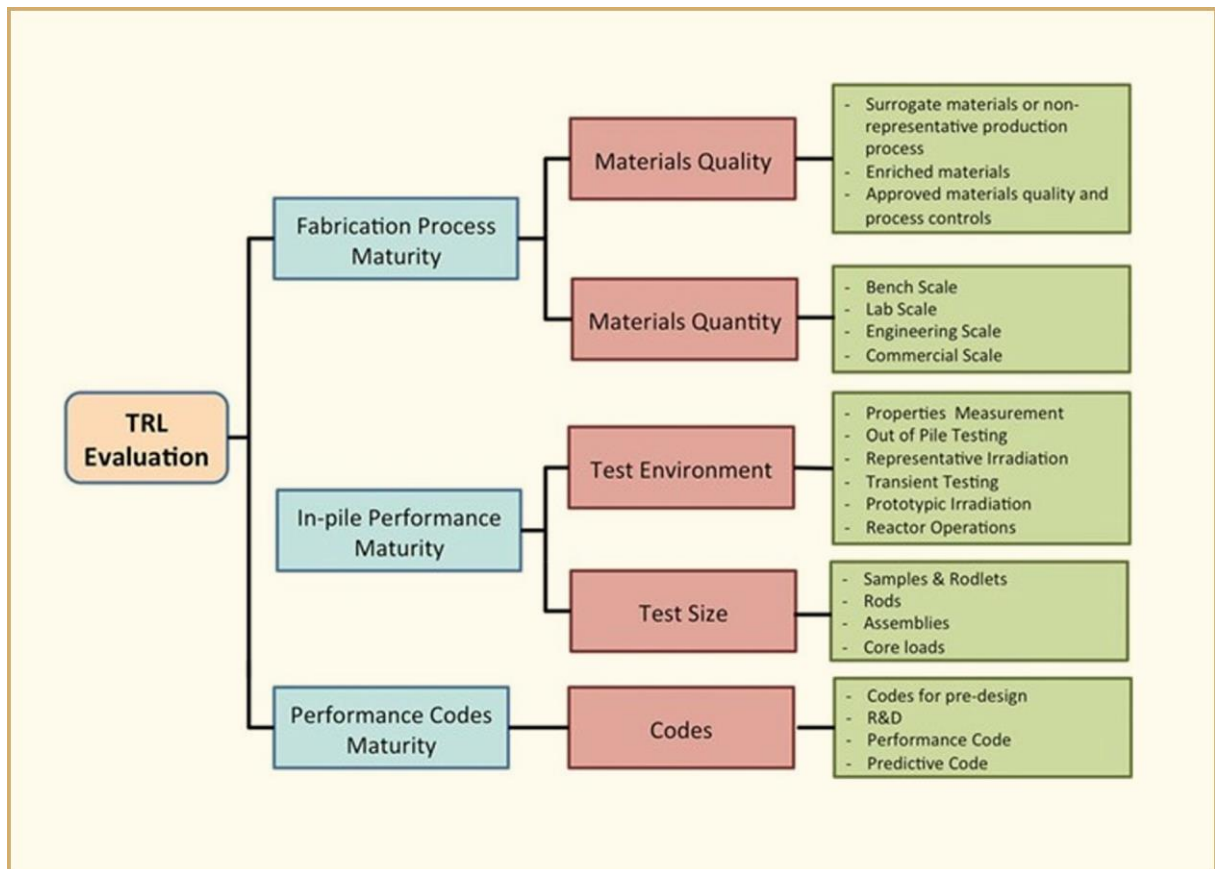


Figure 9-4: Summary of TRL evaluation elements and attributes [NEA, 2018].

### 9.3.1 National Laboratory, Industry, and University Directed Efforts

Table 9-2 gives a summary of the major US DOE-funded ATF projects that are being led by a national laboratory, industry, or a university.

Table 9-2: Major US DOE-funded ATF projects [Bragg-Sitton, 2015].

Lead Organization	Category – Major Technology Area	Additional Collaborators
Oak Ridge National Laboratory	<b>Fuel:</b> Fully Ceramic Microencapsulated (FCM)-UO <sub>2</sub> ; FCM-UN <b>Cladding:</b> FeCrAl alloy; silicon carbide (SiC)	LANL, INL support FeCrAl weld development work
Los Alamos National Lab.	<b>Fuel:</b> Enhanced UO <sub>2</sub> , Composite Fuels	
EPRI + LANL	<b>Cladding:</b> Advanced molybdenum alloys (multi-layer design)	ORNL
AREVA (FOA, NEUP)	<b>Fuel:</b> High conductivity fuel (UO <sub>2</sub> +Cr <sub>2</sub> O <sub>3</sub> +SiC) <b>Cladding:</b> Coated Zr-alloys (protective materials, MAX phase)	U. Wisconsin, U. Florida, SRNL, TVA, Duke
Westinghouse (FOA, NEUP)	<b>Fuel:</b> U <sub>3</sub> Si <sub>2</sub> , and UN+U <sub>3</sub> Si <sub>2</sub> fuel <b>Cladding:</b> Coated Zr-alloy; SiC concepts	General Atomics, EWI, INL, LANL, MIT, TAMU, Southern Nuclear Operating Company
GE Global Research (FOA)	<b>Cladding:</b> Advanced Steel (Ferritic / Martensitic, including FeCrAl)	Global Nuclear Fuels, LANL, U. Michigan
University of Illinois (IRP)	<b>Cladding:</b> Modified Zr-based cladding (coating or modification of bulk cladding composition)	U. Michigan, U. Florida, INL, U. Manchester, ATI Wah Chang
University of Tennessee (IRP)	<b>Cladding:</b> Ceramic Coatings for Cladding (MAX phase, multilayer ceramic coatings)	Penn State, U. Michigan, UC Boulder, LANL, Westinghouse, Oxford, U. Manchester, U. Sheffield, U. Huddersfield, ANSTO
<b>Additional laboratories are providing analysis support (INL, BNL, ANL).</b>		
© ANT International 2018		

The major fuel vendors, Framatome, GNF, and Westinghouse, are pursuing a wide range of promising ATF concepts under this DOE funded effort (Figure 9-5). This DOE program makes use of international collaborations as well, as shown in Figure 9-6 [McCaughey, 2017].

## 10 Storage and Transportation of Commercial Spent Nuclear Fuel Under Dry Inert Conditions (Albert Machiels)

### 10.1 Introduction

In last year's Annual Report Section 10, the degradation of cladding tube ductility by hydrides was reviewed given the topic's relevance to accident analyses, especially in the context of transportation of spent fuel after long dry storage times [Patterson et al., 2017]. The conclusions of the review were as follows:

- Moderate concentrations (<500 wppm of H) of circumferential hydrides do not significantly degrade the ductility of Zr-alloy claddings, even at room temperature. However, radial hydrides with a high degree of radial continuity can degrade ductility below a critical temperature.
- Irradiated Zr-based alloys experience a greater loss of ductility as a function of increasing H concentration than unirradiated hydrided materials due to the additive effects of irradiation damage and precipitated hydrides.
- According to [Kubo et al., 2013], brittle failure can only occur when the strength of the Zr-alloy cladding, which decreases with increasing temperature, is greater than the fracture strength of the hydrides, which, as a first approximation, is independent of temperature in the range of interest to dry storage. Consequently, radiation damage annealing may prevent brittle cracking for RXA claddings, because the strength of RXA claddings (~600 MPa at room temperature) is smaller than the fracture strength of hydrides (~710 MPa). While annealing of irradiation damage can be beneficial with respect to ductility and impact resistance, reductions in alloy strength could decrease the resistance of fuel cladding to creep during dry storage. However, given that fuel rods are closed systems, creep always results in an increase in rod internal void volume, and, consequently, in a decrease of the rod internal pressure and cladding stress. Creep of closed systems tend to be self-limiting; as a result, creep rupture is not predicted.
- The experiments by [Daum et al., 2008] indicate that thick oxide layers can initiate brittle cracks. Given the larger number of such cracks in thick oxide layers, the likelihood that a crack connects with a radial hydride, i.e., crack growth, is greater.
- For accident scenarios involving pinch loading, cladding deformation takes place only during closure of the pellet-cladding gap. In high-burnup fuel, the gap is either non-existent or small. As a result, impact loads are transferred to the fuel column; this load transfer is the main contributor to the robust behavior of the cladding under hypothetical accident conditions, as has been documented in best-estimate system performance evaluations [EPRI, 2005].

In this year's report, thermal creep of Zr-based cladding tubing is reviewed in more details. Prior to discussing the technical aspects of Zr-alloy cladding creep, a brief historical note is provided to help in appreciating the evolution and present relatively low concern for the impact of thermal creep during dry storage [Patterson et al., 2015].

In the early assessments of the impact of dry storage on fuel performance, consideration was given to whether thermal creep or diffusion-controlled cavity growth (DCCG) of the Zr-based cladding would dominate or have the potential to result in gross rupture. In the first US regulatory analyses, DCCG was used as the limiting cladding failure mechanism for its potential to result in gross rupture (specifically, loss in cohesion of the alloy grain structure) and thermal limits were based on calculations consistent with a DCCG model. However, between 1995 and 1999, better technical information became available and US regulators indicated a shift toward a thermal creep basis for cladding degradation.



In the Standard Review Plan published in 1997 [NRC, 1997], cladding temperatures were allowed to reach 570 °C during water removal and vacuum drying, as well as under accident conditions and short-term, off-normal conditions. The basis for 570 °C was derived from creep testing conducted on irradiated Zircaloy-4 rods [Einziger et al., 1982]. It was recognized, however, that this 570 °C limit was obtained by creep testing of low-burnup fuel rod with low internal fuel-rod gas pressure.

Revision 1 of the Standard Review Plan [NRC, 2010] reflects an improved understanding in the guidance to NRC reviewers. Consistent with Interim Staff Guidance 11, Rev. 3 [NRC, 2003], the revised Standard Review Plan limits peak cladding temperatures to 400 °C for all normal operations, including drying. Cladding temperatures up to 570 °C can still be justified for short-time loading operations for spent nuclear fuel (SNF) with best-estimate cladding hoop stress equal to or less than 90 MPa. As a result, previously analyzed SNF did not have to be re-analyzed because that SNF had relatively low burnups ( $\leq 45$  GWd/MTU) with cladding stress likely to be less than 90 MPa. NUREG-1536, Rev. 1 [NRC, 2010] also states that for off-normal and accident conditions, the maximum cladding temperature shall not exceed 570 °C. The basis for allowing up to 570 °C for off-normal and accident conditions was, at least in part, based on the previously cited work by [Einziger et al., 1982], which showed no cladding rupture after relatively long creep test times of 30 days and 73 days at 571 °C.

The last sentence of the first paragraph of Section 8.8.1 in [NUREG-1536, Rev. 1] gives the following basis for the apparently reduced concern about creep, where it is concluded that:

“(1) deformation caused by creep will proceed slowly over time and decrease with rod pressure, (2) the decreasing cladding temperature also decreases the hoop stress, and this too will slow the creep rate so that during the later stages of dry storage, further creep deformation will become exceedingly small, and (3) in the unlikely event that a breach of the cladding due to creep occurs, it is believed that this will not result in gross rupture.”

The more detailed creep discussion in the next section provides mechanistic support for the limited effect of creep. In Europe, Asia and in the USA, the allowable peak temperature and cladding hoop stress during drying and dry storage are constrained by licensing criteria. The overall objectives of these constraints are to avoid:

- systematic failure due to creep rupture, and
- mechanical property degradation (with emphasis on loss of ductility) due to the hydrogen-related phenomena discussed in previous Annual Reports.

## 10.2 Thermal Creep of Zr-based Alloys

### 10.2.1 Introduction

Thermal creep is the tendency of solid materials, in this case Zr-based cladding tubing alloys, to deform permanently under the influence of temperature and stress. Thermal creep occurs over time as a result of long-term exposure to levels of stresses that are, at least initially, *below the yield strength* of the material. Excessive deformation results in rupture; an example of such excessive deformation and rupture is shown in Figure 10-1.



Figure 10-1: Illustration of creep rupture in cladding tubing tested to failure under constant load conditions.

Systematic cladding failure by creep must be avoided during dry storage. Regulatory requirements seek to minimize the likelihood of creep rupture failures by limiting

- (1) the maximum allowed, or peak, cladding temperature (for example, USA); or
- (2) the cladding diametral strain to  $\leq 1\%$  (for example, Germany).

Some countries, such as Spain and Switzerland, have deployed dry storage technologies that were originally licensed following either the US or German regulations; such countries tend to maintain a strong relationship between deployed dry storage technology and US or German regulatory guidance. Considerations related to hydride re-orientation also play a significant role in limiting peak temperature and hoop stress used in evaluating creep strain. In Japan, for example, JNES recommendations for disposing of the hydride re-orientation issue limit the range of peak cladding-specific temperature and hoop stress between 200 to 300 °C and between 70 to 100 MPa, respectively [Kamimura, 2010]. For similar reasons, German regulations limit cladding hoop stresses to  $\leq 120$  MPa.

## 10.2.2 Creep Testing Set-up

Given the geometry of fuel rod cladding, only creep testing of tube specimens is considered in this review. A creep testing furnace set-up is illustrated in Figure 10-2. A cladding segment, typically ~10-cm long, with a leak-tight bottom plug and a top fitting allowing connection to a pressurization system is placed in a furnace. Diametral deformation of the cladding tube specimen is monitored using a laser system. Pressurization of the specimen and inerting of the furnace atmosphere is accomplished through the use of an inert gas such as argon. Prior to the start of the test, the temperature is increased to the test temperature followed by a stabilization hold period of several hours. The pressure is then increased up to test pressure at a rate chosen to minimize deformation of the specimen during the time it is pressurized. Determination of the apparent Young's modulus<sup>37</sup> (elastic modulus) can be conducted at each test start-up and shut-down to verify the proper functioning of the equipment. By maintaining furnace temperature and pressure inside the specimen at pre-set values, such a system allows measuring creep deformations on a continuous basis, as illustrated in Figure 10-3a (specimen subjected to testing conditions resulting in relatively small creep strains) and Figure 10-3b (specimen subjected to testing conditions resulting in relatively large creep strains).

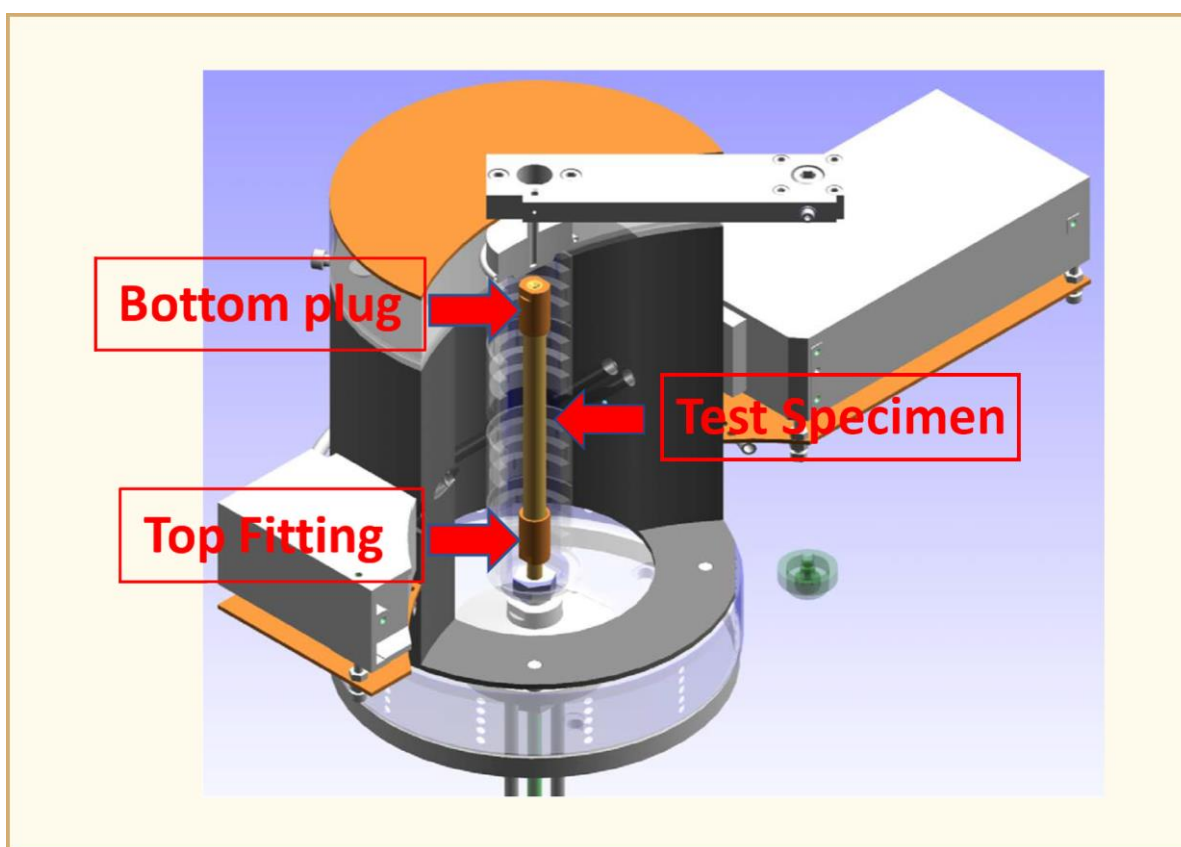


Figure 10-2: Example of creep testing furnace set-up.

Variations of the system illustrated in Figure 10-2 include reliance on Linear Variable Differential Transformers (LVDTs) instead of laser systems. Dimensional measurements can also be performed at room temperature, but this approach obviously requires many thermal cycles between testing temperature and ambient temperature. Another option is introducing a pre-set amount of gas in order to achieve a target pressure inside the specimen at the chosen test temperature followed by sealing both ends of the specimen to maintain a constant gas inventory inside the specimen. Such a specimen can

<sup>37</sup> The relation between Young's modulus and apparent Young's modulus is  $E_{app} = E/(1-\nu/2)$ , where  $E_{app}$  is the Apparent Young's modulus;  $E$  is the Young's modulus; and  $\nu$  is the Poisson's ratio.

then be placed inside a furnace and its deformation monitored preferably in a continuous manner at the testing temperature.

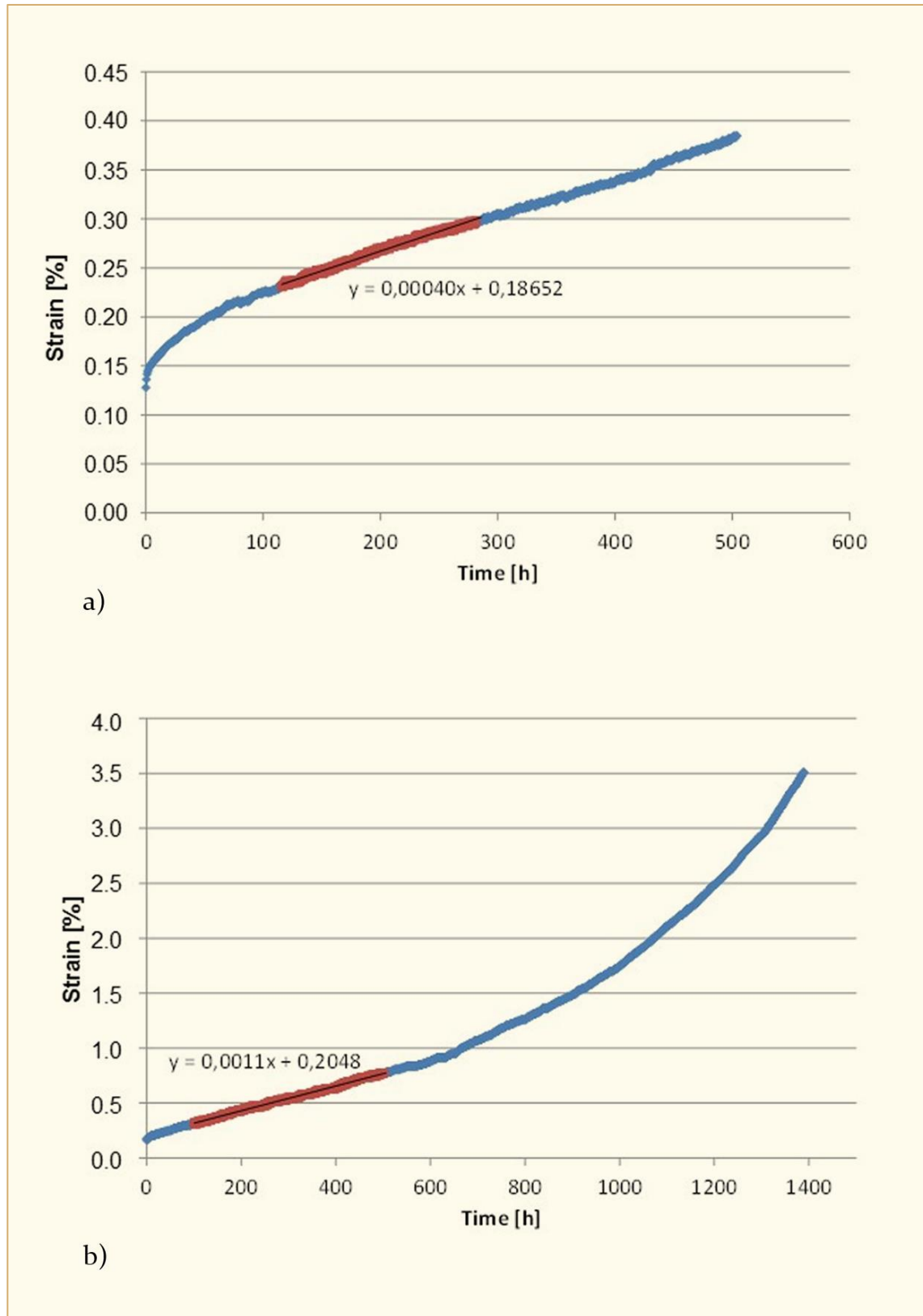


Figure 10-3: Examples of creep curves for relatively small (a) and larger (b) creep strains. The areas highlighted in red show portions of the secondary (steady state) creep, as discussed in Section 10.2.3

### 10.2.3 Experimental Creep Curve Shapes

Depending on the experimental protocol, different creep curve shapes can be generated while maintaining a constant test temperature:

- *Curves generated under constant load conditions:* a constant pressure inside the specimen is maintained throughout the duration of the testing either for a pre-determined length of time, or until specimen rupture. This is the most common creep testing approach.
- *Curves generated under constant stress conditions:* a constant hoop stress is maintained throughout the duration of the testing by adjusting, if necessary, the pressure inside the specimen in order to compensate for changes in specimen diameter and thickness.
- *Curves generated under constant gas content conditions* (specimen sealed at both ends): a constant gas content inside the specimen is maintained throughout the duration of the testing by first pressurizing followed by sealing both ends of the specimen; adjustment of the internal pressure, without changing the furnace temperature, is not possible during testing.

Assuming that the initial testing parameters for these three testing protocols are identical (same temperature and initial internal pressure values), Figure 10-4 provides an illustration of the shape of the curves that would be expected by testing the same material according to the three different protocols referred to above.

Creep curves are typically described as reflecting up to three stages during the deformation process. The first two stages are Stage I, or primary creep, and Stage II, or secondary creep. Primary creep occurs at the beginning of the test, as shown in Figure 10-4, where  $\epsilon_e$  and  $\epsilon_p$  denotes the instantaneous elastic strain and transient primary creep strain, respectively. During the transient primary creep stage, the creep strain rate decreases as the material becomes more creep-resistant as strain increases until Stage II is reached. In Stage II, or secondary creep, the rate at which the specimen deforms (i.e., the slope of the curve) becomes nearly constant; this stage is referred to as steady-state creep; the secondary creep strain is denoted  $\epsilon_s$  in Figure 10-4. For the purpose of the discussion, the curves capturing the primary creep transient and the initial stage of the secondary creep are shown to be identical for all three testing protocols; this assumes that changes in internal pressure and specimen dimensions (diameter and wall thickness) remain small in the early phases of specimen deformation. However, when changes in specimen dimensions become more significant, the shapes of the curves diverge as testing duration increases.

- **Constant load conditions:** As the tubing specimen deforms, changes in tube dimensions (increases in outside and inside diameters and decrease in wall thickness) result in increasing applied stress levels. The applied stress eventually becomes locally greater than the yield stress, and plastic deformation (no longer creep as initially defined) at the structurally weakest location in the cladding tube eventually results in specimen rupture.
- **Constant stress conditions:** The creep rate (i.e., the slope of the creep curve) remains the same as internal pressure is continuously adjusted, if necessary, for accounting for the changes in specimen dimensions in order to maintain a constant hoop stress in the specimen. Stage II is greatly expanded time-wise until the specimen wall becomes so thin that plastic deformation and rupture occur at the structurally weakest location in the cladding tube. Such testing protocol has been documented to result in very large diametral strains (>10%) in a large variety of materials, including Zry-4 [Woodford, 1969].
- **Constant gas content conditions:** When the sealed specimen fuel contains fuel, or more likely dummy fuel pellets, the volume available to the gas content inside the specimen may represent a small fraction of the specimen's internal volume. Such a "fueled" tube specimen experiences a decreasing stress because, as specimen diameters increase as a result of creep, the internal specimen void volume available to the gas content increases significantly when the initial void volume is small.

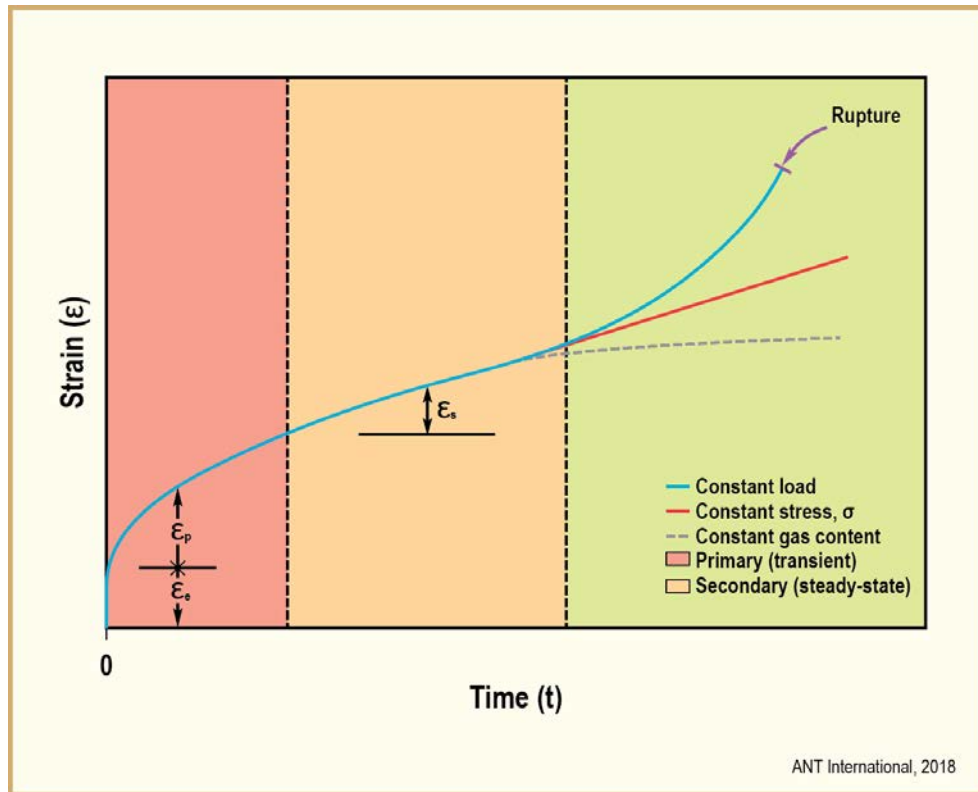


Figure 10-4: Typical shapes of creep curves (diametral strain versus time) obtained under constant load, constant stress, and constant gas content conditions.

## 10.2.4 Thermal Creep Deformation Mechanisms

### 10.2.4.1 Deformation Maps

Detailed accounts of various creep mechanisms can be found in the literature. Based on the different creep deformation mechanisms and experimental data, [Chin et al., 1986] developed a secondary creep deformation map for unirradiated, non-hydrided Zircaloy. Secondary creep rates are shown in black lines going across the different deformation kinetics regions in Figure 10-5, where  $\ln(\sigma/E)$  is plotted against  $T_m/T$ .

- $T_m$  is the melting temperature of Zircaloy equal to 2125 K
- $T$  is the temperature [K]
- $\sigma$  is the applied stress [MPa]
- $E$  is Zircaloy's Young's modulus equal to  $(11.09 - 11.61 T/T_m) \cdot 10^4$  MPa

For reference, a secondary creep rate [ $1/s$ ] of  $10^{-10} s^{-1}$  means that it takes ~3 years to achieve a 1% strain for as-fabricated Zircaloy tubing. Therefore, there is little interest in secondary creep rates that are below  $10^{-10} s^{-1}$ .

By inspection, it can be seen that for normal dry storage conditions ( $T < 673$  K and  $\sigma < 120$  MPa), grain boundary sliding and low/high temperature climb dominate. A boundary between two adjacent deformation kinetics regions means the two mechanisms involved contribute equally to the secondary creep strain rate value.

## 11 Trends and Needs

Improved fuel reliability and operating economics are the driving forces for changing operating conditions, while at the same time maintaining acceptable margins to operating and regulatory safety limits. Table 11-1 gives the trends for Burn Up (BU) achieved compared to regulatory limits in various countries. An approximate (“rule of thumb”) conversion of BU to fluence is 50 GWd/MT is equivalent to about  $1 \times 10^{26}$  n/cm<sup>2</sup>, E>1 MeV (or about 17 dpa), but this depends on many nuclear parameters such as enrichment, extent of moderation and neutron energy spectrum. In general, PWRs operate to higher discharge BUs compared with BWRs because of higher PWR power densities and neutron fluxes, but the differences are decreasing with improvements in fuel design and operating practices. There are some incentives to reach BUs of 60-70 GWd/MT batch average, but the economic benefits vary among countries and, in some instances, reactors within a country.. A majority of US plants and many in Europe have undergone power uprates, from a few percent to up to 20%. This increases the number of Fuel Assemblies (FAs) in a core that operates at high power, thereby decreasing the margin to established limits. In cooperation with utilities, fuel suppliers have operated Lead Test Assemblies (LTAs) or Lead Use Assemblies (LUAs) to very high BUs, in some cases approaching 100 GWd/MT peak rod exposures.

Table 11-1: Maximum BUs achieved vs. regulatory limits, (excludes LTAs).

Country	Batch	BU (GWD/MT)			
		Assembly	Rod	Pellet	Regulatory Limit
USA	57	60	62	73	62.5 peak rod
Belgium		50-55			55 UO <sub>2</sub> assy., 50 MOX assy.
Czech Republic	51	56	61		60 peak rod
Finland	45.6*	48.6	58		57 assy. (for PWR)
France	47	51 UO <sub>2</sub> 42 MOX			52 assy.
Germany	58	62	68		65 assy.
Hungary		50	62		
Japan	53	55	62		55 UO <sub>2</sub> assy., 45 MOX assy.
Korean Republic	46				60 rod
Netherlands	52	55	59		60 rod
Russia	60	65			
Spain	50.4	57.4	61.7	69	
Sweden	47	57.2	63.6	65	60 assy., 64 rod
Switzerland	68	71	73		80 pellet
Taiwan					60 rod (P), 54 assy. (B)
UK	44.3	46.5	50		55 pellet
Ukraine		50			
*Current batch design for 50 GWD/MT in BWR					
© ANT International, 2018					



As discussed in earlier sections, material properties and microstructure evolve as BU and fluence increase. Examples include:

- In PWRs, Zircaloy-4 no longer meets corrosion and hydriding performance needs; therefore, virtually all current PWR claddings now use a zirconium alloy containing Nb.
- Although not a new phenomenon, observed Second Phase Particle (SPP) dissolution and re-precipitation phenomena have required a new perspective on alloy development and Hydrogen Pick Up (HPU).
- BWR channel bow at high BU has requires a new understanding of the relationships between HPU, shadow corrosion and irradiation growth.

Current fuel performance limitations,:

- During Normal Operation are related to
  - Corrosion and Hydrogen Pickup (HPU)
  - Liftoff (reopening of the fuel cladding gap)(creep)
  - FA bowing (PWRs and VVERs) (HPU, creep, growth)
  - Fuel channel bowing (BWRs)(HPU, growth)
- During Anticipated Operational Occurrences (AOO)<sup>40</sup> are related to
  - Pellet Cladding Interaction (PCI) (ductility)
  - Pellet Cladding Mechanical Interaction (PCMI) (HPU, ductility)
- During Design Basis Accidents (DBA) are related to
  - HPU
- During Interim Dry Storage are related to
  - HPU

A broader listing of issues needing resolution include the following

HPU and Hydrogen Pickup Fraction (HPUF)<sup>41</sup>

- BWRs and PWRs:
  - Hydrogen Pickup - how the hydrogen gets into the Zr material (driving force and mechanisms), including roles of sub-oxides, oxide porosity, and localized electrical charges

---

<sup>40</sup> PCI seems to be re-emerging as a regulatory issue for fuel that is not resistant to I-SCC. This applies to PWRs because many are being forced to use control blades for rapid changes in power to compensate for irregularities in wind and solar production. The issue of AOOs also extend to I-SCC as discussed in Section 2 of this Report. PCMI, corrosion and hydriding are a separate item based on the effects of hydrides on cladding ductility.

<sup>41</sup> Hydrogen Pickup Fraction (HPUF) is the fraction of corrosion hydrogen released by the zirconium alloy - water corrosion reaction that is picked up by the zirconium alloy. 100 % HPUF means that all of the hydrogen from the water molecule is being picked up by the zirconium alloy.

- Role and kinetics of Fe, Cr, Ni and Nb from dissolving SPPs in Zry and Zr-Nb alloys on mechanical properties (and corrosion and dimensional stability.)
- Effect of <c> loops on strength and ductility

Dimensional stability:

- Effect of hydrogen on irradiation growth mechanisms.
- PWR FA bowing mechanism. Not only a material problem, but also a mechanical engineering design concern.
- BWR fuel channel bowing mechanism and parameters affecting it such as: texture, residual stress, flux gradient, hydrogen and hydrogen gradient.
- Mechanism of <c> loop formation in zirconium alloys.
- Mechanisms of both irradiation and post-irradiation creep.
- Roles of Nb and Fe in decreasing irradiation growth.
- The effects of texture and HPU of Zr-Nb alloys as related to growth of PWR guide tubes.
- Effects of thermal and radiation induced relaxation of Zr and Ni- alloys, particularly relative to steam generators.
- The extent of interdependency of creep and growth
- The mechanism of post- breakaway increase of growth rate in Zircaloy and , perhaps, Zr-Nb alloys.
- Effects of tin and carbon on irradiation growth
- Effect of hydrogen and hydrides on irradiation creep
- Effects of temperature in the range 300 – 400 °C on growth and SPP stability

PCI and PCMI:

- PCMI failure mechanism during outside in-cracking, and possible relevance to failure mechanism for high BU fuel?
- Outside in-cracking both for BWR and PWR (new) claddings at high burnups. Requires discussion about crack growth direction. In some cases may be the reverse due to PIE micrographic artefact.
- PCI failure mechanisms due to Missing Pellet Surfaces (MPSs).
- PCI mechanism and performance of liner/barrier and/or pellets with additives at high BU.
- Refined knowledge of the embrittling species for SCC during power ramps

LOCA:

- Verification of coolant blockage with real fuel rods in lattice design, related to maintenance of coolable geometry.
- Conditions leading to formation of brittle alpha-Zr layers.

## References

- 10 CFR Part 50 Appendix A, *General Design Criteria for Nuclear Power Plants*, U.S. Government Printing Office, Washington, 1990a.
- 10 CFR Part 100.11, *Determination of Exclusion Area, Low Population Zone, and Population Centre Distance*, U.S. Government Printing Office, Washington, 1990b.
- Abolhassani S., Bart G., Bertsch J., Grosse M., Hallstadius L., Hermann A., and Wiese H., (2015), *Corrosion and Hydrogen Uptake in Zirconium Claddings Irradiated in Light Water Reactors*, 17th Zirconium in the Nuclear Industry ASTM-STP 1543. p. 540-573.
- ACRS, *Susquehanna Steam Electric Station Units 1 and 2 Extended Power Uprate Application*, United States Nuclear Regulatory Commission Advisory Committee on Reactor Safeguards, Washington, D.C., USA, 2007.
- Adamson R. B., *Effects of Neutron Irradiation on Microstructure and Properties of Zircaloy*, Zirconium in the Nuclear Industry; Twelfth International Symposium, ASTM STP 1354, pp. 15-31, West Conshohocken, PA, 2000.
- Adamson R. B., *Recovery of Irradiation Damage by Posts-Irradiation Thermal Annealing-Relevance to Hydrogen Solubility and Dry Storage Issues*, EPRI Technical Report 1013446, June 2006.
- Adamson R. et al., *Pellet-Cladding Interaction (PCI and PCMI)*, Vol ZIRAT-11 Special Topic Report, Advanced Nuclear Technology International, Skultuna, Sweden, 2006.
- Adamson R. et al., *Corrosion Mechanism in Zirconium Alloys*, ZIRAT12, Advanced Nuclear Technology International, Skultuna, Sweden, 2007.
- Adamson R., Garzarolli F. and Patterson C., *In-Reactor Creep of Zirconium Alloys*, ZIRAT14/IZNA9 Special Topical Report, ANT International, Mölnlycke, Sweden, 2009a.
- Adamson R. et al., *ZIRAT14/IZNA9 Annual Report*, ANT International, Mölnlycke, Sweden, 2009b.
- Adamson R., *Zirconium Production and Technology: The Kroll Medal Papers 1975-2010*, ASTM RPS2, ASTM I, West Conshohocken, PA, 2010.
- Adamson R. et al., *ZIRAT16 Annual Report*, Advanced Nuclear Technology International, Mölnlycke, Sweden, 2011.
- Adamson R., Coleman K., Mahmood T. and Rudling P., *Mechanical Testing of Zirconium Alloys*, ZIRAT18/IZNA13 Special Topic Report, Vols. I and II, Advanced Nuclear Technology International, Mölnlycke, Sweden, 2013.
- Adamson R., *Charged Particle Bombardment in Zirconium Alloys – A Review*, ZIRAT19/IZNA14 Special Topic Report, ANT International, Mölnlycke, Sweden, 2014.
- Adamson R. et al., *ZIRAT21 Annual Report*, ANT International, Mölnlycke, Sweden, 2016.
- Adamson R., Griffiths M. and Patterson C., *Irradiation Growth of Zirconium Alloys*, ZIRAT 22 Special Topic 3674 Report, A.N.T. International, Tollerød, Sweden, 2017.
- Adamson R., Griffiths M. and Coleman C. E., *Irradiation Creep and Growth of Zirconium Alloys*, J. Nucl. Mat., 2019, in press.
- Adrych-Brunning A. et al., *Modelling the Interaction of Primary Irradiation Damage and Precipitates: Implications for Experimental Irradiation of Zirconium Alloys*, J. Nucl. Mater. 498, pp. 282-289, 2018.
- Ahmedabadi P.M. and Was G.S., “Stress Corrosion Cracking of Ferritic-Martensitic Steels in Simulated Boiling Water Reactor Environment”, Corrosion, Vol. 72, January 2016, pp. 66-77, 2016.

- Beale J., *Fuel Performance Data*, International Utility Nuclear Fuel Performance Conference, June 22-23, 2016, Charlotte, North Carolina, USA, 2016.
- Beale J., Yoon B., Daum R. and Hanlon S., *Estimation of Hydrogen in Zircaloy Using Multi Frequency Eddy Current*, TopFuel, Paper AO211, 2018.
- Bell B.D. et al., *The Influence of Alloying Elements on the Corrosion of Zr Alloys*, Corrosion Science 105 (2016) 36–43.
- Bentejac F. and Hourdequin N., *TOUTATIS: An Application of the Cast3M Finite Element Code for PCI Three-Dimensional Modelling*, Pellet-clad Interaction in Water Reactor Fuels, Aix-en-Provence, France, OECD Nuclear Energy Agency, NEA No. 6004, 2004.
- Bergmann U. C., King J., “Triton11<sup>TM</sup> – Westinghouse 11x11 BWR Fuel Design,” In proceedings of Top Fuel 2016, Boise, ID, USA, September 11-15, 2016, paper 17668, (2016).
- Bergmann et al., “Out-of-pile Verification of Triton11 BWR Fuel”, TopFuel Prague, 2018.
- Bernaumat C. et al., “Updated RIA Criteria in France”, TopFuel, Prague, 2018.
- Besch O. A. et al., *Corrosion Behavior of Duplex and Reference Cladding in NPP Grohnde*, Zirconium in the Nuclear Industry — Eleventh Inter. Symp., ASTM STP 1295, E.R. Bradley and G.P. Sabol (Eds), ASTM, West Conshohocken, PA. pp. 805–824, 1996.
- Besmann T., *SOLGASMIX-PV, A Computer Program to Calculate Equilibrium Relationships in Complex Chemical Systems*, Oak Ridge National Laboratory, Oak Ridge, Tennessee, USA, 1977.
- Besmann T. et al., *Modelling Thermochemistry of Fuel and Coupling to Fuel Performance Codes*, Top Fuel 2016, Boise, Idaho, USA, American Nuclear Society, 2016.
- Bickel G.A., and Griffiths M., *Manufacturing Variability*, Microstructure and Deformation of Zr-2.5Nb Pressure Tubes, Fifteenth International Symposium on Zirconium in the Nuclear Industry, STP 1505, 2009. Published by J. of ASTM Int., Vol. 4, No. 10, DOI: 10.1520/STP48153S, pp. 529-540, 2009.
- Bickel G. A. et al., *Development of Zr 2.5Nb Pressure Tubes for Advanced CANDU Reactor*, Sixteenth International Symposium on Zirconium in the Nuclear Industry, Chengdu, China, June 2010.
- Bickel G.A., “Improved Zr-2.5Nb Pressure Tubing for Future HW Reactors,” [www.iaea.org/inis/collection/NCLCollectionStore/\\_Public/45/017/45017242.pdf](http://www.iaea.org/inis/collection/NCLCollectionStore/_Public/45/017/45017242.pdf), 2013.
- Bickel G.A., private communication, 2018.
- Billone M., Yan Y., Burtseva T. and Daum R., *Cladding Embrittlement During Postulated Loss-of-Coolant Accidents*, USNRC Report, NUREG/CR-6967, 2008.
- Bischoff J. et al., *AREVA NP'S Enhanced Accident Tolerant Fuel Developments: Focus on Cr Coated M5<sup>TM</sup> Cladding*, WRFPM 2017, Korea.
- Bischoff J. et al., *Cr-coated Cladding Development at Framatome*, TopFuel 2018, Prague, Czech Republic, Paper AO152, 2018.
- Bossis P. et al., *In PWR Comprehensive Study of High Burn-up Corrosion and Growth Behaviour of M5 and Recrystallised Low-Tin Zircaloy-4*, 15th ASTM International Symposium: Zirconium in the Nuclear Industry, ASTM I, STP 1505, pp. 430-456, Sunriver, OR, June 25-27, 2009.
- Bouffieux P. and Rupa N., *Impact of Hydrogen on Plasticity and Creep of Unirradiated Zry-4 Cladding Tubes*, Zirconium in the Nuclear Industry: Twelfth International Symposium, ASTM STP 1354, Sabol G. and Moan G., Eds., American Society for Testing and Materials, pp. 399-422, West Conshohocken, PA, 2000.

- Carpenter G. J. C., Coleman C. E. and MacEwen S. R., *Proceedings of the International Conference on Fundamental Mechanisms of Radiation Induced Creep and Growth*, Chalk River, May 8-10, 1979 (also J. Nucl. Mat. 90, 1980).
- Carpenter G.J.C., Murgatroyd R.A. and Rogerson A., Watters J.F., *Irradiation Growth of Zirconium Single Crystals*, J. Nucl. Mater. 101 (1981) 28.
- Causey A. R., Fidleris V., MacEwen S. R. and Schulte C. W., *In-reactor Deformation of Zr<sub>2</sub>5Nb Pressure Tubes*, ASTM Spec. Techn. Publ. 956, pp. 54-, 1988a.
- Causey A.R., Woo C.H. and Holt R.A., *The Effects of Intergranular Stresses on the Texture Dependence of Irradiation Growth in Zirconium*, J. Nucl. Mater., Vol. 159, pp. 225-236, 1988b.
- Causey A. R., Butcher F. J. and Donohue S. A., *Measurements of Irradiation Creep of Zr Alloys Using Stress Relaxation*, J. Nucl. Mat. 159, pp. 101-113, 1988c.
- Causey A. R., Elder J. E., Holt R. A. and Fleck R. G., *On the Anisotropy of In-reactor Creep of Zr-2.5Nb Tubes*, ASTM STP 1245, pp. 202-220, 1994.
- Chabretou V. and Mardon J.P., *M5 Alloy High Burnup Behaviour*, KTG Fachtag on Status of LWR Fuel Development and Design Methods, Dresden, March 2-3, 2006.
- Chapin D. L. et al., *Optimized ZIRLO Qualification Program for EDF Reactors*, In *Proceedings of Top Fuel 2009*, number Paper 2040, pages 60-65, Paris, France, September 6-10, 2009.
- Chapman R. H. and Crowley J. L., Longest A. W. and Sewell E. G. Effect of Creep Time and Heating Rate on Deformation of Zircaloy-4 Tubes Tested in Steam with Internal Heaters. Technical Report NUREG/CR-0343, ORNL/NUREG/TM-245, US NRC, October 1978.
- Chapman R. H., Crowley J. L., Longest A. W. and Hofmann G. Zirconium Cladding Deformation in a Steam Environment with Transient Heating. In *Zirconium in the Nuclear Industry: Fourth Conference*, volume ASTM STP 681, pages 393-408. American Society for Testing and Materials, 1979.
- Cheadle B. A., *The Development of Zr-2.5Nb Pressure Tubes for CANDU Reactors*, J. ASTM International, Vol. 7, No. 8, pp. 1-15, 2010.
- Cheng B. et al., *Zr-Alloy Lined Molybdenum Fuel Cladding To Enhanced Accident Tolerance*, 2017 Water Reactor Fuel Performance Meeting, Jeju Island, South Korea, Sep. 10-14, 2017.
- Chin B. A., Khan M. A. and Tarn J. C. L., *Deformation and Fracture Map Methodology for Predicting Cladding Behaviour During Dry Storage*, PNL Report 5998, 1986.
- Chiu W-J., Cheng S-C., Shiu Y-H. and Tseng C-C., *Results of Post-Irradiation Examinations for BWR Failure Rods*, Proceedings of Top Fuel 2009, Paris, France, September 6-10, 2009.
- Christensen M. et al., *Effect of Hydrogen on Dimensional Changes of Zirconium and the Influence of Alloying Elements: First Principles and Classic Simulations of Point Defects, Dislocation Loops and Hydrides*, Zirconium in the Nuclear Industry: 17th International Symposium, STP 1543, Robert Comstock and Pierre Barberis, Eds., p. 55, doi:10.1520/STP154320120170, ASTM International, West Conshohocken, PA, 2015.
- Christodoulou N. et al., "Modelling the Effect of Texture and Dislocation Structure on Irradiation Creep of Zirconium alloys," Effects of Radiation on Materials: 16th International Symposium. ASTM STP 1175, A.S. Kumar, D.S. Gelles, R.K. Nanstad, and E.A. Little, Eds., ASTM Philadelphia, pp. 1111-1128, 1993.
- Christodoulou N. et al., *Modelling In-reactor Deformation of Zr-2.5Nb Pressure Tubes in CANDU Power Reactors*, Zirconium in the Nuclear Industry: Eleventh International Symposium, ASTM 1295, E.R. Bradely and G. P. Sabol, Eds. American Society for Testing and Materials, Philadelphia, pp. 518-537, 1996.

- DeCarlan Y. et al., *Influence of Iron on the Nucleation of c-Component Dislocation Loops in Irradiated Zircaloy-4*, Proc. 11th Int. Symp. on Zr in the Nuclear Industry, Garmisch, Germany, Sept. 1995, ASTM STP 1295, p.638, 1996.
- Deck C. P. et al., *Demonstration of Engineered Multi-Layered SiC/SiC Cladding with Enhanced Accident Tolerance*, TopFuel Conference, Prague, 2018.
- Del Rio Luna I., Muñoz Sicilia A., Pan G. and Long, Y., “In-reactor Creep Behavior of ZIRLO® and Optimized ZIRLO™ Cladding,” Top Fuel 2018, Prague, Sept.-Oct. 2018.
- Delafoy C. et al., *Benefits of Framatome’s E-ATF Evolutionary Solution: Cr-coated Cladding with Cr<sub>2</sub>O<sub>3</sub>-doped UO<sub>2</sub> Fuel*, TopFuel 2018, Prague, Czech Republic, Paper AO149, 2018.
- Desquines J. and Guilbert S., *Effect of An Oxide Layer on the Result of a Ring Compression Test on a Fuel Cladding Sample After a Simulated LOCA Transient*, TopFuel 2018, Prague, Czech Republic, Paper AO040, 2018.
- Dieter G.E., *Mechanical Metallurgy*, McGraw-Hill Book Company, NY., 1988.
- DOE, *Development of Light Water Reactor Fuels with Enhanced Accident Tolerance*, US Department of Energy, Report to Congress, April 2015.
- Dollins C. C. and Nichols F. A., "Mechanisms of Irradiation Creep in Zirconium-Base Alloys," *Zirconium in Nuclear Applications*, ASTM STP 551, American Society for Testing and Materials, p. 229, 1974.
- Dollins C.C., *In-Pile Dimensional Changes in Neutron Irradiated Zirconium Base Alloys*, J. Nucl. Mater. 59, pp 61-76, 1976.
- Donaldson A.T., and Healey, T., *Creep Deformation of Westinghouse Zircaloy-4 Fuel Cladding Tubes in Alpha Plus Beta Phase Temperature Range*. Technical Report TRPD/B/0564/N85, Central Electricity Generating Board, Berkeley, Gloucestershire, UK, 1984.
- Donaldson A.T., Healey T., and Horwood R.A.L., *Creep Behaviour of Westinghouse Zr-4 Fuel Between 973 and 1073 K*, Technical Report TRPD/B/0008/N82, Central Electricity Generating Board, Berkeley, Gloucestershire, UK, 1985.
- Du D.X. and Woo C.H., “Effect of Grain-Structure Topology in Modelling Aggregate Irradiation Creep behaviour of Two-Phase Alloys”, *Comp. Mat. Sci.*, Vol. 23, pp. 260–269, 2002.
- Dutton R., Nuttall K., Puls M.P. and Simpson L.A., *Mechanisms of Hydrogen Induced Delayed Cracking in Hydride Forming Materials*, *Met. Trans. A*, 8A, pp. 1553-1562, 1977.
- EIA, *Spent Nuclear Fuel, Average Discharge Burnups, Table 3*. [https://www.eia.gov/nuclear/spent\\_fuel](https://www.eia.gov/nuclear/spent_fuel), U.S. Energy Information Agency, 2015.
- Einstein A., *Über die von der molekularkinetischen Theorie der Wärme geforderte Bewegung von in ruhenden Flüssigkeiten suspendierten Teilchen*, *Annalen der Physik*, 322, pp. 549-560, 1905.
- Einziger R.E., Atkin S.D., Stellrecht D.E. and Pasupathi V., *High Temperature Postirradiation Materials Performance of Spent Pressurized Water Reactor Fuel Rods under Dry Storage Conditions*, *Nuclear Technology*, Vol 57, Issue 1, pp. 65-80, 1982.
- Ensor B. et al., (2017), The Role of Hydrogen in Zirconium Alloy Corrosion, *Journal of Nuclear Materials*, vol. 496, p. 301-312.
- EPRI, *Spent Fuel Transportation Applications: Fuel Rod Failure Evaluation under Simulated Cask Side Drop Conditions*. EPRI, Palo Alto, CA. 2005. 1009929.
- EPRI, *Fuel Reliability Program: Proposed RIA Acceptance Criteria*, EPRI TR 1021036, December 2010.

- Forgeron T. et al., Experiment and Modeling of Advanced Fuel Rod Cladding Behavior under LOCA Conditions: Alpha-Beta Phase Transformation Kinetics and EDGAR Methodology. In G. P. Sabol and G. D. Moan, editors, *Zirconium in the Nuclear Industry: Twelfth International Symposium*, volume ASTM STP 1354, pages 256-278, West Conshohocken, PA, USA, 2000. American Society for Testing and Materials.
- Foster J., Yueh H. K. and Comstock, R.J., *ZIRLO Cladding Improvement*, ASTM 15<sup>th</sup> International Symposium, Sunriver, OR, June, 2007.
- Foster J. P. et al., *ZIRLO Cladding Improvement*, Journal of ASTM International, Vol. 5, No. 7, Paper ID JAI101188, 2008.
- Foster J. P., Yueh H. K. and Comstock R. J., *ZIRLO Cladding Improvement, Zirconium in the Nuclear Industry*, 15th International Symposium, ASTM STP1505, B. Kammezdind and M. Limbäck, Eds., ASTM International, West Conshohocken, PA, pp. 457-469, 2009.
- Foster J.P., Pan G., Cai L., and Atwood A.R., *Effect of Hydrogen on Irradiation Creep and Growth for ZIRLO™ Alloy and Zr-1.0Nb*, Zirconium in the Nuclear Industry, 18<sup>th</sup> International Symposium, ASTM STP 1597, R.J. Comstock and A.T. Motta, Eds., ASTM International, West Conshohocken, PA, (2018), pp. 725-747, <http://dx.doi.org/10.1520/STP159720160058>.
- Franklin D. G., Lucas G. E. and Bement A. L., *Creep of Zirconium Alloys in Nuclear Reactors*, ASTM PCN 04-815000-35, ASTM, Philadelphia, 1983.
- Franklin D. G. and Adamson R. B., *Implications of Zircaloy Creep and Growth to Light Water Reactor Performance*, J. Nucl. Mat. 159, pp. 12-21, 1988.
- Franklin D.G., *Performance of Zirconium Alloys in Light Water Reactors with A Review of Nodular Corrosion*, J. ASTM Intl., 7, doi:10.1520/JAI103032, 2010.
- Frenkel J. M. and Weisz M., *Influence of Metallurgical Parameters and Neutron Flux on Creep of Zircaloy 4 Cladding Tubes*, Int. Conf. On Nuclear Fuel Performance, London, 15-19. October, 1973.
- F-SECT Nuclear Application System – *User’s Manual*, CESI Report B4013589, 2014.
- Fuketa T., Sasajima H. and Sugiyama T., *Behaviour of High-burnup PWR Fuels with Low-tin Zircaloy-4 Cladding Under Reactivity-initiated-accident Conditions*, Nucl. Technology, 133, pp. 50-62, 2001.
- Fuse M., *Analysis of Irradiation Growth in Zirconium-Base Alloy*, J. Nucl. mater. Vol. 140, pp. 131-139, 1986.
- Garat V., Personal communication, 2016.
- Garde A.M., (1991) *Enhancement of Aqueous Corrosion of Zircaloy-4 due to Hydride Precipitation at the Metal-oxide Interface*, in: Zirconium in the Nuclear Industry: 9<sup>th</sup> International Symposium, ASTM STP 1132, pp. 566-594.
- Garde A., Slagle W. and Mitchell D., *Hydrogen Pick-Up Fraction for ZIRLO Cladding Corrosion and Resulting Impact on the Cladding Integrity*, TopFuel Conference, Paris France, September 2009.
- Garner A., et al., *The Effect of Sn Concentration on Oxide Texture and Microstructure Formation in Zirconium Alloys*, Acta Materialia 99 (2015) 259–272.
- Garner A. et al., (2018), *Investigating the Effect of Zirconium Oxide Microstructure on Corrosion Performance: A Comparison between Neutron, Proton and Non-irradiated Oxides*, In : 18<sup>th</sup> International Symposium on Zirconium in the Nuclear Industry, ASTM STP 1597, p. 491-523.
- Garnier C. et al., *The COPERNIC Mechanical Model And Its Application To Doped Fuel, Pellet-clad Interaction in Water Reactor Fuels*, Aix-en-Provence, France, OECD Nuclear Energy Agency, NEA No. 6004, 2004.



- Golubov S. I., Barashev A. V., Stollar R. E. and Singh B. N., *Breakthrough in Understanding Radiation Growth of Zirconium*, Zirconium in the Nuclear Industry: 17th International Symposium, STP 1543, R.Comstock and P. Barberis, Eds., p. 729, ASTM International, West Conshohocken, PA, 2015.
- Gong W., Trtik P., Valance S. and Bertsch J., *Hydrogen Diffusion Under Stress in Zircaloy: High-resolution Neutron Radiography and Finite Element Modeling*, J. Nucl. Mater., 508, pp. 459-464, 2018.
- Grandjean C., *A State of Art Review of Past Programs Devoted to Fuel Behavior under LOCA Conditions: Part I*, Technical Report NT SEMCA 2005-313, IRSN, Cadarache, France, December 2005.
- Grapengiesser B. and Hallstadius L., “*Non-destructive Pool-side Methods for Fission Gas Release Determination and Fuel Column Characterisation of Intact Fuel Rods*”, Ninth International Conference on Non-destructive Evaluation in the Nuclear Industry, Tokyo, Japan, April 25-28, (1998).
- Griffiths M., White J., Loretto M.H. and Smallman R.E., *Radiation Damage in Zr and Ti*, Proc. Yamada Conf. V on Point Defects and Defect Interactions in Metals, Kyoto, University of Tokyo Press, J. Takamura, M. Doyama and M. Kiritani, Eds., p. 880, 1982.
- Griffiths M., Loretto M.H. and Smallman R.E., *Anisotropic Distribution of Dislocation Loops in HVEM-irradiated Zr*, Phil. Mag. A, Vol.49, No.5, p.613, 1984.
- Griffiths M. and Gilbert R.W., *The Formation of c-Component Defects In Zirconium Alloys During Neutron Irradiation*, J. Nucl. Mater., Vol. 150, pp. 169-181, 1987.
- Griffiths M., Gilbert R.W. and Fidleris W., Adamson R.B. and Tucker, R.P., *Neutron Damage in Zirconium Alloys Irradiated at 644 to 710K*, J. Nucl. Mater., Vol. 150, p. 159, 1987.
- Griffiths M., *A Review of Microstructure Evolution in Zirconium Alloys*, Journal of Nuclear Materials, Vol.159, pp.190-218, 1988.
- Griffiths M., Gilbert R. W. and Coleman C. E., *Grain Boundary Sinks in Neutron-irradiated Zr and Zr-alloys*, Journal of Nuclear Materials, Vol. 159, pp. 405-416, 1988.
- Griffiths M., Gilbert R.W. and Fidleris V., *Accelerated Irradiation Growth of Zirconium Alloys*, Proc. 8th Int. Symp. on Zr in the Nuclear Industry, ASTM STP 1023 p. 658, 1989.
- Griffiths M., *Evolution of Microstructure in HCP Metals During Irradiation*, J. Nucl. Mater. Vol. 205, pp. 225-241, 1993.
- Griffiths M. et al., *Evolution of Microstructure in Zirconium Alloy Core Components of Nuclear Reactors during Service*, Effects of Radiation on Materials: 16th. International Symposium, ASTM STP 1175, A.S. Kumar, D.S. Gelles, R.K. Nanstad, E.A. Little, Eds., American Society for Testing and Materials, 1077 – 1110, Philadelphia, 1993a.
- Griffiths M., Gilbon D., Regnard C. and Lemaignan C., *HVEM Study of the Effects of Alloying Elements and Impurities on Radiation Damage in Zr-Alloys*, J. Nucl. Mater., Vol. 205, pp. 273-283, 1993b.
- Griffiths M. et al., *Study of Point Defect Mobilities in Zirconium During Electron Irradiation in a High-Voltage Electron Microscope*, J. Nucl. Mat. 208, pp. 324-334, North-Holland, 1994.
- Griffiths M., Holt R.A., and A. Rogerson, A., *Microstructural Aspects of Accelerated Deformation of Zirconium Alloy Nuclear Reactor Components*, J. Nucl. Mater., Vol. 225, p. 245, 1995.
- Griffiths M., Mecke J. F. and Winegar J. E., *Evolution of Microstructure in Zirconium Alloys During Irradiation*, Zirconium in the Nuclear Industry: 11th Int'l Symposium, ASTM STP 1295, E. R. Bradley and G. P. Sabol, Eds., American Society for Testing and Materials, pp. 580-602, 1996.

- Jezequel T. et al., *Stress Corrosion Crack Initiation of Zircaloy-4 Cladding Tubes in an Iodine Vapor Environment during Creep, Relaxation, and Constant Strain Rate Tests*. Journal of Nuclear Materials, 499, pp 641-651, 2018.
- Jostsons A., Kelly P. M. and Blake R. G., *Faulted Loops in Neutron-Irradiated Zirconium*, J. Nucl. Mater., Vol. 68, pp. 267-276, 1977.
- Jostsons A., Kelly P. M., Blake R. G. and Farrell K., *Neutron Irradiation-Induced Defect Structures in Zirconium*, Effects of Radiation on Structural Materials. ASTM STP 683. J. A. Sprague and D. Kramer, Eds., American Society for Testing and Materials, pp. 46-61, 1979.
- Julien J. et al., *Adjustment of Fuel Creep Behaviour Based on Post-Ramp Dish Filling Observations and 3D Simulations, Impact on Clad Ridges*, Top Fuel 2012, Manchester, UK, European Nuclear Society, 2012.
- Jung Y-I et al., *Formation of A Dispersed Oxide Layer on Zircaloy-4 By A Laser-Beam-Induced Surface Treatment*, 2017 Water Reactor Fuel Performance Meeting, Jeju Island, South Korea, Sep. 10-14, 2017.
- Jyrkhamä M.I., Bickel G. A. and Pandey M.D., *Statistical Analysis and Modelling of In-reactor Diametral Creep of Zr-2.5Nb Pressure Tubes*, Nuclear Engineering and Design, Vol. 300, pp. 241-248, 2016.
- Kakiuchi K. et al., *Irradiated Behavior for BWR Advanced Zr Alloy (HiFi alloy)*, Water Reactor Fuel Performance Meeting Kyoto, Japan, 2005.
- Kakiuchi K. et al., *Progress on ATF development of SiC for LWR*, Top Fuel, Boise, ID, September 2016.
- Kamimura K. et al., *Thermal Creep Tests of BWR and PWR Spent Fuel Cladding*, Conference on Storage of Spent Fuel in Power Reactors, Conference 2003, pp. 375-386, IAEA-CSP-20/CD, Vienna, October, 2003.
- Kamimura K., *Integrity Criteria of Spent Fuel for Dry Storage in Japan*, International Seminar on Spent Fuel Storage (ISSF) 2010, Tokyo, Japan, November 15-17, 2010.
- Karb E. H. et al., *LWR Fuel Rod Behavior during Reactor Tests under Loss-of-coolant Conditions: Results of the FR2 In-pile Tests*. J. Nucl. Mater., 107:55-77, 1982.
- Karb E. H. et al., *LWR Fuel Rod Behavior in the FR2 In-pile Tests Simulating the Heatup Phase of a LOCA*, Technical Report KfK 3346, Kernforschungszentrum Karlsruhe, Germany, March 1983.
- Karlsson J. et al., “Modelling Out-of-Pile LOCA Tests on High Burnup Fuel Rods. Results of the fourth SCIP Modelling Workshop”, TopFuel Prague, 2018.
- Karoutas Z. E. et al., *Westinghouse Accident Tolerant Fuel Plant Benefits*, 2017 Water Reactor Fuel Performance Meeting, Jeju Island, South Korea, Sep. 10-14, 2017.
- Karoutas Z. et al., *Update On Westinghouse Benefits Of Encore® Fuel*, Topfuel Conference, Prague, 2018.
- Kaspar G., Peehs M. and Steinberg E., *Experimental Investigation of Post Pile Creep of Zircaloy Cladding Tubes*, 8<sup>th</sup> SMIRT Conference, Brüssel, Belgium, 1985.
- Kearns J. J., *Thermal Expansion and Preferred Orientation in Zircaloy*, WAPD-TM-472, 1965.
- Kearns J., *Terminal Solubility and Partitioning of Hydrogen in the  $\alpha$  Phase of Zirconium, Zircaloy-2, and Zircaloy-4*, Journal of Nuclear Materials, Vol. 22, p. 292, 1967.
- Kelly A.F. and Knowles, *Crystallography and Crystal Defects*, Wiley, 2012.

- Pizzocri D. et al., “IAEA FUMAC Benchmark on the Halden, Studsvik and Quench-L1 LOCA Tests”, TopFuel Prague, 2018.
- Platt P. et al., (2015), A Study into the Impact of Interface Roughness Development on Mechanical Degradation of Oxides Formed on Zirconium Alloys, *J Nucl Mater*, vol. 459, p. 166-174.
- PNNL Report 22549, *Pellet-Cladding Mechanical Interaction Failure Threshold for Reactivity Initiated Accidents for Pressurized Water Reactors and Boiling Water Reactors*, (ADAMS ML13277A368) June 2013.
- Porter I. E., *FAST: The Merger of NRC'S Fuel Performance Codes FRAPCON and FRAPTRAN for Scoping and Regulatory Decision Making*, 2017 Water Reactor Fuel Performance Meeting, Jeju Island, South Korea, Sep. 10-14, 2017.
- Powers D. A. and Meyer, R. O., *Cladding Swelling and Rupture Models for LOCA Analysis*, Technical Report NUREG-0630, US NRC, April 1980.
- Procedure for Conducting Oxidation and Post-Quench Ductility Tests with Zirconium- based Cladding Alloys, Argonne National Laboratory (ANL), March 31, 2009.
- Puls M.P., *The Effect of Hydrogen and Hydrides on the Integrity of Zirconium Alloy Components*, Springer-Verlag, London, 2012.
- Powers J. J. and Terrani K. A., *Uranium Nitride: Enabling New Applications for TRISO Fuel Particles*, Top Fuel 2013, Charlotte, North Carolina, September 15-19, 2013.
- Rautenberg M. et al., *Improvements of PCMI Criterion for Anticipated Operational Occurrences*, Top Fuel 2018 Reactor Fuel Performance, Prague, Czech Republic, 2018.
- Ray S., *Benefits of Accident Tolerant Fuels for Today's Reactors – The US Perspective*, Plenary session presentation, 2017 Water Reactor Fuel Performance Meeting, Jeju Island, South Korea, Sep. 10-14, 2017.
- Rebak R.B., Brown N. R. and Terrani K. A., “Assessment of Advanced Steels as Accident Tolerant Fuel Cladding for Commercial LWRs”, Paper 227, 17th International Conference on Environmental Degradation of Materials in Nuclear Power Systems – Water Reactors, 9-12 August 2015, Ottawa, Ontario, 2015.
- Rebak R.B., Jurewicz T. B. and Kim Y-J, *Oxidation Resistance of FeCrAl in Simulated BWR and PWR Water Chemistries*, WRFPM 2017, Jeju Island, 2017.
- Rebeyrolle V. et al., *Influence of Sulfur Addition on Irradiation Creep of M5 Alloy*, poster, 14th International Symposium on Zirconium in the Nuclear Industry, Stockholm, Sweden, June, 2004.
- RG-1.77, Regulatory Guide 1.77 – Assumptions Used for Evaluating a Control Rod Ejection Accident for Pressurized Water Reactors, US Atomic Energy Commission, 1974.
- Ribis J. et al., *Experimental and Modelling Approach of Irradiation Defects Recovery in Zirconium Alloys Impact of Applied Stress*, (ASTM Zr meeting, Sunriver, June, 2007), Journal of ASTM International, June, 2007.
- Richmond D. and Geelhood K., *Expanded Assessment of Fast For Power Ramp Cases with Short Hold Times and Advanced UO<sub>2</sub> Fuel with Various Dopants*, Top Fuel 2018 Reactor Fuel Performance, Prague, Czech Republic, Eurpeperan Nuclear Society, 2018.
- Rickover H. G., *The Decision to Use Zirconium in Nuclear Reactors, Zirconium Production and Technology: The Kroll Medal Papers 1975-2010*, R.B. Adamson, Ed., ASTM International, RPS2, pp. 9-17, 2010.
- Rishel D. M., Eklund K. L. and Kammenzind B. F., *In-situ EIS Measurements of Irradiated Zircaloy-4 Post-Transition Corrosion Kinetic Behaviour*, Journal of ASTM International, Vol. 5, No. 7, Paper ID JAI101206, 2008.

- Waeckel N., *Using e-ATF in Nuclear Power Plants: Utility Perspectives*, Plenary session paper, 2017 Water Reactor Fuel Performance Meeting, Jeju Island, South Korea, Sep. 10-14, 2017.
- Walker C. et al., *On the Oxidation State of UO<sub>2</sub> Nuclear Fuel at a Burn-up of around 100 MWd/kgHM*, Journal of Nuclear Materials, 345, pp 192-205, 2005.
- Walters L., Bickel G. A. and Griffiths M., *The Effects of Microstructure and Operating Conditions on Irradiation Creep of Zr<sub>2.5</sub>Nb Pressure Tubing*, ASTM Zirconium in the Nuclear Industry, Hyderabad, India, 2013.
- Walters L., Bickel G. A. and Griffiths M., *The Effects of Microstructure and Operating Conditions on Irradiation Creep of Zr<sub>2.5</sub>Nb Pressure Tubing*, Zirconium in the Nuclear Industry: 17th International Symposium, ASTM STP 1543, R.J. Comstock, P. Barberis, Eds, ASTM International, West Conshohocken, PA, pp. 693-725, 2015.
- Walters L., Douglas S.R. and Griffiths, M., *Equivalent Radiation Damage in Zirconium Alloys Irradiated in Various Reactors*, Zirconium in the Nuclear Industry: 18th International Symposium, STP 1597, R.J. Comstock and A.T. Motta, Eds., ASTM International, West Conshocken, PA, pp. 676-690, 2018.
- Watkins B. and Wood D. S., *The Significance of Irradiation-induced Creep on Reactor Performance of Zircaloy-2 Pressure Tubes*, ASTM STP 458, P226, 1969.
- Weidinger H.G., *Fabrication of Zirconium Alloy Cladding Tubes and Other Fuel Assembly Components for Water-cooled Reactors*, Workshop on Modelling and Quality Control for Advanced and Innovative Fuel Technologies, Trieste, 2005.
- White J. T. et al., "Thermophysical properties of U<sub>3</sub>Si<sub>2</sub> to 1773 K", Journal of Nuclear Materials 484 386-387, 2017.
- Williamson R.L. et al., *Multidimensional Multiphysics Simulation of Nuclear Fuel Behavior*, J. Nucl. Mater., 423, pp.149-163, 2012.
- WNA, *Nuclear Power in the USA*, World Nuclear Association, London, UK, 2017a.
- WNA, Data obtained from World Nuclear Association, [www.world-nuclear.org/](http://www.world-nuclear.org/), accessed June 5, 2017b.
- WNA, *World Nuclear Performance Report, 2018*, World Nuclear Association, London, UK, 2018.
- WNN (World Nuclear News), June 14, 2017.
- Woo C. H. and Gosele U., *Dislocation Bias in an Anisotropic Diffusive Medium and Irradiation Growth*, J. Nucl. Mater., Vol. 119, pp. 219-228, 1983.
- Woo C. H., Irradiation Creep due to Elasto Diffusion, J. Nucl. Mat., Vol. 120, pp. 55-64, 1984.
- Woo C. H., *Polycrystalline Effects on Irradiation Creep and Growth in Textured Zirconium*, J. Nucl. Mater. Vol. 131, pp. 105-117, 1985.
- Woo C.H., *Effect of Intergranular Interaction In the Anisotropy of Irradiation Creep and Growth in Zirconium*, Materials for nuclear Reactor Core Applications, BNES, London, Vol. 1, pp. 65-71, 1987a.
- Woo C.H., *Effects of Anisotropic Diffusion on Irradiation Deformation*, ASTM STP 955, pp. 70-89, 1987b.
- Woo C. H., Theory of Irradiation Deformation in Non-Cubic Metals: Effects of Anisotropic Diffusion, Journal of Nuclear Materials 159, 237-256, North-Holland, Amsterdam, 1988.

## Appendix A - Determination of the Creep Anisotropy Factors, F, G and H

As outlined in section 5.2.2.2.2, irradiation creep can be represented by the Hill's compliance tensor that, when referred to principal axes of stress, is given by Equation 5-27 and Equation 5-28. These equations are equivalent in defining the creep compliance tensor. The tensor relates the deformation (creep rate) with applied stress. Another way to think of the compliance tensor is as a set of balance equations describing the response of the material to an imposed stress state. In this case it does not matter what controls the anisotropy, rather that there are a set of parameters, F, G and H, that describe the response of the material to an imposed stress. There may be a number of different physical processes that govern the response but, ultimately, one needs only define F, G and H to be able to describe the response of a given material to a given stress state. F, G and H will change as the microstructure changes and are likely to be most sensitive to dislocation structure, grain structure and crystallographic texture. In the case of thermal creep the dislocation structure and texture are most important with the grain boundaries acting as sinks for gliding dislocations thus aiding thermal creep cessation as the gliding dislocations are exhausted. For irradiation creep, grain structure is very important and that is largely due to the effect of the grain boundaries as sinks for point defects. The dependence of creep on mass transport is the most likely reason why there is a linear stress dependence of irradiation creep – diffusional creep is linear in stress and has an inverse relationship with grain dimensions. There are two ways in which the compliance tensor for irradiation creep can be obtained:

1. by measurement;
2. by using a polycrystalline model.

### A.1 Determination of F, G and H by Measurement

Just as one can determine the yield anisotropy of a given material by measuring the yield stress in three orthogonal directions, or three directions sufficiently different to sample the yield surface adequately, one can, in principle, determine the creep anisotropy by measuring the creep strain rate for two different stress states, effectively defining the radius-normal to the compliance tensor surface for each stress locus thus allowing one to extract the F, G and H parameters defining that surface, see Figure A-1.

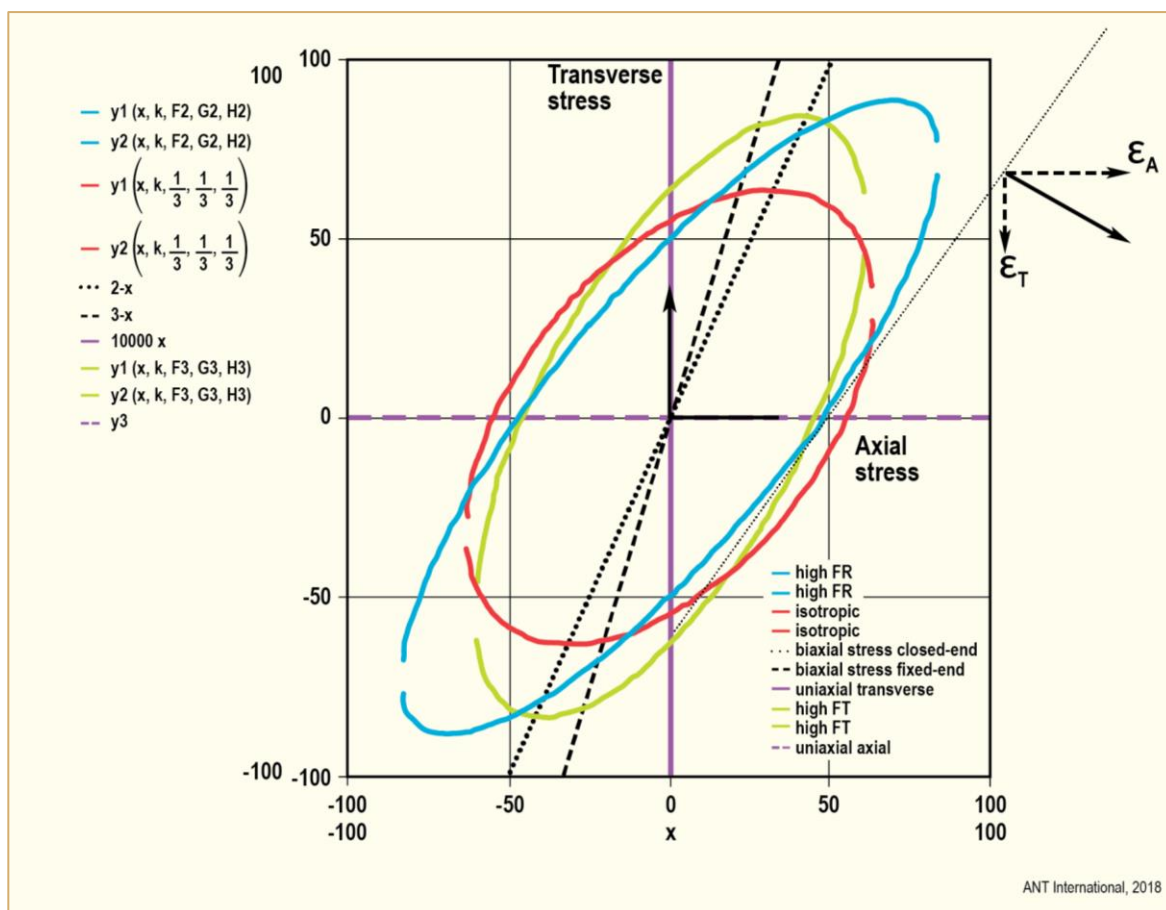


Figure A-1: Example of stress loci and yield surfaces defined by the creep compliance tensor in the plane of a tube for a range of different anisotropy factors. An example is given for the strain rate vector ( $\dot{\epsilon}$ ), defined by the normal to the surface at the intersection with an axial tensile stress for an axial tensile specimen and has components  $\dot{\epsilon}_A$  and  $\dot{\epsilon}_T$  corresponding with the axial and transverse directions respectively;  $\dot{\epsilon}$  is the strain rate.

Given that the irradiation creep response can be described by an equation of the form described in Equation 5-20, one can design an experiment that allows one to determine  $F$ ,  $G$  and  $H$ . A number of different examples of tests that one could conduct to derive  $F$ ,  $G$  and  $H$  have been described by [Woo et al., 1999]. Ideally one should measure the strain rate of tensile specimens under a constant stress in at least three directions. Assuming that the stress exponent = 1, if one is able to obtain creep specimens from three orthogonal directions corresponding with the axes defining the compliance tensor, the strain rates will be proportional to  $(G+H)\sigma$ ,  $(G+F)\sigma$  and  $(H+F)\sigma$  thus enabling one to determine  $F$ ,  $G$  and  $H$ . The sum of the diagonals,  $2(G + F + H)$  is a tensor invariant and is constant.

However, the nuclear reactor core components for which irradiation creep is most important are internally-pressurised tubes. In the case of a thin-walled tube one cannot obtain a simple tensile response in a direction that is sufficiently inclined to the surface of the tube that would provide enough information from which to extract the anisotropy factors. However, if one can measure both the strain along the axis of the tensile specimen and perpendicular to the gauge at the same time then one could deduce  $F$ ,  $G$  and  $H$ . Perhaps the simplest creep experiment that can be practically achieved in a reactor environment is the stress relaxation test. A stress relaxation test provides a measure of the creep compliance for a given strain direction for a tensile stress state [Fraser et al., 1973].

If one conducts tensile or stress relaxation tests with specimens cut from the axial and transverse directions of the tube of interest (Figure A-2), the strain rate in the axial and transverse directions is defined by the normal to the yield surface at the point where the stress locus intersects the yield surface, as shown in Figure A-1.

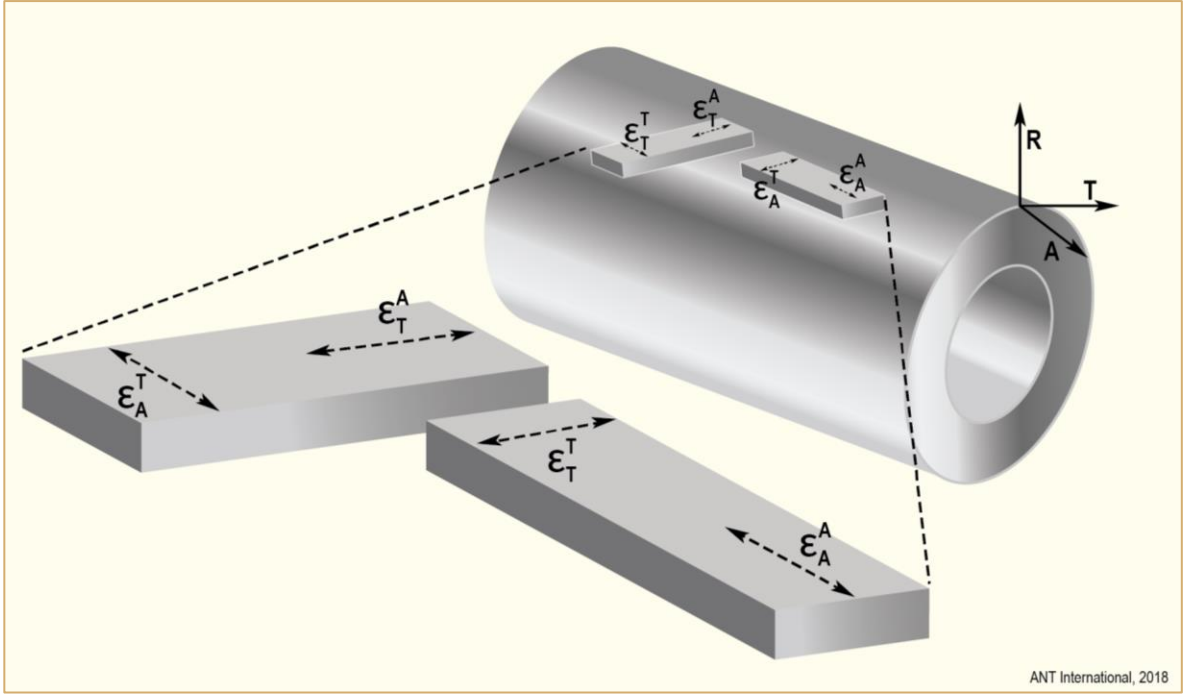


Figure A-2: Orientation of specimens and measurement directions of bent beam stress-relaxation specimens. The subscript defines the orientation with respect to the material of interest (tube), the superscript defines the orientation with respect to the bent beam and  $\epsilon$  is the strain rate.

For bent beam stress-relaxation tests the strains are those determined in the outer fibre of the bent beam with appropriate fiducial markings on the surface from which to determine the strain rates in the two orthogonal directions corresponding with the principal axes of stress and strain.

At the intersection of the stress locus with the creep compliance (yield) surface one can deduce F, G and H as follows:

$$\text{Equation A-1:} \quad \begin{pmatrix} \dot{\epsilon}_R^A \\ \dot{\epsilon}_T^A \\ \dot{\epsilon}_A^A \end{pmatrix} = f(M, \Phi, T) \cdot \begin{pmatrix} G+H & -G & -H \\ -G & G+F & -F \\ -H & -F & H+F \end{pmatrix} \cdot \begin{pmatrix} 0 \\ 0 \\ \sigma \end{pmatrix}$$

$$\text{Equation A-2:} \quad \begin{pmatrix} \dot{\epsilon}_R^T \\ \dot{\epsilon}_T^T \\ \dot{\epsilon}_A^T \end{pmatrix} = f(M, \Phi, T) \cdot \begin{pmatrix} G+H & -G & -H \\ -G & G+F & -F \\ -H & -F & H+F \end{pmatrix} \cdot \begin{pmatrix} 0 \\ \sigma \\ 0 \end{pmatrix}$$

$$\begin{aligned} \text{Equation A-3:} \quad \dot{\epsilon}_R^A &= -f(M, \Phi, T) \cdot \sigma \cdot H; \\ \dot{\epsilon}_T^A &= -f(M, \Phi, T) \cdot \sigma \cdot F; \\ \dot{\epsilon}_A^A &= f(M, \Phi, T) \cdot \sigma \cdot [H+F] \end{aligned}$$

$$\begin{aligned} \text{Equation A-4:} \quad \dot{\epsilon}_R^T &= -f(M, \Phi, T) \cdot \sigma \cdot G; \\ \dot{\epsilon}_T^T &= f(M, \Phi, T) \cdot \sigma \cdot [G+F]; \\ \dot{\epsilon}_A^T &= -f(M, \Phi, T) \cdot \sigma \cdot F \end{aligned}$$



## Appendix B - References

- Backofen, Walter A., *Deformation Processing*, Addison-Wesley Pub. Co. (1972), 1972.
- Causey A. R., Fidleris V., MacEwen S. R., Schulte C. W., *In-reactor Deformation of Zr2.5Nb Pressure Tubes*, ASTM Spec. Techn. Publ. 956, pp. 54-, 1988.
- Causey A. R., Elder J. E., Holt R. A. and Fleck R. G., *On the Anisotropy of in-reactor creep of Zr-2.5Nb tubes*, ASTM STP 1245, pp. 202-220, 1994.
- Christodoulou, N., Causey, A. R., Woo, C. H., Tome, C. N., Klassen, R. J., and Holt, R. A., "Modelling the Effect of Texture and Dislocation Structure on Irradiation Creep of Zirconium alloys," *Effects of Radiation on Materials: 16th International Symposium*. ASTM STP 1175, A.S. Kumar, D.S. Gelles, R.K. Nanstad, and E.A. Little, Eds., ASTM Philadelphia, pp. 1111-1128, 1993.
- Christodoulou N. Causey A. R., Holt R. A., Tomé C. N., Badie N., Klassen R. J., Sauvé R. and Woo C. H., *Modelling in-reactor deformation of Zr-2.5Nb pressure tubes in CANDU power reactors*, *Zirconium in the Nuclear Industry: Eleventh International Symposium*, ASTM 1295, E.R. Bradely and G. P. Sabol, Eds. American Society for Testing and Materials, Philadelphia, pp. 518-537, 1996.
- Coleman C. E. et al., *Rejuvenation of fracture properties of irradiated Zr-2.5 Nb by heat-treatment*, *Effects of Irradiation on Materials: 15th International Symposium*, ASTM STP 1125, Stoller R. E., Kumar A. S., Gelles D. S., (Eds.,) American Society for Testing and Materials, 318-336, Philadelphia, 1992.
- DeAbreu, R.F., Bickel, G.A., Buyers, A.W., Donohue, S.A., Dunn, K., Griffiths, M., Walters, L., *Temperature and neutron flux dependence of in-reactor creep for cold-worked Zr-2.5Nb*, *Zirconium in the Nuclear Industry: Eighteenth International Symposium*, ASTM STP 1507, pp. 938-964, 2018.
- Fraser, D.E., Ross-Ross, P.A. and Causey, A.R., *The relation between stress-relaxation and creep for some alloys during neutron irradiation*, *J. Nucl. Mater.*, Vol. 46, pp. 281-292, 1973.
- Groves, G.W. and Kelly, A., *Independent slip systems in crystals*, *The Philosophical Magazine: A Journal of Theoretical Experimental and Applied Physics*, 8:89, 877-887, DOI: 10.1080/14786436308213843, 1963.
- Holt R. A., *In-reactor Deformation of Cold-worked Zr-2.5Nb Pressure Tubes*, *Journal of Nuclear materials*, Vol. 372, pp. 182-214, 2008.
- Hutchinson, J.W., "Bounds and Self-Consistent Estimates for Creep of Polycrystalline Materials", *Proc. R. Soc. Lond. A*. 348, pp. 101-127, 1976.
- Ibrahim F. E., *Deformation of cold drawn tubes of Zr2.5Nb after 7 years in reactor*, *J. Nucl. Mat*, Vol. 118, pp. 297-304, 1981.
- Kelly, A.F. and Knowles, *Crystallography and Crystal Defects*, Wiley, 2012.
- Nye, J.F., *Physical Properties of Crystals. Their Representation by Tensors and Matrices*, Oxford University press, ISBN: 9780198511656, 1957.
- Ross Ross, P.A. and Hunt, C.E.L., *The In-Reactor Creep of Cold-Worked Zircaloy-2 and Zirconium-2.5wt.%Niobium Pressure Tubes*, *J. Nuclear Materials* 26, pp. 2-17, 1968.
- Spilker H. et al., *Spent LWR Fuel Dry Storage in Large Transport and Storage Casks after Extended Burnup*, *Journal of Nuclear Materials* 250, pp. 63-74, 1997.
- Tome C. N., So C.B. and Woo C.H., *Self-Consistent Calculation of Steady-State Creep and Growth in Textured Zirconium*, *Philos. Mag. A*, Vol. 67 pp. 917-930, 1993.

## Nomenclature

ADS	Automatic Depressurization System
ACRS	Advisory Committee on Reactor Safety (NRC)
AE	Acoustic Emission
ALCYONE	Computer code developed by CEA, EDF and Framatome for analyses of the thermal, chemical and mechanical conditions in PWR fuel
ANL	Argonne National Laboratory
ANS	American National Standards or American Nuclear Society Standards Committee
ANSI	American Nuclear Standards Institute
ANT	Advanced Nuclear Technology
AOA	Axial Offset Anomaly
AOO	Anticipated Operational Occurrences
APT	Atom Probe Tomography
AR	Annual Report
AREVA	French Equipment Manufacturer
ASTM	American Society for Testing and Materials
AT	Axial Tensile
ATEM	Analytical Transmission Electron Microscope
ATP	Atom Probe Tomography
ATR	Advanced Test Reactor
B&W	Babcock & Wilcox
BCC	Body Centered Cubic
BDB	Beyond Design Basis
BE	Back End
BN	Belgo-Nucleare
BNL	Brookhaven National Laboratory
BOL	Beginning of Life
BU	Burn-Up
BWR	Boiling Water Reactor
CANDU	Canadian Deuterium Uranium
CB	Channel Bow
CCT	“C”-shaped ring Compression test
CEA	Commissariat à l'énergie atomique et aux énergies alternatives
CFR	U.S. Code of Federal Regulations
CIEMAT	Centro de Investigaciones Energéticas, Medioambientales y Tecnológicas
CILC	CRUD Induced Localised Corrosion
CIM	Channel Interference Metric
CPR	Critical Power Ratio
CRP	Coordinated Research Project
CRUD	Chalk River Unidentified Deposits
CT	Central Tube
CT	Compact Tension
CVD	Chemical Vapour Deposition
CW	Cold Work
CWSR	Cold Work and Stress Relieved
CZP	Cold Zero Power
DB	Deep Bed
DBA	Design Base Accident
DCF	Dual Cooled Fuel
DCP	Distinctive CRUD Pattern
DEC	Design extension condition
DFT	Density Functional Theory
DHC	Delayed Hydride Cracking
DNB	Post-Departure from Nucleate Boiling
DNBR	Departure from Nucleate Boiling Ratio
DOE	Department of Energy
DS	Dimensional Stability
DZO	Depleted Zinc Oxide

EB	Electron Beam
EBR	Experimental Breeder Reactor
EBSD	Electron Backscatter Diffraction
ECCS	Emergency Core Cooling System
ECR	Equivalent Cladding Reacted
EDC	Expansion Due to Compression
EdF	Electricité de France
EDS	Energy Dispersive Spectroscopy
EDX	Energy Dispersive X-ray spectroscopy
EELS	Electron Energy Loss Spectroscopy
EFPD	Effective Full Power Days
EOL	End Of Life
EPMA	Electron Probe Micro-Analysis
EPRI	Electric Power Research Institute
EPU	Extended power uprate.
ESCP	Extended Storage Collaboration Program
ESSC	Enhanced Spacer Shadow Corrosion
ETR	Engineering Test Reactor
FA	Fuel Assembly
FAST	A thermal-mechanical code with transient as well as steady-state capabilities, which is being developed for the U.S. NRC. FAST incorporates the capabilities of FRAPCON and FRAPTRAN and is intended to replace both of these codes in the near future
FBR	Fast Breeder Reactor
FC	Fuel Channel
FCC	Face Centered Cubic
FCI	Fuel Cladding Interaction
FCM	Fully Ceramic Micro-Encapsulated
FCT	Fuel Centreline Temperature
FE	Front End
FFRD	Fuel Fragmentation, Relocation, and Dispersal
FGR	Fission Gas Release
FIB	Field Ion Bombardment
FIB	Focused Ion Beam
FIMA	Fissions per Initial Metal Atom
FR	Fuel Rod
FRAPCON	Thermal-mechanical code sponsored by the U.S. NRC for steady-state and quasi-transient analysis of water reactor fuel rods; used for sensitivity studies and referee (regulatory) evaluations
FRAPTRAN	Thermal mechanical and hydraulic code sponsored by the U.S. NRC for analyses fuel rod transients; e.g., RIA and LOCA
FWHM	Full Width Half Maximum
GB	Grain Boundary
GDC	General Design Criteria
GE	General Electric
GNF	Global Nuclear Fuel
GT	Guide Tube
GTRF	Grid-to-Rod Fretting
HAADF	High Angle Annular Dark Field
HANA	High performance Alloy for Nuclear Application
HB	High Burnup
HBS	High Burnup Structure
HBWR	Halden BWR
HDS	Hold-Down Spring
HFIR	High Flux Irradiation Reactor
HGCIM	Half-Gap Channel Interference Metric
HIP	Hot Isostatic Pressing
HPCI	High-Pressure Coolant Injections
HPSC	High Potential Stress Corrosion
HPU	Hydrogen Pick-Up

## Unit conversion

TEMPERATURE		
$^{\circ}\text{C} + 273.15 = \text{K}$	$^{\circ}\text{C} \times 1.8 + 32 = ^{\circ}\text{F}$	
T(K)	T( $^{\circ}\text{C}$ )	T( $^{\circ}\text{F}$ )
273	0	32
289	16	61
298	25	77
373	100	212
473	200	392
573	300	572
633	360	680
673	400	752
773	500	932
783	510	950
793	520	968
823	550	1022
833	560	1040
873	600	1112
878	605	1121
893	620	1148
923	650	1202
973	700	1292
1023	750	1382
1053	780	1436
1073	800	1472
1136	863	1585
1143	870	1598
1173	900	1652
1273	1000	1832
1343	1070	1958
1478	1204	2200

Radioactivity	
1 Sv	= 100 Rem
1 Ci	= $3.7 \times 10^{10}$ Bq = 37 GBq
1 Bq	= $1 \text{ s}^{-1}$

MASS	
kg	lbs
0.454	1
1	2.20

DISTANCE	
x ( $\mu\text{m}$ )	x (mils)
0.6	0.02
1	0.04
5	0.20
10	0.39
20	0.79
25	0.98
25.4	1.00
100	3.94

PRESSURE		
bar	MPa	psi
1	0.1	14
10	1	142
70	7	995
70.4	7.04	1000
100	10	1421
130	13	1847
155	15.5	2203
704	70.4	10000
1000	100	14211

STRESS INTENSITY FACTOR	
MPa $\sqrt{\text{m}}$	ksi $\sqrt{\text{inch}}$
0.91	1
1	1.10